# Multivariable Control of a Rougher Flotation Cell


| | |
|---|---|
| By: | Theo van Schalkwyk |
| First supervisor: | Prof Martin Braae |
| Second supervisor: | Dr Dee Bradshaw |

# Declaration

I declare that this thesis, submitted for the degree of Master in Science in Engineering at the University of Cape Town is my own work. It has not been submitted prior to this for any degree or examination, at this or any other university.

Theo van Schalkwyk.
December 2002

# Acknowledgements

My sincere thanks goes to all those that was involved in this project in various ways. In specific to the following people and institutions:

- Anglo Platinum for full financial sponsorship of the project.
- A special thanks to Prof Martin Braae for his supervision, patience and for the great effort of teaching me control theory.
- Dr Dee Bradshaw for her supervision, facilitation and the many other aspects she was involved in that made this project possible.
- Leon Coetzer for his assistance in motivating and initiating this project as well as for his continual support throughout the project.
- Michelle Dry and UCT students that assisted with the many hours of step tests.
- All the staff at Bafokeng Rasimone Platinum Mine (BRPM) that was involved in the project for their contributions, in particular Alan Delaney, Hennie Jansen and Jacques van Niekerk for their assistance.
- Roger Leighton and Craig Sweet for their support and advice throughout the project.
- All the people from UCT (machine vision) and Stone Three for their efforts to ensure that the machine vision system was always operational.
- Tina van Schalkwyk for her never ending support and motivation.

# Abstract

This project focussed on the investigation, development and evaluation of a closed loop control system on a rougher flotation cell that could improve PGM flotation performance.

A PGM rougher flotation cell equipped with Online Stream Analysis (OSA) and machine vision system (SmartFroth) was used during the investigation. Online measurements included bubble velocity, average bubble area, bubble colour; Pt, Ni and Cu concentrate grade and concentrate flow rate and density. Air addition and pulp level was used as the manipulated variables.

A system identification exercise was performed to model the dynamic responses of all the available outputs to step changes in the air addition and pulp level. Brief analysis of the consistency of the output gains for different initial conditions was done to determine whether the process for the measured outputs were linear. None of the outputs that were selected to be controlled exhibited non-linear behaviour so that linear control theory could be applied for the development of a closed loop controller.

Linear dynamic models of the machine vision outputs were analysed and it was determined that the biggest operating region for MIMO control exists when the air addition is manipulated to control the bubble velocity and the pulp level is manipulated to control the blue bubble colour. The multivariable control application was relatively simple as the interaction between the two control loops was intermittent. Different decoupling structures with PI controllers were tested in a simulation environment and it was found that the difference between the decoupling structures were small with no single decoupling structure outperforming any of the other structures. LQG and IMC MIMO controllers were also designed and compared in the simulation environment. All the controllers performed similarly with the exception of LQG control, which was worse.

Implementation of the designed controllers on site exhibited mixed results. The blue colour measurement proved to be unreliable while the bubble velocity showed good control potential as an industrial measurement by manipulating the air addition. Research should focus on relating machine vision outputs directly to the metallurgical performance of flotation so that optimal machine vision setpoints can be selected.

# Table of Contents

## LIST OF TABLES

# 1. Introduction

Flotation, originally patented in 1906 [Wills, 1992] is a solids separation process with the objective of separating mixed material on the basis that the different composites of the bulk material possess different hydrophobicity levels on their particle surface. Flotation has mostly found its application in the minerals processing industry. In particular coal, base metals and the PGM (Platinum Group Metals) industries use flotation in the extraction of valuable metal bearing minerals from run of mine ore that is ground down to a specific particle size.

Automated flotation control has been described by most researchers in the field as a difficult task to achieve for various reasons [Lynch et al, 1981; McKee, 1992; Moolman et al, 1996]. The introduction of new measurement technology in the process provides new opportunities that could simplify this task. One of the latest online measurements of the flotation process utilises froth surface image analysis algorithms or machine vision to monitor some of the flotation process outputs. This measurement device has shown the potential to measure and extract information from the process that was previously not available [Sweet, 2000; Moolman et al, 1996; Hargrave et al, 1997].

This project focuses on the closed loop control possibilities for machine vision as well as researching and investigating traditional measurements and control of the process. The difficulties of automated flotation control have been ascribed to unmeasured disturbances, long delays between process measurements, measurement inaccuracies, strong variable interactions and the lack of accurate process models to determine optimum setpoints. With the introduction of machine vision techniques, new flotation control strategies are possible and Anglo Platinum has initiated various projects on flotation control in order to improve and maximise the performance of their flotation circuits.

Shown below is a schematic presentation of the current status of automated flotation control from which the research objective for this control project originated. This project primarily focuses on the stabilisation block highlighted.

# Online Flotation Control

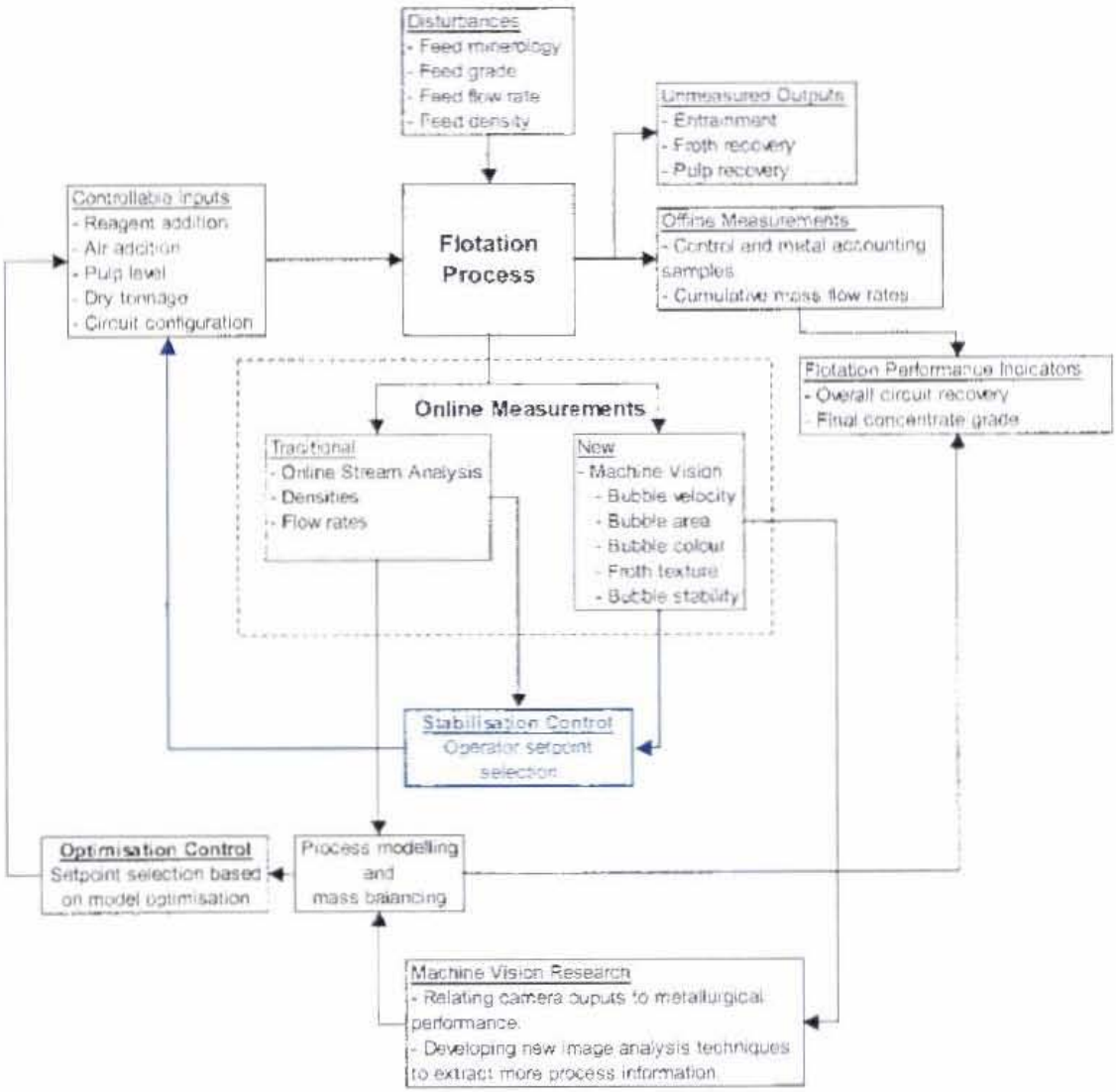

# 2. Literature Review

The literature review primarily focuses on flotation control. After a brief outline of the principles of flotation, the variables that is available for manipulation, is discussed – both physical and chemical. Available online measurements such as OSA and machine vision are then reviewed.

Existing flotation control application and their limitations are then evaluated which lead to the research objectives of this thesis.

## *2.1) Flotation Operation*

Flotation is a physico-chemical process for separating valuable minerals from unwanted waste based on the difference in surface properties. Flotation is mainly used for the concentration of mineral sulphides, oxides and coal [Lynch et al, 1981]. Run of mine ore is prepared for flotation by crushing and grinding that reduces the particle size until most or all of the valuable minerals are liberated. This is done under wet conditions such that the run of mine material is turned into a slurry or pulp (mixture of solids and water). The slurry is fed to an agitated flotation vessel where air is bubbled through the slurry. Separation is then based on the different levels of hydrophobicity of the particle surfaces. In a turbulent environment particles and air bubbles collide and those particles with high hydrophobicity attach to the air bubbles and are carried to the pulp surface by the air bubbles.

The air bubbles form a froth layer on top of the pulp level. The pulp level is maintained some distance beneath the top of the open-ended flotation vessel such that the top of the froth layer overflows over the top edge (or cell lip) of the flotation cell. The froth that overflows over the cell lip is called the concentrate and contains the hydrophobic material that was recovered from the pulp phase as well as material recovered unselectively by entrainment. The chemical environment is manipulated with the addition of chemicals, which are added to the slurry to perform different roles: collectors render certain valuable minerals hydrophobic, depressant depress gangue material and frothers

support froth formation and structure. Various operating conditions have an influence on the performance of the flotation cell. Some of these conditions can be directly manipulated and are discussed in more detail in the next paragraph. The success of the process is measured in term of the concentrate grade and recovery of the valuable minerals.

## *2.2) Manipulated Variables of the Flotation Process*

The flotation circuit receives pulp from the milling circuit and the following variables are measured from the milling circuit but not easily controlled.

- Density
- Flow rate
- Grind

The variables that can be manipulated in an on-line manner to control flotation outputs are:

- Physical
  - Pulp level
  - Air addition
- Chemical
  - Frother addition
  - Collector addition
  - Depressant addition
  - Activator addition

### 2.2.1) Pulp level

Froth height affects the residence time of the froth phase and consequently has a big influence on particle drainage from the froth [Lynch et al, 1981]. This generally applies to gangue particles that are present in the froth due to entrainment. The concentrate grade of the froth can be increased with a deeper level but with a loss in recovery. A deeper

froth bed allows for better water drainage from the froth [Lynch et al, 1981]. Hyotyniemi el al [2001] reports that bubble stability has a big influence on the recovery of a flotation cell. Bubble stability decreases with a deeper level so that any particles that are attached to a bubble that bursts then report to the channels in between the remaining bubbles and are subjected to drainage as fundamentally modelled and reported by Ventura et al [2002]. An optimised pulp level setpoint might then be at the point just before a certain threshold for bubble stability. This would allow for maximum drainage of gangue material without collapsing bubbles that have valuable particles attached to them.

Various operations (e.g. Clarabelle and Kotalahti mines) have used pulp level to control their rougher concentrate grade [Lynch and McKee, 1984]. The difficulties with this type of control occurred as a result of the long measuring times associated with the measuring sensor (OSA) as well as the problem of selecting optimised grade setpoints. In order to select an optimised grade setpoint the theoretical maximum performance that can be achieved needs to be calculated. This is dependent on the feed conditions to the flotation section which include the measured variables:

- Feed grade
- Size distribution
- Flow rate and density

### 2.2.2) Air addition

An increase in air addition increases the probability of collision between the particles and bubbles in the pulp phase. More particles, bubbles and water are then transferred to the froth phase and this reduces the residence time of the froth phase. Air addition can be used to control the concentrate grade, tailings grade or mass pull [Lynch et al, 1981]. The flotation process also responds rapidly to changes in air addition and was found to be more effective than pulp level as a control variable [Lynch et al, 1981]. Test work done by Smar et al [1994] indicate that the recovery increases with an increase in air addition up to a certain maximum after which it remains constant. This is accompanied by a decrease in concentrate grade.

Flotation performance can be limited when not enough air is fed to the flotation cell. This results in a saturated or overloaded froth with little or no concentrate being collected and this condition should be avoided. There is some evidence that froth saturation can be detected by monitoring the froth solids content since this tends to rise to a maximum as the mineral loading in the froth phase increases [Lynch et al, 1981].

### 2.2.3) Collector addition

Collector addition increases the recovery of the valuable mineral until a plateau region is reached after which a reduction in the recovery is possible with increased levels of collector [Lynch et al, 1981]. An increase in collector addition also increases the recovery of gangue material. Lynch et al describe feed forward ratio control based on the mass flow rate of the valuable mineral in the feed to the flotation section that has been applied on various concentrators. Other applications of collector control that he discusses involve feedback control based on the tailings grade of the rougher section. The collector addition on most PGM flotation circuits is only ratio controlled to the mill feed rate. This is mainly due to the fact that the PGM concentration in the rougher feed and tailings are too low to measure by OSA [Sweet, 2000].

### 2.2.4) Frother addition

Froth stability depends on, among other things, the amount of frother added to the system. At low frother concentrations the froth tends to collapse and at higher frother concentrations the mass pull from the cell would be excessively high. Consequently a change in the frother addition rate may significantly affect the recovery and concentrate grade from a system [Lynch et al, 1981].

Frother addition affects both the grade and recovery of a flotation system and can greatly impact negatively on the process when it is under or over dosed. Over and under dosage can be detected on the froth surface [Sweet, 2000; Moolman et al, 1996] by means of machine vision. Since every other parameter of the flotation process also affects the grade and the recovery, it is very difficult to detect insufficient or excessive

frother dosages with an OSA measurement. For this reason there are few implementations of automated control utilising frother addition as a manipulated variable with only OSA measurements available.

Frother addition is manually controlled by the operator that makes the frother adjustment based on the froth appearance or bubble stability. Research on changes in machine vision outputs as a result of frother type and addition rates seems promising for the development of an automated control strategy for frother addition [Sweet, 2000; Moolman et al, 1996].

### 2.2.5) Activators and Depressants

As with frother addition, depressant and activator additions are mostly detected in the froth appearance and the most viable control variables for these are machine vision outputs [Sweet, 2000; Moolman et al, 1996]. Hyotyniemi et al [2000] and Sweet [2000] report on control actions for these reagents and these are discussed later in more detail.

## *2.3) Online Measurements for Flotation Control*

Automated control starts with reliable, online measurements of the process. Without instrumentation that supplies an accurate measure of the plant condition and operating state, automated control of the plant is limited or not possible at all. Some instrumentation on flotation plants has been in use for some time while others are new developments of which some are still under investigation.

### 2.3.1) Online Stream Analysis (OSA)

An OSA analyser measures the metal concentration in slurry streams. The basic principle of such analysers is to excite and measure the characteristic X-rays of the elements in the sample. The energy or wavelength of that radiation uniquely determines

which element it is derived from. The excitation of the characteristic X-rays is done with X-rays from a radioactive source or an X-ray-tube.

Advantages of OSA:

a) Direct measurement of the concentrate grade.
b) If the concentrate mass pull can be measured, the recovery of the plant or at least certain sections of it can be calculated from this and the OSA measurement.

Disadvantages of OSA:

a) High capital and maintenance costs.
b) Require a lot of labour to calibrate and maintain.
c) Cannot directly measure the Pt concentration of flotation feed and tails.
d) Turn around time of an analysis of about 12 minutes.

### 2.3.2) Machine Vision (SmartFroth)

Traditionally operators have controlled plants by visual inspection. With the advent of increased computer capacity, machine vision techniques have been developed to assist the operator and be available for process control. Anglo Platinum has sponsored a project at UCT (University of Cape Town) to develop froth imaging software (SmartFroth). Although the software is still undergoing development, a prototype of the system has already proved to assist with automated control. A camera that is installed above the flotation froth sends 25 images per second of the froth to a PC that performs image analysis on the images. The current measurements from the image analysis algorithms that are reliable are bubble velocity and bubble size distribution. Other measurements that are available but need to be improved are bubble colour, froth type classification and bubble stability [Sweet, 2000].

Advantages of froth image analysis

a) 100% availability with low maintenance.
b) Relatively low capital costs.
c) Measurement available every 2 seconds.

d) Non-intrusive soft sensor.
e) Continuous development possible.

Disadvantages of froth image analysis

a) Does not directly measure the metallurgical performance of a flotation cell.
b) Some camera output measurements (e.g. colour) are influenced by ambient light.

## *2.4) An Overview of Flotation Control.*

From the literature on flotation control three fields within this topic emerged. The first of these and also the most extensively covered is automated flotation control using online stream analysis (OSA) measurements. Research on automated OSA control dates back to the early 1970's when OSA sensors first became reliable instruments [McKee, 1992; Lynch et al, 1981]. In the mid 1990's froth surface image analysis or machine vision appeared as another viable measurement for automated flotation control [Moolman et al, 1996]. One drawback of machine vision is that it does not directly measure the metallurgical performance of the flotation process. Research to date has focussed on the development of machine vision measurements and the interpretation thereof in terms of metallurgical performance [Sweet, 2000; Moolman et al, 1996; Hargrave et al, 1996]. The third field of research with very few publications in the literature is the utilisation of machine vision in closed loop control [Hyotyniemi et al, 2000; Kittel et al, 2001; Cipriano et al, 1998]. Still completely absent from the literature is the combined and integrated usage of OSA and machine vision to form an overall control strategy for the flotation process.

Initial attempts at automatic control of flotation circuits started in the early 1970's with the introduction of online stream analysis (OSA). Lynch and others stated that automatic flotation control has proved to be an elusive goal [Hodouin et al, 2001; McKee, 1992]. Success was limited due to problems encountered with the variability in ore type that could not be compensated for and operators frequently had to manually adjust setpoints to compensate for changes in ore type. This problem has not been solved yet and in recent years the trend has been to simplify strategies and objectives of flotation control

systems [Lynch et al, 1981]. Most flotation control systems only involve feedback stabilisation control loops and no general method has been developed for the automatic selection of optimum setpoints. The economic incentive for the implementation of flotation control still remains valid and for this reason work on flotation control has continued [Lynch and McKee, 1984].

A flotation circuit has very few output variables that define the performance of the process. Concentrate grade and recovery are the two degrees of freedom that describe flotation circuit targets. The number of process variables that can be manipulated are extraordinarily large compared to the two degrees of freedom output variables. This often results in the overall objective of flotation control being cascaded down to various flotation stages [Hodouin et al, 2001]. Hodouin et al also identify non-linearity as a problem with regard to flotation reagent control. He lists the following control approaches being used in more advanced flotation control simulations and applications:

- Model predictive SISO control.
- Multivariable control.
- Non-linear control using mathematical models.
- Adaptive control.
- Rule based expert control.
- Fuzzy logic control.
- Artificial neural networks.
- Adaptive generic algorithm.

McKee [1992] discusses various case studies of flotation control that utilise OSA measurements. He puts emphasis on specifying realistic control objectives and suggests the following structured approach towards developing a suitable flotation control strategy:

- Define the precise metallurgical objectives of the circuit.
- Isolate and understand the constraints present in the circuit.
- Develop an understanding of the types of disturbances that might be encountered.

- After thorough examination of above factors, formulate an initial set of objectives for the desired control system.
- Decide on a general control approach – stabilising, setpoint control or optimising.
- Select a control approach and commence the development of strategies.

The three major difficulties of stabilising control are identified by McKee as:

a) Recognising when changes in ore type occur.
b) Developing loops that can accommodate long process delays (OSA).
c) Developing methods for appropriate setpoint and selection of limits.

PID and adaptive control algorithms were mostly used in the case studies that are discussed [McKee, 1992].

More recent developments such as more reliable flotation models, froth imaging and expert systems are not covered in these case studies that he presents.

### 2.4.1) Flotation Control Applications: OSA

Self-tuning minimum variance control strategies have been successfully applied to rougher flotation at Mount Isa Mines. Manlapig et al [1987] report that manipulating the collector addition, controlled the rougher tailings grade and therefore the recovery of the rougher stage. However, operators were still required to provide a manual setpoint for the tailings grade to compensate for ore type changes. Initially this was PI controlled, but due to the non-linearity and time varying nature of the process it was found that the PI controller needed to be retuned on a regular basis. An adaptive control algorithm with a sampling interval of seven minutes (OSA cycle time between measurements) was then successfully implemented. The benefits were more stable operation of the flotation bank and a reduction in the collector addition by 10 %.

Bergh et al [1995] report on the successful implementation of an expert system for two flotation columns and a cleaning stage at Salvador concentrator. The final concentrate

grade was increased by 1.2% without a loss in recovery and the operation of the cleaning stage was stabilised. The expert system acted as an overall supervisor that co-ordinated the actions of distributed controllers according to some specific objective function that relates to metallurgical and economic benefits. The supervising expert system mainly improved the overall performance of the plant by implementing fault detection followed by appropriate corrective action that includes the management of local control loops. Manipulated variables included froth depth, gas flow rate and wash water flow rate. As each of these has a strong influence on the concentrate grade, optimum setpoints for these variables were calculated based on the combined effect of all three variables. The objective of the control strategy was to keep the concentrate grade within a narrow band while the recovery had to be more than a minimum value. When the recovery decreased to below the minimum value the concentrate grade control was overruled by a procedure that increased the recovery. Constraints were imposed on the three manipulated variables that had to be within upper and lower limits. Again, when a constraint was reached, the concentrate grade control was overruled with corrective action to get rid of the constraint. Another manipulated variable was frother addition that was maintained at a minimum unless the operation variables got saturated. The frother addition was then incrementally increased. Control action intervals were only performed every 10 minutes. This was not a restriction imposed by the OSA measurement intervals but as a result of the response time of the process. The response time of a frother addition change would be 2 to 3 times the residence time of the flotation cell or stage. The residence time for a flotation cell would typically be a few minutes, while for a flotation stage it can be up to an hour depending on the amount of cells in the circuit.

Suichies et al [1999] report on the successful implementation of a SISO Generalised Predictive Controller on an expert system shell. The controller made use of a linear ARX model with a sampling interval of two minutes and controlled the concentrate grade by manipulation of the xanthate addition. The concentrate grade was stabilised and improved by 1.4%.

### 2.4.2) Flotation Control: Machine Vision Outputs

Most of the literature on flotation control only discusses the application of OSA measurements as the only flotation control variable. Since the early 1990's froth image analysis has developed output measurement of the flotation process. Papers on the interpretation of froth image analysis have been produced by various researchers [Moolman et al, 1996; Hargrave and Hall 1997], but there are few publications on the application of froth image analysis in closed loop control [Hyotyniemi et al, 2000; Kittel et al, 2001; Cipriano et al, 1998]. The reason for this is that certain froth image analysis outputs only recently became reliable [Holtham and Nguyen, 2002] and the application of these measurements still need to be accepted and implemented successfully by the industry. Commercial units have only appeared on the market since 1998. Froth image analysis is still a very active field of investigation with researchers attempting to extract more information from froth images, and relating and interpreting these to the metallurgical performance of the flotation process.

Sweet [2000] found that machine vision could be used to detect dosage levels of depressant and frother that could negatively influence flotation performance. The ore type, Merensky reef (Bushveld complex), on which his work focused is similar to the ore type found at BRPM where this project was done, which is also Merensky reef but from a different location. From his work he suggests a logic algorithm that would identify frother and depressant over and under dosages. Since this current project focuses mainly on the air addition and pulp level as manipulated variables, Sweet's work could be combined with the results of this project to incorporate reagent addition rates, air addition and pulp level in a general control philosophy for PGM Merensky ore flotation.

Hyotyniemi et al [2001] report that the most important measurements from a machine vision system that could be used for automated control (using only reagents as manipulated variables) of the flotation process are:

- Bubble collapse rate
- Transparency of bubbles
- Bubble size
- Bubble colour

- Bubble velocity

He shows that the bubble collapse rate strongly relates to the activation flotation reagent, $CuSO_4$, which is added to the zinc flotation feed (Pyhäsalmi concentrator). Bubble collapse rate further has a strong influence on the recovery of the flotation process. When the bubbles collapse rate increases, the recovery of the process is significantly reduced. He also reports that an over dosage of $CuSO_4$ can be detected by a low transparency of the bubbles. A rule based control algorithm was constructed to control the $CuSO_4$ in the feed. The reagent was increased or decreased by 2% depending on the froth vision outputs with the objective to minimise bubble collapse rate and to prevent over dosage of $CuSO_4$. The whole rule based control consisted of seven if-then rules that made fixed incremental changes to the manipulated variables. They managed to control the $CuSO_4$ addition so that the bubble collapse rate was stabilised. Their simple, but effective control actions were successful and the control philosophy was implemented on other flotation plants within the same company. As Lynch et al suggested on the trend to simplify flotation control actions; Hyotyniemi reports, '*Even though the industrial application seems to be promising, something seems to be missing from the artificial intelligence point of view: The somewhat obscure feel of "intelligence" vanishes when explicit algorithms can be written for implementing all specific tasks.*' and that '*...seen from outside, the consistent operation of the controlled plant still looks rather intelligent*'.

Another implementation of froth image analysis was at Escondida copper mine in Chile. They have implemented rule based control on an expert system that adjusts the air addition and pulp level based on the bubble velocity. Kittel et al report a 1.2 % increase in recovery on two rougher banks of the concentrator. From metallurgical test work they determined that air addition has the greatest effect on copper recovery and that pulp level had the greatest effect on concentrate grade. Their flotation control philosophy was to first adjust the air addition (in feedback with bubble velocity) and only when the air addition reached a specified minimum or maximum, was the pulp level adjusted.

Froth image analysis is capable of producing many measurements and features to describe the froth surface. An online measurement is only useful if it can be used for control or modelling purposes. Since all outputs from froth image analysis can only be

used as inferential measurements of the metallurgical performance of flotation, it makes the selection of usable measurements difficult. From the literature various researchers have found different image analysis measurements useful in that they could relate these to the metallurgical performance. Some researchers reported that froth colour is correlated to the concentrate grade for some ore types [Hargrave and Hall, 1997; Bonifazi et al 2000; Niemi et al, 1997]. Moolman et al [1996] and Ventura [2000] identified bubble velocity as an important froth feature that correlates to mass pull. Bubble area has been reported to respond to perturbations in the process inputs by various researchers [Sweet, 2000; Hargrave and Hall, 1997; Moolman et al, 1996]. Another machine vision measurement that came from the literature as having a big influence on recovery is bubble stability [Hyotyniemi et al, 2001; Aldrich et al, 1997]. Froth surface texture analysis also showed correlation to cell performance [Bezuidenhout et al, 1997; Hargrave and Hall 1997].

From the literature on the interpretation of the relationship of froth surface features to metallurgical performance it can be said that the topic has been investigated to a relatively broad degree, but that consensus on a generic understanding of the calibration of machine vision outputs to metallurgical performance has not been reached yet. This is evident in the few closed loop control applications of froth image analysis that this would be the next step after general quantification of machine vision outputs.

# 3. Research Objectives

The literature review showns that there exists a need to investigate further the use of machine vision in closed loop control. Different machine vision outputs seem to be more beneficial for control for different kinds of ore types. With regard to PGM ore types, in particular Merensky reef, some work has been done on the metallurgical interpretation of machine vision outputs, but system identification and a control evaluation of the best machine vision outputs for closed loop control has not been done. To date research on machine vision control has focussed more on which outputs to control, while the actual controller designs have been neglected and seemed to be sub optimal as if-then rule based control and single loop control loops are mostly applied.

Objectives of this project are to:

- Identify and evaluate possible online measurements for flotation control.
- Investigate control possibilities around a single PGM, Merensky reef flotation cell utilisation machine vision outputs from SmartFroth.
- Investigate more advanced controller design techniques and evaluate the potential benefits of their use.
- Make recommendations and identify difficulties towards an advanced control strategy for PGM flotation that is primarily focussed on machine vision outputs, but consideration should also be given to the benefits and use of online stream analysis.

# 4. Process Description and Measurements

The concentrator plant where the test work was done is a typical mill-float, mill-float concentrator. ROM Merensky reef (Bushveld complex) is crushed to minus 8 mm and fed to a primary ball mill. Cyclone overflow from the primary milling section gravity flows to the primary rougher flotation section. Final concentrate of the plant is produced by a recleaning stage, which is fed by concentrate from the first rougher and cleaner sections. Secondary rougher concentrate goes to the cleaning stage and secondary cleaner concentrate gets recycled to the cleaner feed. Depressant, xanthate, dithiophosphate, $CuSO_4$ and frother are added at various stages of the process. Primary rougher flotation tails are pumped to the secondary ball mill with a flotation circuit that is identical to the primary flotation circuit.

Figure 4-1 below shows the first and second primary rougher cells. All the test work was done on these two cells.

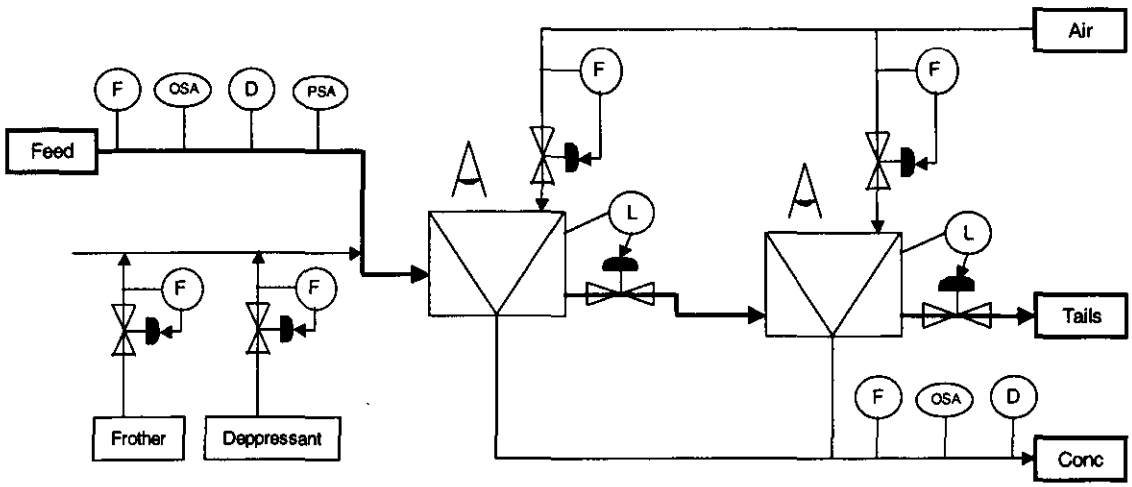


**Figure 4-1: Process flow diagram.**

Figure 4-1 shows the measured and manipulated variables that are available for automation. Other information about the process that is not shown is the xanhtate and dithiophosphate addition at the feed. These collectors are essential for optimal recoveries and the manual control approach that is followed by the plant personnel is to slightly overdose these, to ensure that there is always enough collector is the system.

Frother on the other hand requires regular setpoint adjustments depending on the froth appearance (maybe once or twice a shift) and is therefore a good variable to manipulate automatically, if a shortage or over dosage can be detected or measured online. Production staff at BRPM doses depressant at irregular intervals as they are still determining whether it is beneficial to dose depressant at the rougher stage.

Other variables that could be manipulated are the air addition and pulp level of the cells. The operator most often manipulates these variables as their effect can be clearly and quickly detected in the froth appearance form the cell.

Process outputs are measured by two instruments namely froth image analysis from a camera on each cell and online stream analysis (OSA) from a field X-ray analyser. Rougher feed and the combined concentrate from cell one and two are analysed for metal concentration by the X-ray analyser. OSA has been in use for the last 30 years and is reasonably well established in the minerals processing industry. However, automated online control using only OSA measurements has proved to be very difficult in the past [Lynch, 1981; McKee, 1992].

Froth image analysis on the other hand is a fairly new measurement and this technology has been around for last ten years [Moolman, 1996]. Machine vision works on the basis that a camera is placed above the froth so that the froth surface appearance can be characterised by image processing. Traditionally an operator manually controls the flotation process by observing what the froth looks like. If a camera could digitally supply the same information about the froth appearance as the operator interprets from it, a camera system could be used for closed loop control of the variables that the operator manipulates. The development of froth image analysis outputs is still ongoing as programmers and metallurgists work together to extract more accurate and relevant information from the froth appearance by image analysis.

Process measurements on minerals processing plants have always been difficult due to the nature of slurries [Lynch, 1981]. Slurry streams are highly abrasive and often cause blockages in pipelines and instrumentation equipment due to the presence of solids. One of the major advantages of froth image analysis is that it is a non-contact instrument that is relatively low in cost with a high availability and low maintenance.

Other measurements of the process as indicated in Figure 4-1 are online particle size measurements of the rougher feed, density and flow rate measurements of the rougher feed as well as the combined rougher concentrate from cell one and two. The online particle size analysis is done by laser diffraction of a sampled stream, while the flow rate to the roughers is inferred from milling section parameters. Density of the feed and concentrate streams is done by the Online Stream Analyser (OSA), while the flow rate measurement of the concentrate stream is estimated from an inferential measurement on the secondary sampling system of the OSA.

In mathematical form presented below, for a linear plant model, is the G(s) plant transfer function matrix. The outputs include those from both OSA and machine vision measurements and the following section will evaluate which inputs and outputs should be used in a control strategy.

$$\begin{bmatrix} \text{Bubble velocity} \\ \text{Bubble area} \\ \text{Blue bubble colour} \\ \text{\% Ni in concentrate} \\ \text{\% Pt in concentrate} \\ \text{\% Cu in concentrate} \\ \text{Concentrate flow rate} \\ \text{Concentrate density} \end{bmatrix} = \begin{bmatrix} g_{11} & g_{12} & g_{13} & g_{14} \\ g_{21} & g_{22} & g_{23} & g_{24} \\ g_{31} & g_{32} & g_{33} & g_{34} \\ g_{41} & g_{42} & g_{43} & g_{44} \\ g_{51} & g_{52} & g_{53} & g_{54} \\ g_{61} & g_{62} & g_{63} & g_{64} \\ g_{71} & g_{72} & g_{73} & g_{74} \\ g_{81} & g_{82} & g_{83} & g_{84} \end{bmatrix} \begin{bmatrix} \text{Air addition} \\ \text{Pulp level} \\ \text{Frother addition} \\ \text{Depressant addition} \end{bmatrix}$$

where each element $g_{ij}(s)$ is a transfer function [Maciejowski, 1989].

# 5. System Identification and Process Model Analysis

The flotation process is relative well understood in terms of the parameters that influence its performance [Lynch, 1981]. Fundamental modelling of the process has however not progressed so far that the process outputs can be predicted accurately by taking into consideration all the input variables [Hodouin, 2001; Lynch, 1981]. The main reason for this is the many input variables present and the inability to accurately measure and determine the exact quantity of these input variables. It is therefore not possible to determine the dynamic response of a flotation cell fundamentally, and so the system identification of the process was determined empirically by stepping the manipulated inputs and monitoring the responses in the measured variables.

From the start of the project it was decided to focus mainly on the air addition and pulp level as possible manipulated variables. Since a camera system was only available on the first two cells of the rougher stage, accurate accounting of reagent addition effects on the froth surface down the whole rougher bank was not possible. Air addition and pulp level are however individual variables to each flotation tank cell of the rougher stage so that these could to a certain degree be independently controlled from the other cells. The outputs of the process that was monitored are given in Table 5-3 with their low, nominal and high values.

A series of step tests were performed on the air addition and pulp level of the first two rougher cells for a period of one and a half weeks. During this time the plant operated at varies feed tonnages ranging from 220 to 310 t/h. The feed rate to the plant is determined by the ore availability, which fluctuates over a large range. The design throughput capacity of the concentrator is 310 t/h.

## *5.1) Step Test Procedure*

Step changes were made to the air addition and pulp level of the flotation cells. The setpoints for the step changes were such that the minimum and maximum values were spread over the widest range possible so that a decent mass pull, typical to normal

deviations of the process, was still achieved. Table 5-1 shows the step tests that were performed with the corresponding low (L), medium (M) and high (H) values as indicated in Table 5-2. The step test routine was altered by changing from low to high instead of high to low as indicated in Table 5-1; each consecutive time the routine was repeated. The routine was repeated 12 times. Thirty to 40 minute intervals between step changes was allowed for steady state to be reached. This interval was determined by the time it took the OSA measurements to reach steady state. Camera measurements reached steady state after only a few minutes. Occasionally the values in Table 5-2 were changed when the mass pull was so high or so low so that it would impact negatively on the process.

**Table 5-1: Step tests routine.**

| No | Air Cell 1 | Air Cell 2 | Level Cell 1 | Level Cell 2 |
|---|---|---|---|---|
| 1 | H | M | M | M |
| 2 | L | M | M | M |
| 3 | M | M | M | M |
| 4 | M | H | M | M |
| 5 | M | L | M | M |
| 6 | M | M | M | M |
| 7 | M | M | H | M |
| 8 | M | M | L | M |
| 9 | M | M | M | M |
| 10 | M | M | M | H |
| 11 | M | M | M | L |
| 12 | M | M | M | M |

**Table 5-2: Low, medium and high values of table 4.1.**

| MV | Low | Medium | High | Units |
|---|---|---|---|---|
| Air cell1 | 5 | 7 | 10 | $m^3$/min |
| Air cell 2 | 5 | 7 | 10 | $m^3$/min |
| Level cell 1 | 15 | 40 | 65 | % froth height |
| Level cell 2 | 15 | 40 | 65 | % froth height |

The corresponding outputs of the process that were recorded are given in Table 5-3. Concentrate measurements were on the combined concentrate from both cells (Figure 4-1). The concentrate flow rate was inferred from the secondary sampling system of the Courier OSA.

Table 5-3: Process outputs.

| No | Measurement | Instrument | Span | Units |
|---|---|---|---|---|
| 1 | Bubble velocity | Camera | 0-1.8 | Pixels/s |
| 2 | Average bubble area | Camera | 0-155 | $Pixels^2$ |
| 3 | Bubble colour, blue | Camera | 0-255 | RGB Colours |
| 4 | Concentrate Ni content | OSA | 0-8 | % |
| 5 | Concentrate Cu content | OSA | 0-8 | % |
| 6 | Concentrate Pt content | OSA | 0-250 | g/t |
| 7 | Concentrate % solids | OSA | 0-85 | % |
| 8 | Concentrate flow rate | OSA | 0-1.5 | $m^3/min$ |

## *5.2) Process Response*

The output data was scaled and normalised according to the size of the input step change. Given in Figure 5-1, Figure 5-2, Figure 5-3 and Figure 5-4 are all the normalised bubble velocity and bubble colour responses, including the average response, for the air addition and pulp level step tests to cell one. The time units that are given in the figures are twenty second intervals.

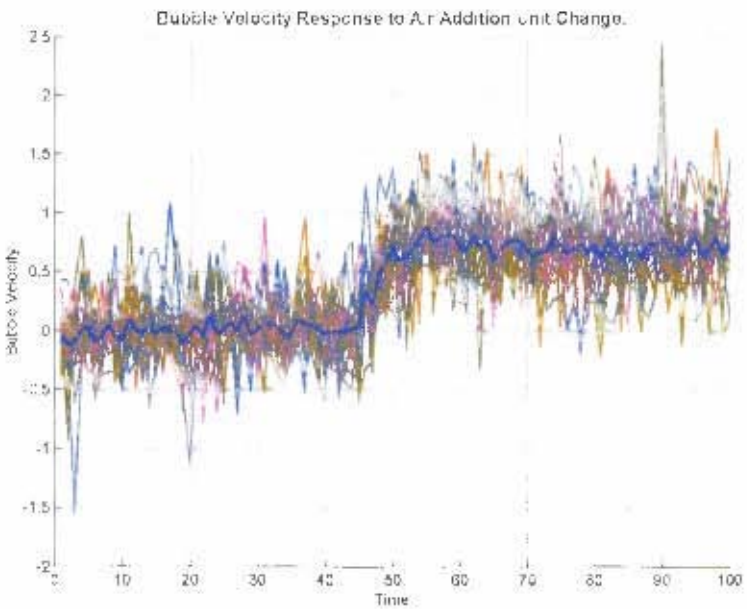


**Figure 5-1: Bubble velocity response for air addition step change to cell one.**

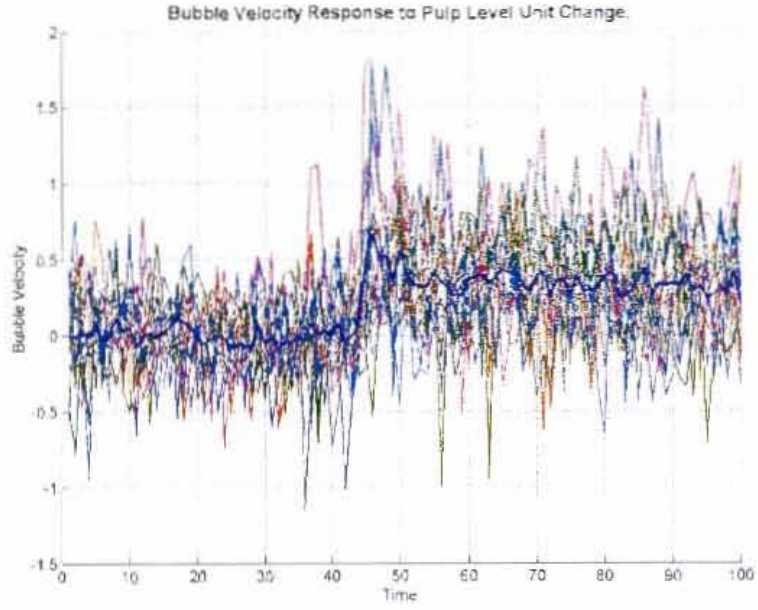


Figure 5-2: Bubble velocity response for pulp level step change to cell one.

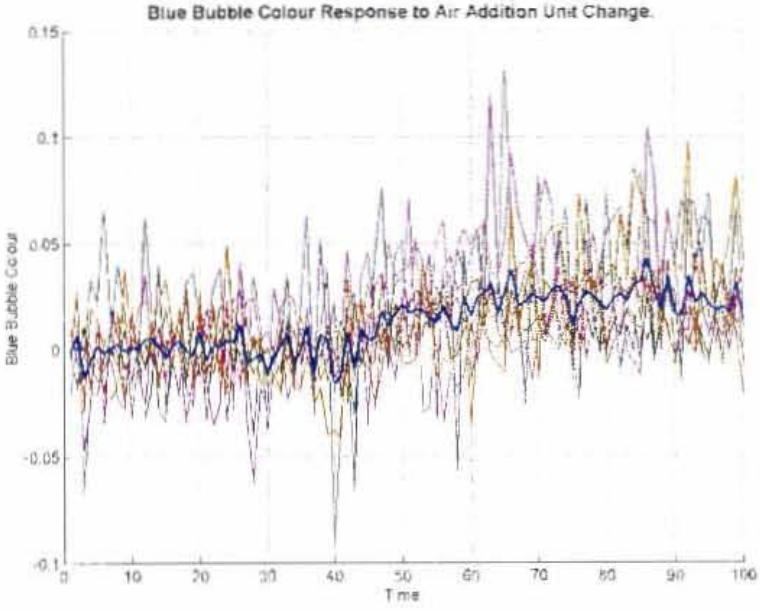


Figure 5-3: Bubble colour response for air addition step change to cell one.

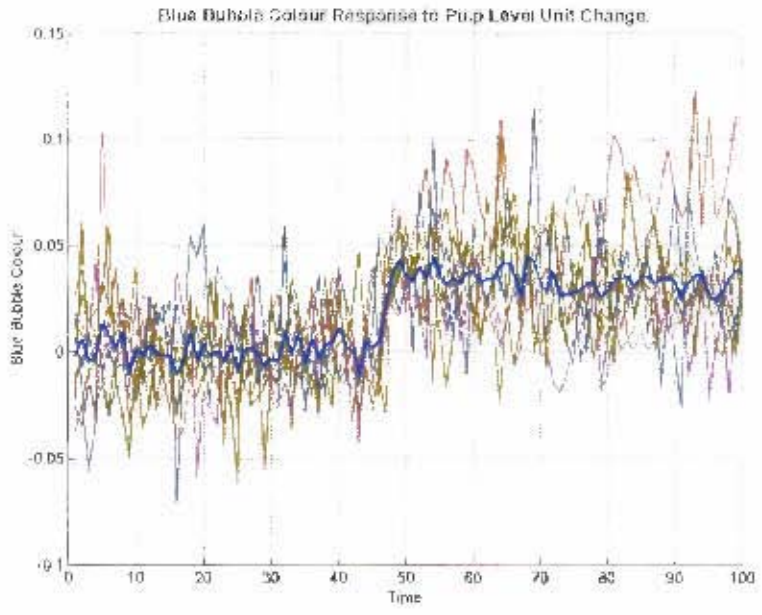


**Figure 5-4: Bubble colour response for pulp level step change to cell one.**

The rest of the output response plots are given in appendix A. For all given figures the setpoint change occurred at time point 45 with a sampling interval of 20 seconds between the points.

After completion of the step tests two problematic issues were realised. Firstly there was a problem with the camera on cell two so that the machine vision data were not reliable. Secondly ambient light had a big influence on the colour measurements from the camera so that only the data from step tests done during the night could be used (when the ambient light was more or less constant) for the dynamic modelling of the bubble colour response.

From the graphs above it can be seen that the data exhibits a lot of variance. This is reflected in Table 5-4 that contains some statistical information on the step tests data sets. For all the runs of each output variable, the average value before the step change occurred was removed and an average value of the standard deviation of these data sets were calculated as given in the table below. Ten data points (200 seconds) were skipped after the step change occurred and the average of the next 45 data points were averaged to get a second average steady state gain for each output variable of all the

runs. From the output response graphs ten data points would ensure that the dynamic response was excluded from the steady state average calculation. The 95% confidence intervals were calculated for the difference in the average value before and after the step change. This was done using a paired t-test [Napier-Munn 1996] and the results are given in Table 5-4 and Table 5-5. The confidence limits for all the output variables are relatively small compared to the difference of the average values, which indicates a distinct change with good confidence.

The air addition and pulp level data were logged every 20 seconds while the camera outputs were calculated and logged every three seconds. The minimum sampling interval could therefore only be 20 seconds. Three sampling points, on and before the 20 second interval was averaged and used as the camera output data. The true standard deviation of the raw data would therefore be higher than the values given in Table 5-4 and Table 5-5.

**Table 5-4:Statistical information of the step test data for air addition to cell one.**

| Output Variables | STD | Averages Before | After | Confidence (95%) limits |
|---|---|---|---|---|
| Bubble velocity | 0.2356 | 0 | 0.7186 | ±0.0261 |
| Bubble ave area | 0.2772 | 0 | 0.7761 | ±0.0294 |
| Bubble colour blue | 0.0183 | 0 | 0.0233 | ±0.0029 |
| Concentrate Ni content | 0.0309 | 0 | 0.1382 | ±0.0156 |
| Concentrate Cu content | 0.0306 | 0 | 0.3742 | ±0.0300 |
| Concentrate Pt content | 0.1302 | 0 | 0.1551 | ±0.0426 |
| Concentrate % solids | 0.0147 | 0 | 0.1215 | ±0.0061 |
| Concentrate flow rate | 0.1938 | 0 | 1.233 | ±0.0995 |

**Table 5-5: Statistical information of the step test data for pulp level to cell one.**

| Output Variables | Ave STD Before | Averages Before | After | Confidence (95%) limits |
|---|---|---|---|---|
| Bubble velocity | 0.2534 | 0 | 0.3321 | ±0.0233 |
| Bubble ave area | 0.2073 | 0 | 0.3565 | ±0.0259 |
| Bubble colour blue | 0.0200 | 0 | 0.0329 | ±0.0023 |
| Concentrate Ni content | 0.0296 | 0 | 0.1775 | ±0.0121 |
| Concentrate Cu content | 0.0372 | 0 | 0.2260 | ±0.0407 |
| Concentrate Pt content | 0.1317 | 0 | 0.2284 | ±0.0470 |
| Concentrate % solids | 0.0183 | 0 | 0.0819 | ±0.0087 |
| Concentrate flow rate | 0.1624 | 0 | 0.5998 | ±0.0698 |

## 5.3) Dynamic Process Modelling

A dynamic process model is required to simulate the process for the purposes of developing, testing and tuning a controller. Two ways of obtaining this dynamic process model is by theoretical modelling of the fundamentals of the process or by empirical model estimation from process data with the latter being referred to as system identification [Ogunnaike, 1994; Ljung, 2001]. When the fundamentals of the process are not well understood or are too complicated, the next modelling option is system identification. This "black-box" empirical method constructs a dynamic process model from experimental input-output data of the process. No fundamental knowledge of the process is required to obtain a dynamic process model with this method.

Prior to the system identification as described below, an analysis was done on whether the assumption can be made that the process is relatively linear over the operating range. It was found that the process nonlinearities were not significant as discussed in more detail in section (5.4).

### 5.3.1) Dynamic Process Model Types

Most chemical and metallurgical processes exhibit dynamics that can be related to one of the following continues model types [Ogunnaike, 1994]:

$$G_p = \frac{K_p e^{-\alpha s}}{\tau s + 1} \tag{5.1}$$

$$G_p = \frac{K_p e^{-\alpha s}}{(\tau_1 s + 1)(\tau_2 s + 1)} \tag{5.2}$$

$$G_p = \frac{K_p (\xi s + 1) e^{-\alpha s}}{(\tau_1 s + 1)(\tau_2 s + 1)} \tag{5.3}$$

$$G_p = \frac{K_p(\xi s + 1)e^{-\alpha s}}{(\tau s + 1)} \qquad (5.4)$$

Equation 5.1 presents a first-order-plus-time-delay model that is most commonly used. For the given model types, $K_p$ is the steady state gain and $e^{-\alpha s}$ represents the time delay of the system. $\tau$ are the time constants of the system and $\xi$ sets the zero position.

The transfer function model types given above are for continuous model identification and the parameters are regressed to produce values that most closely predict the sampled data that was obtained during the step tests. Discrete model identification involves the direct regression on consecutive sampling points.

The simplest and most commonly used linear discrete system identification model is the ARX (Autoregressive with external input model estimator) [Ljung, 2001]. The general form of the model is given by:

$$y(t) + a_1 \cdot y(t-1) + \ldots + a_{na} \cdot y(t-na) = b_1 \cdot u(t-nk) + \ldots + b_{nb} \cdot u(t-nk-nb+1) \qquad (5.5)$$

where $a_n$ and $b_n$ are model parameters,

$y$ represents the output and

$u$ represents the input variable.

$k$ is the dead time in sampling period intervals.

This model is in the discrete-time format for which many z-domain design methods exist. However the design of multivariable control systems, especially in the local mineral extraction industry, is well established in continuous s-domain and will be used in this work. Therefore any model obtained in the discrete time domain would have to be converted to an equivalent s-domain continuous model for further evaluation and controller design. Thus it was decided to do the system identification regression on continuous model types for the following reasons:

- The experimental data seems to fit the predefined model structures of Eq. (5.1) and (5.3).

- No conversion back to s-domain is required.

### 5.3.2) Regression Technique and Results

The regression analysis was done utilising a differential evolution optimisation routine [Storn]. Differential Evolution (DE) is a population-based, stochastic minimisation algorithm that has good convergence properties and is simple to understand and implement. Initially a predefined population of randomly selected values in the parameter space is selected. DE then generates new parameter vectors by adding the weighted difference between two population vectors to a third vector. If the resulting vector yields a lower objective function than a predetermined population member, the newly generated vector replaces the vector, with which it was compared, in the next generation; otherwise, the old vector is retained [Storn].

The experimental data is regressed to the time domain functions of Eq. (5.1) and (5.3), which are given by:

$$y(t) = AK_p(1 - e^{-(t-\alpha)/\tau}) \tag{5.6}$$

$$y(t) = AK_p\left[1 - \left(\frac{\tau_1 - \xi}{\tau_1 - \tau_2}\right)e^{-(t-\alpha)/\tau_1} - \left(\frac{\tau_2 - \xi}{\tau_2 - \tau_1}\right)e^{-(t-\alpha)/\tau_2}\right] \tag{5.7}$$

where $t \geq \alpha$; $y(t) = 0$ for $t < \alpha$,

$A$ is the step size of the input variable and the rest of the parameters are the same as described for Eq. (5.1) to (5.4). Each step test data set was divided by the step size so that A for all the step responses was equal to one.

The objective function that was minimised is the sum of the squared error between the predicted and measured outputs. Differential evolution optimisation m-files can be downloaded from http://www.icsi.berkeley.edu/~storn/code.html. The system identification toolbox was also used to obtain some of the discrete plant models and when converted to the continuous domain was similar to that from the DE regression.

Given below in Figure 5-5 and Figure 5-8 are the average bubble velocities and blue bubble colour responses for an air addition and pulp level step changes respectively. The bubble velocity response to an air addition step change is first order (given in Eq. 5.1) while the response for a pulp level step change is a second order response with one zero (given in Eq. 5.3). Both responses from the blue bubble colour were first order as well. The lead-lag model, given in Eq. (5.4), could also be accurately fitted to the bubble velocity response for a pulp level step change. This might have been a better modelling approach to follow due to the less complicated model that would be obtained. Under the circumstances though a more complicated model fit that included an extra pole, given in Eq. (5.3), was chosen as this simplified the design of the decouplers as explained later in the controller design section.

None of the models given in Figure 5-5 and Figure 5-6 has a time delay. This is however not the case for the real system. The precise delay of the system could not be detected in the data because it is less than the sampling interval of 20 seconds. The 20 second sampling interval are close to the maximum sampling interval that can be used as this is just below 10% of the settling time (i.e. the dynamic response before steady state). For future system identification exercises more accurate models that could include dead time might be obtained with a smaller sampling interval. It can however be said that the time delay of the system is less than 10% of the settling time so that this is not a crucial shortcoming in the dynamic models.

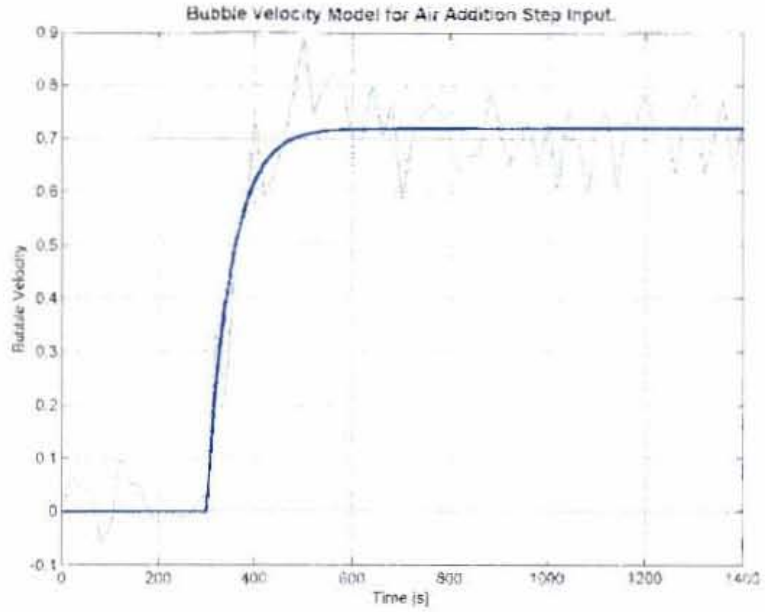


**Figure 5-5: Average bubble velocity response to a unit air addition step change.**

From Figure 5-5 it can be seen that there is a slight over shoot of the dynamic response roughly at time step t = 500. The model type given in Eq. (5.3) would therefore have been a more appropriate model type to use. For simplicity and the fact that the response almost resembles a first order response, it was decided to fit the first order model instead. Further the slight over shoot is only about 5% above of the steady state gain when the model type of Eq. (5.3) is used. It is therefore assumed that the absence of higher order dynamics in return for a less complicated model would still be sufficient to describe the system without sacrificing crucial information about the dynamic model.

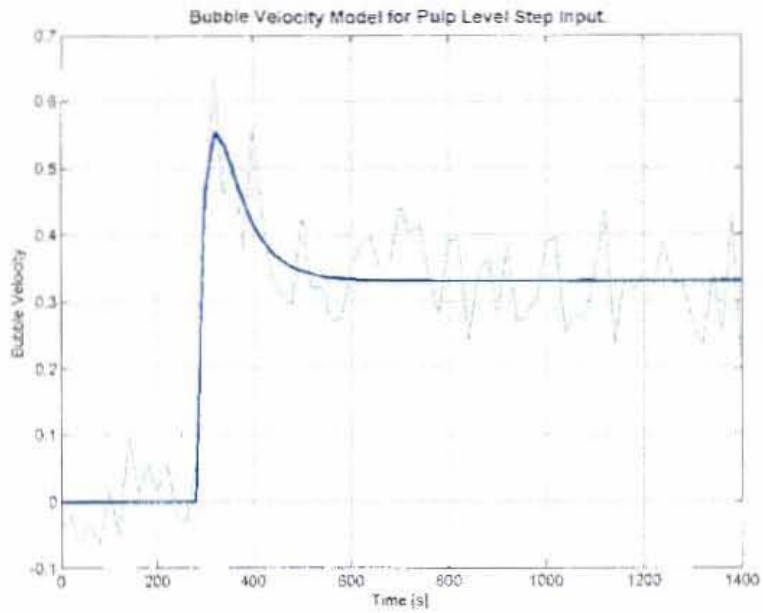


Figure 5-6: Average bubble velocity response to a unit pulp level step change.

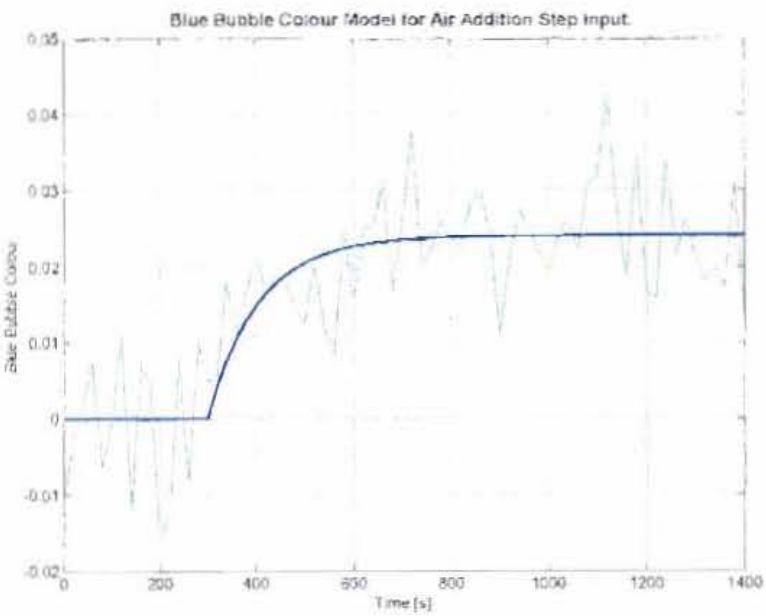


Figure 5-7: Average bubble colour response to a unit air addition step change.


**Figure 5-8: Average bubble colour response to a unit pulp level step change.**

Only first-order and second-order-with-one-zero model types were used in the system identification. For completeness all the responses, including the above, are given in Appendix A while all the parameters of the dynamic models that was determined are given in Table 5-6. The model parameters correspond to equations (5.1) and (5.3). The data sets that are plotted above were scaled between zero and some maximum value of the output variables. The steady state gain of the models given in Table 5-6 is of the raw signals (inputs and outputs), while the time constants are given in seconds. Air addition and pulp level input ranges for the models given in Table 5-6 are 0 to 5 [$m^3$/min] and 0 to 50 [%] respectively (total range (100%) of the pulp level is approximately 480 mm).

**Table 5-6: System identification model parameters.**

| OP Variables / Camera Outputs | Air Addition Input | | | | | Pulp Level Input | | | | |
|---|---|---|---|---|---|---|---|---|---|---|
| | $K_p$ | $\tau_1$ | $\tau_2$ | $\xi$ | $\alpha$ | $K_p$ | $\tau_1$ | $\tau_2$ | $\xi$ | $\alpha$ |
| Bubble velocity | 0.07922 | 50.13 | 0 | 0 | 0 | 0.003641 | 55.5 | 19.9 | 137.5 | 0 |
| Average bubble area | 9.597 | 121.9 | 0 | 0 | 0 | 0.4303 | 59.73 | 0 | 0 | 40 |
| Blue bubble colour | 0.4344 | 105.5 | 0 | 0 | 0 | 0.06064 | 29.31 | 0 | 0 | 0 |
| | | | | | | | | | | |
| %Ni in concentrate | 0.06558 | 352.6 | 0 | 0 | 600 | 0.007714 | 184.4 | 0 | 0 | 480 |
| %Cu in concentrate | 0.1099 | 453.5 | 325.1 | 864.2 | 360 | 0.005761 | 450.1 | 431.7 | 1365 | 240 |
| Pt grade in concentrate | 2.46 | 328.9 | 0 | 0 | 480 | 0.3555 | 327.6 | 0 | 0 | 240 |
| %Solids of concentrate | 0.8073 | 269.6 | 0 | 0 | 360 | 0.05434 | 283.8 | 0 | 0 | 360 |
| Concentrate flow rate | 0.1110 | 358.7 | 301.9 | 907.6 | 240 | 0.00576 | 195.5 | 206 | 632.5 | 240 |

Given in Eq. (5.8) and (5.9) are the matrix representation of the dynamic models in Table 5-6 above. To give the reader a feel for the relative gains from the two outputs, the gain values were normalised so that both inputs range between 0 and 1.

$$\begin{bmatrix} \text{Bubble velocity} \\ \text{Bubble area} \\ \text{Blue bubble colour} \end{bmatrix} = \begin{bmatrix} \dfrac{0.3961}{(50.13s+1)} & \dfrac{0.1821(137.5s+1)}{(55.5s+1)(19.9s+1)} \\ \dfrac{47.99}{(121.9s+1)} & \dfrac{21.52e^{-40s}}{(59.73s+1)} \\ \dfrac{2.172}{(105.5s+1)} & \dfrac{3.032}{(29.31s+1)} \end{bmatrix} \begin{bmatrix} \text{Air addition SP} \\ \text{Pulp level SP} \end{bmatrix} \tag{5.8}$$

$$\begin{bmatrix} \%\,\text{Ni} \\ \%\,\text{Cu} \\ \%\,\text{Pt} \\ \%\,\text{Solids} \\ \text{Flow rate} \end{bmatrix} = \begin{bmatrix} \dfrac{0.3279e^{-600s}}{(352.6s+1)} & \dfrac{0.3857e^{-480s}}{(184.4s+1)} \\ \dfrac{0.5494(864s+1)e^{-360s}}{(325s+1)(453.5s+1)} & \dfrac{0.288(1365s+1)e^{-240s}}{(450.1s+1)(431.7s+1)} \\ \dfrac{12.3e^{-480s}}{(328.9s+1)} & \dfrac{17.78e^{-240s}}{(327.6s+1)} \\ \dfrac{4.037e^{-360s}}{(269.6s+1)} & \dfrac{2.717e^{-360s}}{(283.8s+1)} \\ \dfrac{0.555(908s+1)e^{-240s}}{(358.7s+1)(302s+1)} & \dfrac{0.288(632.5s+1)e^{-240s}}{(195.5s+1)(206s+1)} \end{bmatrix} \begin{bmatrix} \text{Air addition SP} \\ \text{Pulp level SP} \end{bmatrix} \tag{5.9}$$

The dead times of the Courier OSA outputs is much longer than that of the camera outputs. The reason for this is that the concentrate from the cells first goes into a sump from where it is pumped to the X-ray analyser. There are five other concentrate streams that are also measured by the OSA. During the step test procedures these streams were bypassed so that only the combined rougher concentrate was measured every 2 minutes. Under normal operating conditions of the plant this measurement would only take place every 12 minutes.

The OSA response data also mostly exhibited higher order dynamics. It is suspected that the higher order dynamics is not a direct result of the actual concentrate grade from a single cell but rather the product of the fact that the concentrates from rougher cell one and two that is mixed and then analysed. It is known that the concentrate grade from a cell is highly depended on the feed grade to the cell [Lynch et al, 1981]. The concentrate grade would therefore increase, if all other conditions stay the constant and the head grade increases. For the system under investigation there are two flotation cells in series. When the concentrate grade from the first cell is increased by lowering the air addition (or pulp level), for instance, less material is floated and consequently the head grade to cell two increases. This would then result in an increase of the concentrate grade from cell two as well and this would only happen after a while as the residence time in cell one is about 4 minutes.

## *5.4) Check on System Linearity*

One of the assumptions that were required for the system identification exercise above was that the process could be modelled as a linear system. From the literature [Lynch et al, 1981; McKee, 1992; Hodouin et al, 2001] it is emphasised that under certain conditions and for certain input variables that the process exhibits extreme non-linear behaviour. Some aspects of the process are however classified as being linear with specific reference to the recovery of a flotation vessel that is described by most researchers as a first order process [Lynch et al, 1981] under constant conditions. No direct reference has however been made to the non-linearity of froth image analysis outputs and of non-linear control theory that has been applied in this field on a real plant.

focuses on identifying possible non-linearities of the process using the data that was obtained from the step tests.

The approach followed was to determine whether there would be an increase or decrease of some function in the gain of the camera outputs for different initial conditions. The four initial process conditions that were selected were the mill feed tonnage, % Cu, % solids and flow rate of the concentrate before the step change occurred.

Figure 5-9 and Figure 5-10 show scatter plots of the camera output gains (bubble velocity, average bubble area and blue bubble colour) for step changes to the air addition and pulp level respectively vs. initial process conditions. Ore throughput, in dry tonnages is indicated with different markers on the graphs.

All the gains are randomly scattered and there is no pattern in the plots that could be detected so that the respective gains obtained from each step test would be dependant on any initial conditions of the process, except for one variable. From Figure 5-10 the average bubble area gain seems to linearly increase with increasing % solids of the concentrate for pulp level changes. Fundamentally this might relate to different bubble stabilities and structures that are obtained with different solids loading on the bubbles. It is however not in the scope of this project to investigate this further. In general it is concluded that the system is sufficiently linear so that linear control theory could be applied to the process.

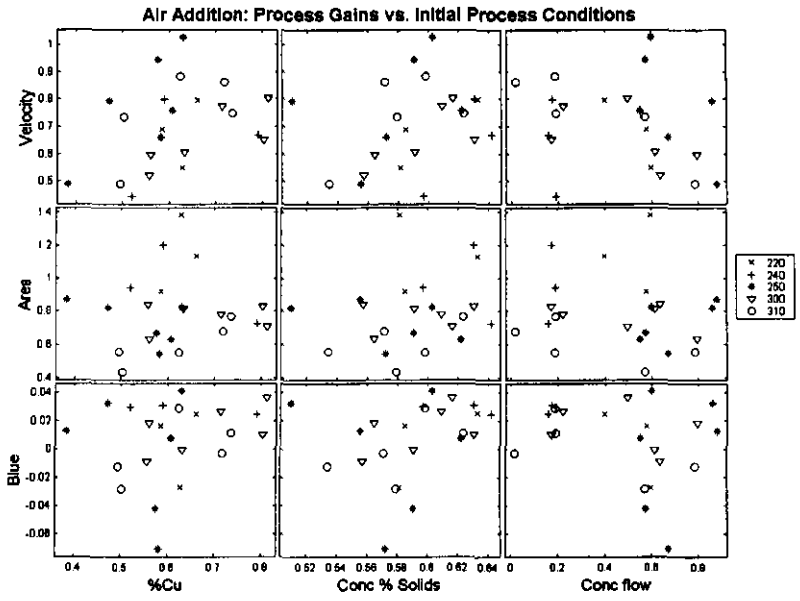


**Figure 5-9: Camera output gains for air addition step changes at different initial process conditions.**

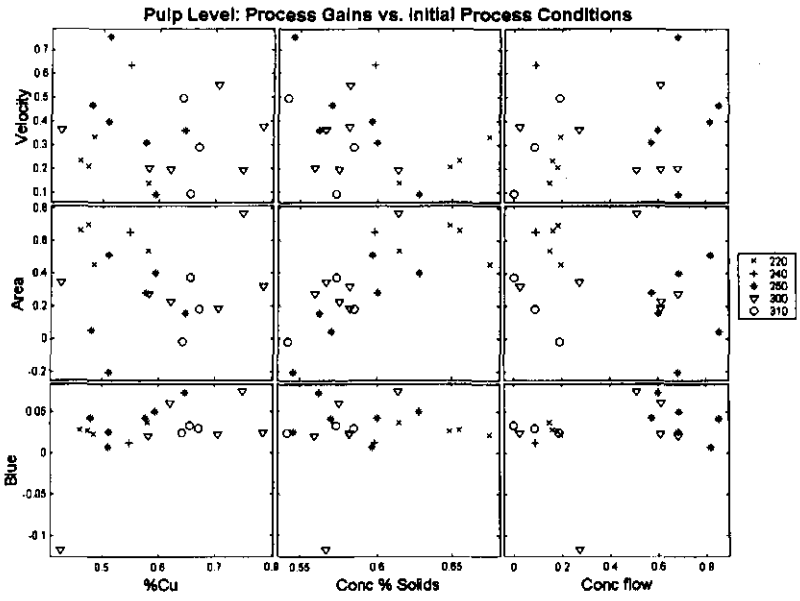


**Figure 5-10: Camera output gains for air addition step changes at different initial process conditions.**

# 6. Controller Design

An appropriate controller needs to be designed for the flotation cell described above. There are only two available inputs and eight output measurements. Output measurements are from two instruments namely froth image analysis and online stream analysis. Froth image analysis is a relatively new measurement technique with only a few online control applications around the world, while OSA online control has been extensively investigated.

The nature of the two measurements is fundamentally different. Considering a whole flotation section, froth image analysis can easily be applied to every cell while the same does not apply to OSA measurements, which require a feed stream from a sump-pump configuration. Most often the concentrates from a few cells are mixed together in a sump and then pumped to the same location. An OSA measurement would only then be available from this mixed stream. Low pass variance in froth image analysis outputs can be seen to describe the stability of a single flotation cell unit in the process, while OSA measurements generally give an indication of the overall metallurgical performance of the circuit.

The current approach of the BRPM concentrator towards flotation automation is to use froth image analysis to stabilise individual flotation cells while OSA measurements would be used to determine optimum setpoints, based on the overall circuit requirements. Since this project only focuses on one cell and not a flotation circuit, it has been decided to focus on and design a stabilisation controller using the machine vision outputs. This controller design could then be rolled out to other single flotation cell units while another project would determine how optimum setpoints for the circuit would be determined from the OSA measurements.

The design of a stabilisation controller for the machine vision outputs is now considered. First the outputs for the controller are selected and then paired with the selected inputs. Different controllers are then designed and compared with each other in terms of effectiveness of the decoupling, setpoint tracking, noise attenuation and input utilisation.

Controllers that were designed include:

- PI controllers with different decoupling structures.
- LQG servo and regulatory controllers.
- Internal model controller.

The objectives of testing different controller structures are to quantify the trade off between simplicity and accuracy for different controller structures and designs, compare classical controller design techniques and to identify whether there are any benefits in having a controller structure with a plant model.

## *6.1) Output Selection for Froth Image Analysis Measurements*

The system under investigation is currently over-defined with three output variables (bubble velocity, average bubble area and blue bubble colour) and two input variables (air addition and pulp level) and it needs to be reduced to a 2x2 multivariable system. Given the gain matrices from the system identification for various possible combinations of the camera outputs to the process inputs, each input had to be paired with an output. One of the outputs would therefore become redundant and consequently be rejected as an independently controllable output. The current system gain matrix (for normalised inputs) is given by:

$$\begin{bmatrix} y1 \\ y2 \\ y3 \end{bmatrix} = \begin{bmatrix} \mathbf{0.3961} & \mathbf{0.1821} \\ \mathbf{47.99} & \mathbf{21.52} \\ \mathbf{2.172} & \mathbf{3.032} \end{bmatrix} \begin{bmatrix} u1 \\ u2 \end{bmatrix} \qquad (6.1)$$

where: $y1$ → Bubble velocity
$y2$ → Average bubble area
$y3$ → Blue bubble colour

and $u1$ → Air addition
$u2$ → Pulp level

The possible output to input combinations that would reduce the over defined system to a defined system are:

$$\begin{bmatrix} y1 \\ y2 \end{bmatrix} = \begin{bmatrix} \mathbf{0.3961} & \mathbf{0.1821} \\ \mathbf{47.99} & \mathbf{21.52} \end{bmatrix} \begin{bmatrix} u1 \\ u2 \end{bmatrix} \tag{6.2}$$

$$\begin{bmatrix} y1 \\ y3 \end{bmatrix} = \begin{bmatrix} \mathbf{0.3961} & \mathbf{0.1821} \\ \mathbf{2.172} & \mathbf{3.032} \end{bmatrix} \begin{bmatrix} u1 \\ u2 \end{bmatrix} \tag{6.3}$$

$$\begin{bmatrix} y2 \\ y3 \end{bmatrix} = \begin{bmatrix} \mathbf{47.99} & \mathbf{21.52} \\ \mathbf{2.172} & \mathbf{3.032} \end{bmatrix} \begin{bmatrix} u1 \\ u2 \end{bmatrix} \tag{6.4}$$

One of the combinations given in equations (6.2) to (6.4) needs to be selected as the system that would be controlled. A simple but very effective way to get a good indication of which process variable to pair for small 2×2 or 3×3 system, is to plot the steady state process outputs for all the combinations of minimum and maximum $u_i$ values. Represented in matrix form for a 2×2 defined system, this equates to:

$$\mathbf{Y = G_0 U} \tag{6.5}$$

Where: $\mathbf{G_0}$ is the steady state gain matrix of the system and

$\mathbf{U} = \begin{bmatrix} 0 & 1 & 0 & 1 \\ 0 & 0 & 1 & 1 \end{bmatrix}$ that contains all possible input extremes.

**Y** is the 2×4 product matrix and the two vectors, $\mathbf{Y_{(1,1\text{-}4)}}$ and $\mathbf{Y_{(2,1\text{-}4)}}$, are plotted against each other. The result is a plot of the achievable operating regime of the system in steady state, assuming a linear system. Figure 6-1 shows the plot of the system given by Eq.(6.3) above.

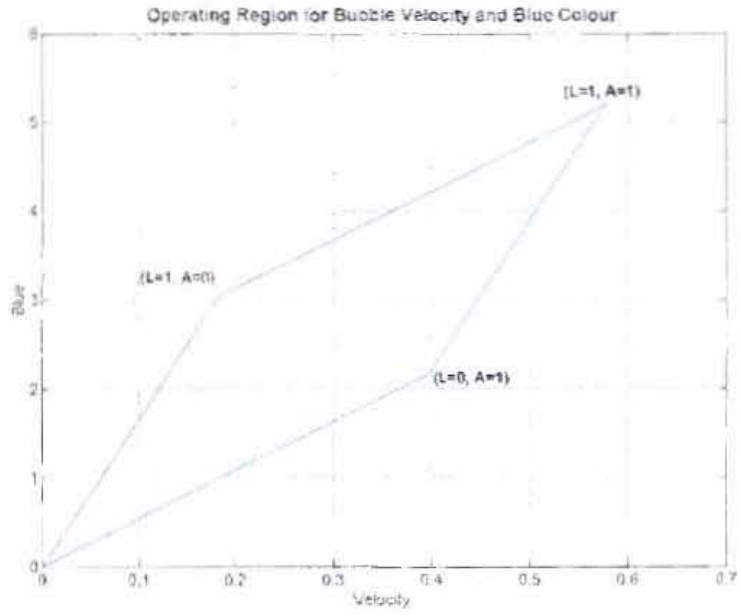


**Figure 6-1: Steady state operating regime for the velocity-blue output combination.**

From Figure 6-1 it can be seen that there is a reasonable operating region where the *blue bubble colour* and *bubble velocity* can be controlled independently by manipulating the air addition and pulp level. Symbols A and L indicates air addition and pulp level. It can also readily be seen from the plot that the air addition has a bigger effect on the bubble velocity than the pulp level. The opposite is true for bubble colour where it is affected more by pulp level then by air addition.

Figure 6-2 below shows the plot for the bubble-velocity and average-bubble-area output combination. From the figure it is clear that these two output variables are not independent. The effect on these two output variables caused by the air addition and pulp level has the same direction while the magnitude caused by the air addition is more. By closer inspection of the steady state gain matrix given in Eq.(6.2) it is easy to see that $u_1$ and $u_2$ are basically the same vector except for their magnitude. This matrix is therefore almost singular with a condition number of 327. Bubble velocity and bubble area can therefore not be controlled independently and this combination of outputs is therefore rejected.

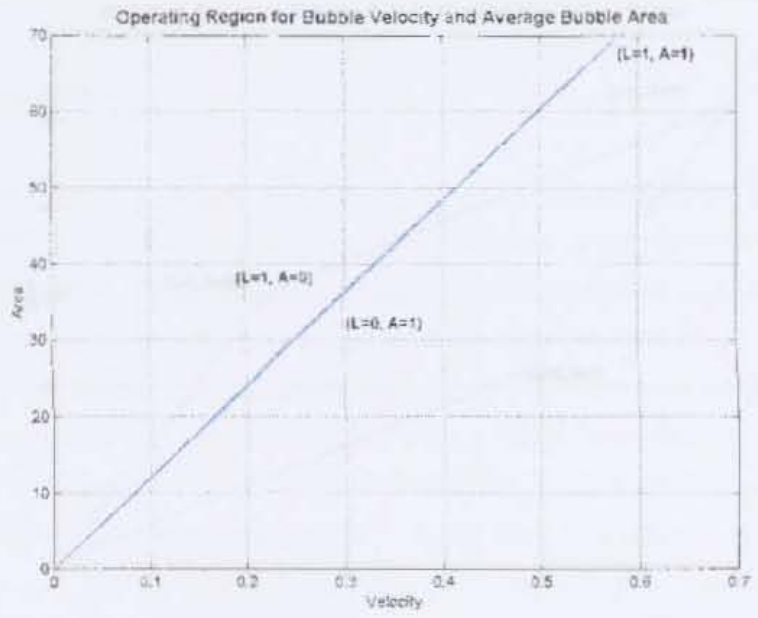


**Figure 6-2: Steady state operating regime for the velocity-area output combination.**

The remaining output combination is that of the blue bubble colour and the average bubble area given by Eq.(6.4) above. Figure 6-3 shows the plot for this system. The characterising parameters for this output combination are almost identical to that of the bubble velocity and blue bubble colour system due to the similar responses between bubble velocity and bubble area.

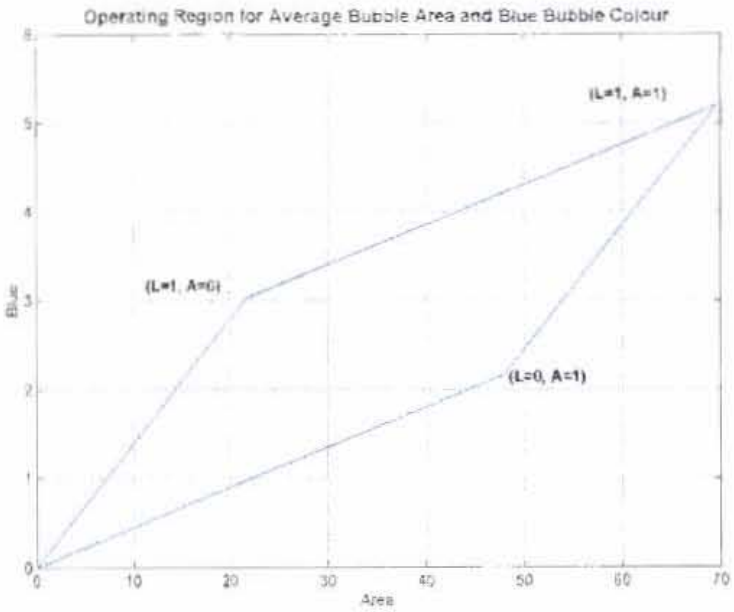


**Figure 6-3: Steady state operating regime for the blue-area output combination.**

With not much separating the $y_1$-$y_3$ and $y_2$-$y_3$ output combinations in terms of their steady state characteristics, the best combination would now be selected based on which of the two output variables, bubble velocity or average bubble area, is most closely related to the metallurgical performance of the process.

One drawback of froth image analysis is that the important metallurgical output variables of the flotation cell are not directly measured and inferential models needs to be employed that would relate the camera output variables to metallurgical performance. A lot of research has been done [Hargrave et al, 1997; Sweet, 2000; Moolman et al, 1996] towards this, but none of the models and correlations is generic enough to apply directly to any flotation process. This is simply attributed to the uniqueness and wide diversity of flotation processes around the world [Lynch et al, 1981].

Given below is a discussion on the three outputs from which two must be selected.

***Bubble velocity***

This output variable is probably the most useful camera output (of the three outputs considered) and is the easiest to correlate to some of the metallurgical outputs of the process [Ventura, 2000; Moolman, 1996]. Traditional manual control on flotation plants involved the operator adjusting the air addition and pulp level to get a certain mass pull (% of the cell concentrate mass flow rate to cell feed mass flow rate), which according to his judgement, is the desirable mass pull for optimal performance. The main feature of the froth appearance that an operator takes into account when making this decision is the bubble velocity over the cell lip. It is logical that the bubble velocity is proportional to the mass pull. Bubble velocity is also the only camera output variable that would indicate when there is no mass pull (bubble velocity zero) or when the mass pull is to high and the cell is "*slimming*" (bubble velocity bigger than a critical value that is predetermined, which usually occurs when too much reagent with frothing characteristics are dosed or when the pulp level is very high.). From the system identification the velocity measurement also gave good and consistent responses.

***Average bubble area***

Judging the performance of a flotation cell based on the bubble size is more difficult. From the system identification the bubble size responded well to changes in air addition and pulp level but it is generally expected that the bubble size is mostly influenced by addition of reagents [Sweet, 2000; Moolman, 1996] especially frother and depressant dosages.

Poor operating conditions of a flotation cell can be identified if the bubble size is very small. This indicates abnormal operation with poor selectivity of the flotation kinetics, high mass pull and low grades, which is usually a result of over dosage of a frother (or some collectors). Any automated control system should take careful consideration of this so that the input causing abnormality is adjusted and not a secondary input that also has an effect on bubble size.

Based on the literature it can be concluded that the bubble size is an important flotation performance parameter, but that correct and accurate manipulation of the bubble size requires more than only air addition and pulp level changes.

***Blue bubble colour***

Bubble colour has been used in zinc and copper flotation to predict the concentrate grade [Hargrave, 1997]. Darker froth usually means higher percent solids in the froth, which indicates to a high amount of hydrophobic particles and consequently a higher concentrate grade. The responses obtained in the system identification are suspected to be the result of changes in the grey scale, rather then only the blue colour, as all three RGB colours responded similarly. Of the three output measurements, the bubble colour gain was also the least consistent, comparing the gains of the individual step tests. The bubble colour signal also had the biggest variance compared to the other output signals.

Currently the biggest problem associated with the colour measurement is the fact that it is highly influenced by an external disturbance, ambient light. Besides the ambient light that varies, the light source of the camera can also degrade or change when the light bulb is replaced, which makes the absolute value of colour not very valuable and appropriate setpoint selection for colour very difficult. However, this measurement can be improved by installing a hood over the camera and to compensate for changes to the light source by having an additional reference light source [Hyotyniemi, 2000].

From the discussions given above the three output variables are then prioritised as being "*most meaningful*" as process measurements for platinum froths according to:

1. Bubble velocity.
2. Bubble area.
3. Bubble colour

Bubble velocity and blue bubble colour were therefore selected as the two camera output variables that would be controlled to setpoints. The transfer function matrix model for this system is given in Eq.(6.6). The gains are scaled for a unit change in the inputs.

$$\begin{bmatrix} y1 \\ y2 \end{bmatrix} = \begin{bmatrix} \dfrac{0.07831}{(50.13s+1)} & \dfrac{0.003654(137.5s+1)}{(55.5s+1)(19.9s+1)} \\ \dfrac{0.4344}{(105.5s+1)} & \dfrac{0.06064}{(29.31s+1)} \end{bmatrix} \begin{bmatrix} u1 \\ u2 \end{bmatrix} \tag{6.6}$$

where: $y1$ → Bubble velocity

$y2$ → Blue bubble colour

and $u1$ → Air addition

$u2$ → Pulp level

This output combination is also confirmed with the calculation of the condition number, with a value of 3.8, in section (6.3.2) that evaluates the degree of ill-conditioning of the system.

## *6.2) Loop Pairing with RGA*

The objective of loop pairing for a MIMO system is to minimise the loop interaction between the single loop controllers of the system by pairing certain inputs with certain outputs. For a 2×2 system the two possible pairings are simply $u_1$-$y_1$ and $u_2$-$y_2$ or $u_1$-$y_2$ and $u_2$-$y_1$.

From inspection of the steady state gain matrix, $\mathbf{G_0}$, given in Eq. (6.7) it can already be seen what the most likely input/output pairing would be $u_1$-$y_1$ and $u_2$-$y_2$ and this is also evident in the *plot* of the system, Figure 6-2. $u_1$ has a bigger influence on $y_1$ compared to $u_2$ and $u_2$ has a bigger effect on $y_2$ compared to $u_1$ at steady state. So the best pairing for the least interaction would be $u_1$-$y_1$ and $u_2$-$y_2$.

$$\mathbf{G_0} = \begin{bmatrix} 0.3961 & 0.1821 \\ 2.172 & 3.032 \end{bmatrix} \tag{6.7}$$

The above intuitive approach works well for small systems though the relative gain array (RGA) is a more systematic approach to do loop paring for bigger systems [Ogunnaike

1994]. For this 2×2 system, shown in Figure 6-4, consider the case where loop 1 is open and loop 2 is closed.

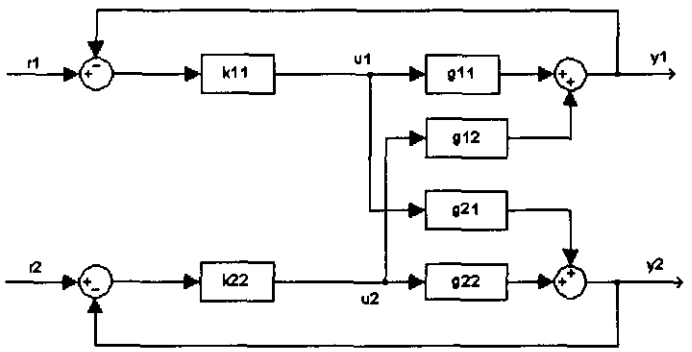


**Figure 6-4: 2×2 system with $u_1$-$y_1$, $u_2$-$y_2$ pairing.**

When $u_1$ is stepped, $y_1$ would have experienced a net change at steady state. This net change is the sum of the direct effect of $u_1$ on $y_1$ ($G_{0,11}\cdot\Delta u_1$) and the effect of the closed loop response of loop 2 ($G_{0,12}\cdot\Delta u_2$), which would have reacted to maintain $y_2$ at its setpoint. The relative gain,$\lambda_{11}$, is then defined by:

$$\lambda_{11} = \frac{G_{0,11}\Delta u_1}{G_{0,11}\Delta u_1 + K_{12}\Delta u_2} \tag{6.8}$$

It can further be showed that $\Delta u_i$ can be substituted by block diagram algebra with $G_{0,ij}$ so that $\lambda_{11}$ is given by:

$$\lambda_{11} = G_{0,11}\left(1 - \frac{G_{0,12}G_{0,21}}{G_{0,11}G_{0,22}}\right) \tag{6.9}$$

Similarly the relative gain, $\lambda_{12}$, with loop 1 closed and loop 2 open can be showed to be $1-\lambda_{11}$. Redefining $\lambda=\lambda_{11}$, the RGA is for the $u_1$-$y_1$ and $u_2$-$y_2$ pairing is then defined as:

$$\Lambda = \begin{bmatrix} \lambda & 1-\lambda \\ 1-\lambda & \lambda \end{bmatrix} \tag{6.10}$$

The RGA for the bubble velocity and blue bubble colour is:

$$\Lambda = \begin{bmatrix} 1.49 & -0.49 \\ -0.49 & 1.49 \end{bmatrix} \tag{6.11}$$

For $\lambda_{11}$ ($u_1$-$y_1$, $u_2$-$y_2$ pairing) the relative gain is 1.49, so that loop 2 form Figure 6-4, opposes the change by $u_1$ and the net contribution to the change in $y_1$ is less than 1. This indicates good pairing except for big values of $\lambda_{11}$. For $\lambda_{12}$ ($u_1$-$y_2$, $u_2$-$y_1$ pairing) = -0.49 so that the closed loop not only opposes the effect of $u_1$ on $y_2$ but that it is also more dominant. This is therefore not a good pairing combination. It is then concluded that the best pairing, is the $u_1$-$y_1$ / $u_2$-$y_2$ combination.

## *6.3) Controllability Analysis*

The controllability of the output selection for the system above are evaluated by looking at the:

- Poles and zeros of the system.
- Singularity of the system.

### 6.3.1) Poles and Zeros

The poles and zeros for the dynamic model given in Eq. (6.6) were calculated using the Matlab *pole* and *zero* functions:

Transmission zeros: -0.0724
-0.0168
-0.0112

Poles: -0.0199
-0.0095
-0.0503
-0.0180
-0.0341

There are no right half plane zeros nor right half plane poles. Thus the system is stable. The one dominant pole (-0.0095) is from the $y_1$-$u_2$ transfer function and dictates that the system would reach steady after approximately 420 seconds. There does not seem to be any obvious pole-zero cancellations.

### 6.3.2) System Singularity

A reliable indication of the controllability or ill-conditioning of a matrix, $\mathbf{G_0}$, is its singular values which is defined as the square root of the eigenvalues of the matrix $\mathbf{G_0}^T\mathbf{G_0}$. The ratio of the largest to the smallest singular value of a matrix is called the condition number. A large condition number is an indication of an ill-conditioned process and would therefore be difficult to control. The significance of the condition number is that it can identify ill-conditioning where the RGA, matrix determinant and eigenvalues might fail to do so [Ogunnaike and Ray, 1994].

Determining the condition number involves scaling the inputs and outputs between 0 and 1 by multiply the steady state gain matrix by the maximum change in u and dividing it by the maximum expected error between the setpoint and output measurements. The maximum expected errors, as observed form process data, for all the process models are given in Table 6-1.

**Table 6-1: Maximum expected errors.**

| No | Output | Max error |
|---|---|---|
| 1 | Bubble velocity | 0.3 |
| 2 | Bubble area | 35 |
| 3 | Blue bubble colour | 2.3 |
| 4 | Nickel conc. | 0.29 |
| 5 | Copper conc. | 0.4 |
| 6 | Platinum conc. | 12.8 |
| 7 | % Solids | 3 |
| 8 | Concentrate flow rate | 0.42 |

As a matter of interest the condition numbers for all the output combinations, as 2x2 systems, were calculated based on the matrix model and are given in Table 6-2.

**Table 6-2: Condition numbers for all output combinations.**

| | Velocity | Area | Blue | Ni | Cu | Pt | Solids | Flow |
|---|---|---|---|---|---|---|---|---|
| Velocity | | 327.5 | 3.8 | 4.6 | 38.5 | 3.7 | 12.4 | 41.8 |
| Area | 327.5 | | 3.7 | 4.5 | 34.4 | 3.6 | 11.9 | 37.1 |
| Blue | 3.8 | 3.7 | | 24.2 | 4.2 | 122.8 | 5.5 | 4.2 |
| Ni | 4.6 | 4.5 | 24.2 | | 5.2 | 20.1 | 7.3 | 5.2 |
| Cu | 38.5 | 34.4 | 4.2 | 5.2 | | 4.1 | 18.2 | 481.8 |
| Pt | 3.7 | 3.6 | 122.8 | 20.1 | 4.1 | | 5.3 | 4.1 |
| Solids | 12.4 | 11.9 | 5.5 | 7.3 | 18.2 | 5.3 | | 17.6 |
| Flow | 41.8 | 37.1 | 4.2 | 5.2 | 481.8 | 4.1 | 17.6 | |

The condition number for the bubble velocity and bubble colour output combination is 3.8, which indicates that steady state targets would be achievable within certain ranges. The singularity of the bubble velocity and average bubble area is confirmed numerically with a condition number of 327.

Of the three elemental OSA measurements the Ni and Cu measurements are the most reliable due to the higher concentration of these elements in the system compared to Pt. It is interesting to note that the Ni and Cu output combination has a low condition number (5.2) so that it might be possible to independently control the concentration of these two elements by manipulating only the air addition and pulp level.

## *6.4) Classical PI Controller Design and Decoupling of the Process*

From the system identification and the sections above the inputs and outputs have been reduced to a linear system given by:

$$y_1 = g_{11} \cdot u_1 + g_{12} \cdot u_2$$
$$y_2 = g_{21} \cdot u_1 + g_{22} \cdot u_2$$

Next different decoupling structures with PI controllers are designed and optimum PI parameters are determined for the process model given in Eq. (6.6). The different decoupling designs are then evaluated and compared.

### 6.4.1) Simplified Decoupling

The objective of decoupling is to eliminate the interaction between variables of a multivariable system. The first decoupling design being considered is "simplified decoupling" as described by Ogunnaike and Ray [1994], which is most commonly used in process control.

Given the system in Figure 6-5 it can be proved by substitution that for $m_1$ to eliminate the effect on $y_2$ when it changes, the decoupling term from $m_1$ to $m_2$ should be:

$$k_{21} = -\frac{g_{21}}{g_{22}} \qquad (6.12)$$

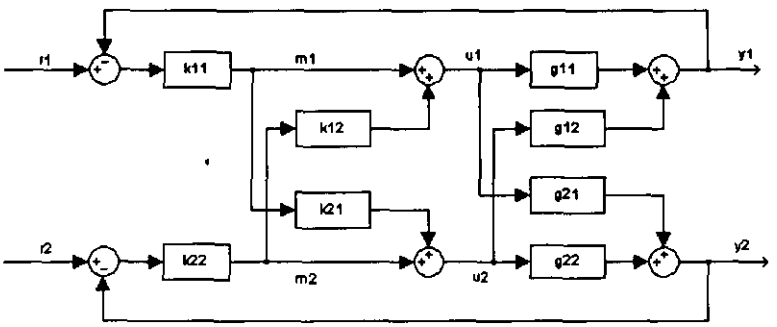


**Figure 6-5: Simplified decoupling of a 2x2 system.**

Similarly for the decoupling term that would eliminate the effect of $m_2$ on $y_1$ is then:

$$k_{12} = -\frac{g_{12}}{g_{11}} \tag{6.13}$$

When the two decoupling terms are inserted in the 2x2 system there is no interaction between the two loops and the two loops can be tuned individually as two SISO systems [Ogunnaike, 1994].

As was mentioned earlier in section (5.3.2) $g_{12}$ was purposefully regressed with an additional pole so that the decoupling term could be realisable (the number of zeros are equal or less than the poles of the system). The decoupling terms for this system is then given by:

$$k_{12} = \frac{-0.29121\,(s+0.01995)\,(s+0.007273)}{(s+0.05025)\,(s+0.01802)} \tag{6.14}$$

$$k_{21} = \frac{-1.9902\,(s+0.03412)}{(s+0.009479)} \tag{6.15}$$

The system can now be viewed as two SISO systems with the following modified transfer functions that represent the process. The inputs to the two processes are $m_i$ (controller outputs as presented in Figure 6-5) and the outputs are still $y_i$.

$$G_{Loop1} = g_{11} + g_{12}k_{21} = g_{11} - \frac{g_{12}g_{21}}{g_{22}} \quad \text{and} \quad G_{Loop2} = g_{22} + g_{21}k_{12} = g_{22} - \frac{g_{12}g_{21}}{g_{11}} \tag{6.16}$$

The detailed transfer functions are then:

$$G_{pm1} = \frac{0.00065678(s+0.0724)(s+0.01678)(s+0.01119)}{(s+0.05025)(s+0.01995)(s+0.01802)(s+0.009479)}$$

$$G_{pm2} = \frac{0.00086985(s+0.0724)(s+0.01678)(s+0.01119)}{(s+0.05025)(s+0.03412)(s+0.01802)(s+0.009479)}$$

Further evaluation of the two decoupling terms indicates that $k_{12}$ might be problematic at high frequencies. Given in Figure 6-6 and Figure 6-7 are the Bode diagrams for $k_{12}$ and $k_{21}$ respectively. The Bode plot for $k_{12}$ shows a high gain at high frequencies and is similar to a lead circuit while the amplitude ratio of $k_{21}$ over the whole frequency range seems to approach that of a first order lag system.

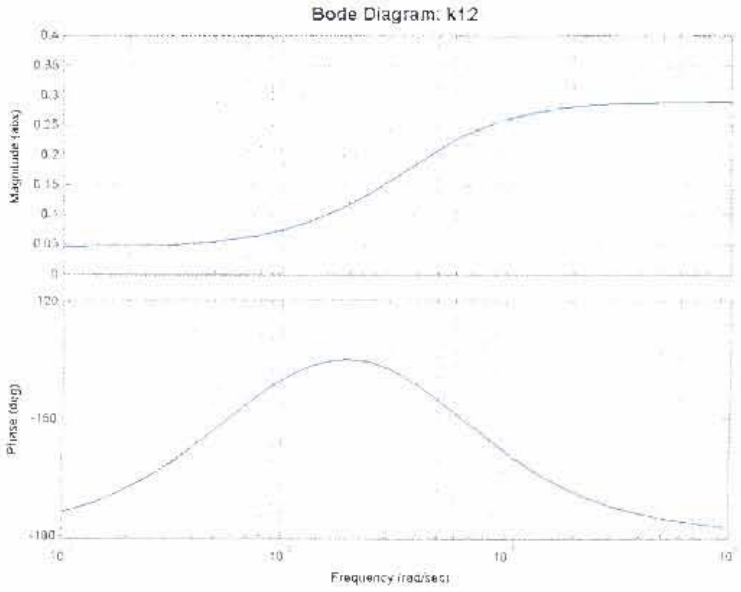


**Figure 6-6: Bode plot of $k_{12}$.**

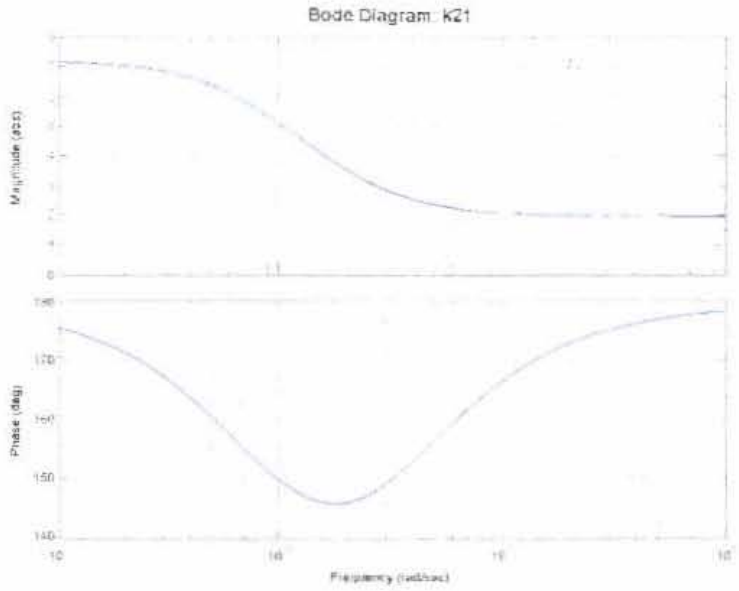


**Figure 6-7: Bode plot of $k_{21}$.**

The step responses of $k_{12}$ and $k_{21}$ clearly show the dynamics that was observed in the Bode diagrams. Figure 6-8 and Figure 6-9 shows the step responses of negative $k_{12}$ and $k_{21}$. From Figure 6-8 it can be seen that the $k_{12}$ decoupler will require $u_1$ to jump to almost five times more than its steady state value in order to fully decouple the two loops. When $u_2$ for instance change by say 50 % (range of $u_2$: 0-100%), it will require $u_1$ to jump to 14.5 $m^3$/min (50*0.29), which is more than the total range of $u_1$ (range of $u_1$: 0-10 $m^3$/min). It is therefore not possible for the process to provide enough air to fully decouple loop one from loop two and this decoupler therefore needs to be modified.

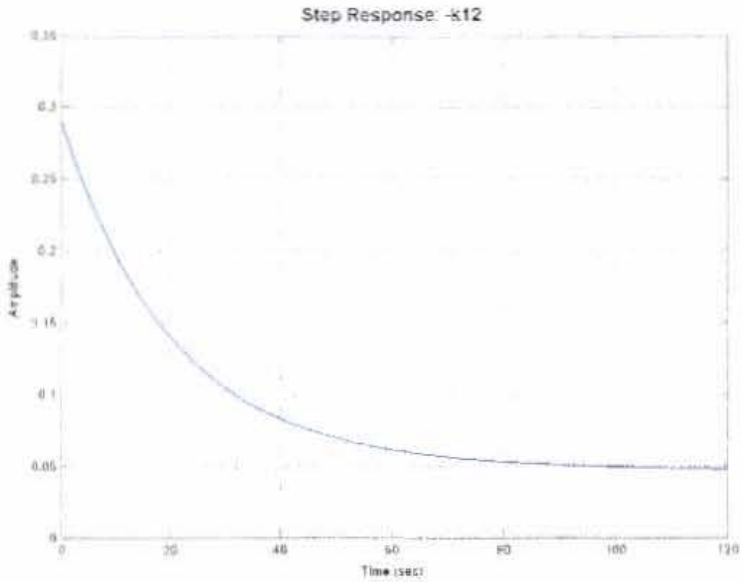


**Figure 6-8: Step response of $-k_{12}$.**

The step response for $k_{21}$, Figure 6-9 below, shows that $u_2$ would require $u_1$ to jump to 28% of its steady state value after which it exhibits a first order decay to its final value. The slow exponential decay from the decoupler would also benefit the stability of the pulp level regulatory control loop (MV=control valve, CV=pulp level) compared to the regulatory air addition setpoint tracking. Possible reasons for the difficulty of the regulatory level setpoint tracking is presented and discussed in appendix F.

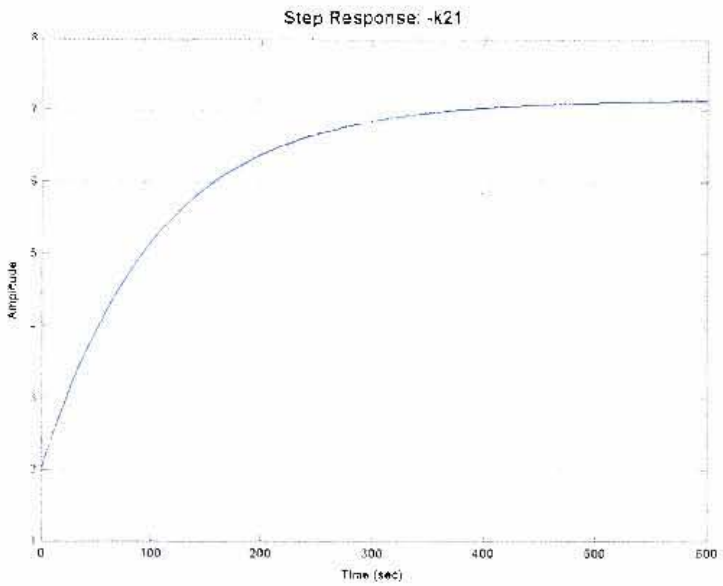


**Figure 6-9: Step response of $-k_{21}$.**

There are a few options to consider for modifying $k_{12}$ so that $u_1$ is not required to act so aggressively. Any modification however would result in loop one not being completely decoupled from loop two. The first option would be to just consider steady state decoupling where the $k_{12}$ term is replaced by only its steady state gain. Considering the requirements of $k_{12}$ for decoupling of the two loops (Figure 6-8), a certain amount of air more than that of the steady state gain value is required. It would therefore benefit the decoupling of the two loops to still allow more air to go into the system at higher frequency ranges. Evaluating the pole zero plot of $k_{12}$ in Figure 6-10 below reveals the problematic zero at -0.0073, closest to the imaginary axis that causes $u_1$ to jump the way it does. Moving this zero more the left on the pole-zero plane (decreasing its value) would result in a smaller jump in $u_1$.

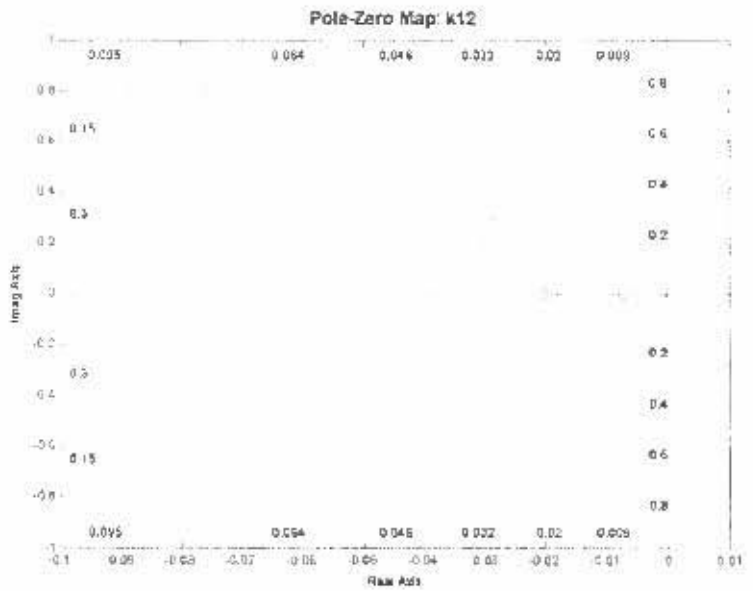


**Figure 6-10: Pole-Zero plot of $k_{12}$.**

Another option would be to filter the high frequency from $k_{12}$ with a first order filter, which would be equivalent to adding an additional pole to $k_{12}$.

Given in Figure 6-11 below are the step responses for $k_{12}$, $k_{12}$ with a first order filter and $k_{12}$ where the dominant zero has been modified to have a value of –0.021. Both the filter and modified-zero option requires $u_1$ to go to 100% more than the steady state gain of $k_{12}$. The modified zero jumps immediately to the maximum amplitude and then settles to the steady state gain while the filtered value gradually increases to reach its maximum amplitude. Judging each option on the basis of how much more air is put into the system before steady state is reached, the filtered value seems to be the better option as the area between the filtered curve and the steady state asymptote is substantially more compared to that of the modified zero curve. Based on this observation it was therefore decided to use a filter instead of modifying a zero in $k_{12}$. The filter given in Figure 6-11 adds an additional pole at -0.032 in $k_{12}$. This pole is non-dominant and restricts the decoupler to 100% overshoot as shown in the figure.

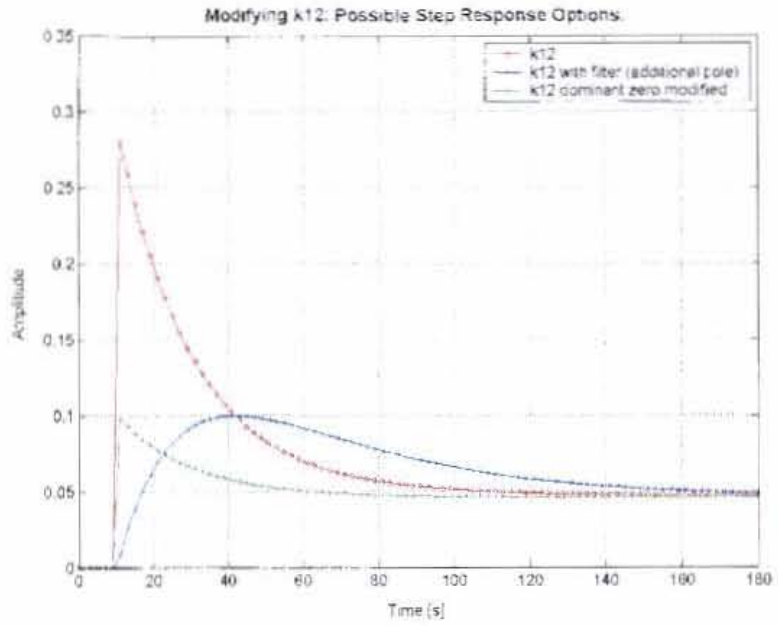


**Figure 6-11: Options for modifying $k_{12}$.**

The final design for the simplified decoupling is given in Figure 6-12 below where $g_f$ is a first order filter given by:

$$g_f = \frac{1}{\alpha s + 1} \tag{6.17}$$

$\alpha$ Is the first order time constant and has a value of 31.3 for this design.

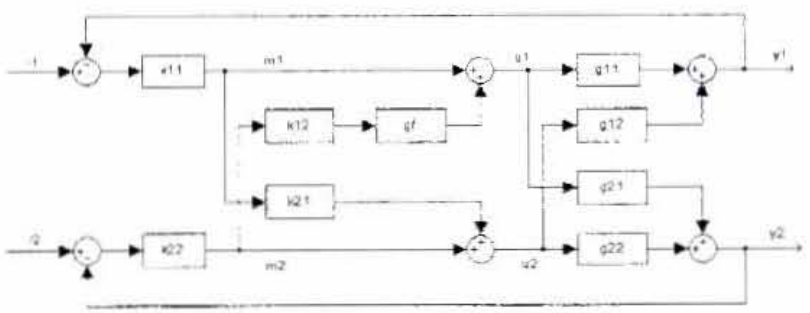


**Figure 6-12: Simplified decoupling, final design.**

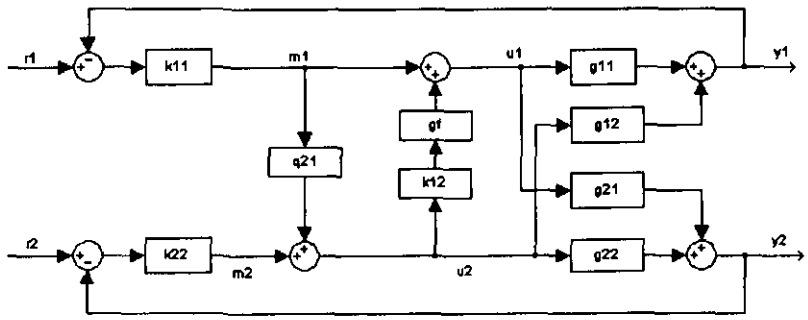


**Figure 6-13: Alternative decoupling design with q21.**

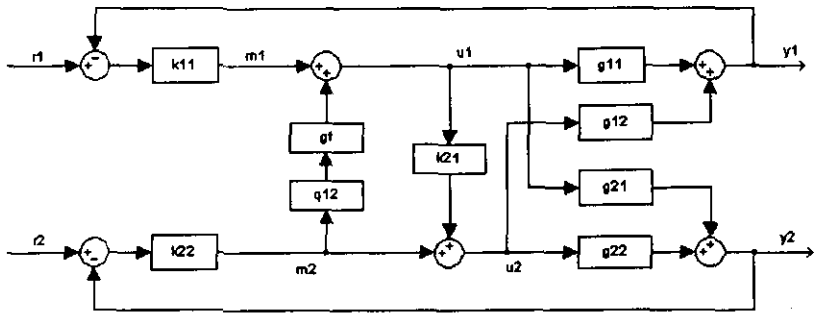


**Figure 6-14: Alternative decoupling design with q12.**

It can be shown by substitution that the q decoupling terms are given by:

$$q_{12} = \frac{-g_{12}}{g_{11} - g_{12}\dfrac{g_{21}}{g_{22}}} \tag{6.18}$$

$$q_{21} = \frac{-g_{21}}{g_{22} - g_{21}\dfrac{g_{12}}{g_{11}}} \tag{6.19}$$

The detailed transfer function are then:

$$q_{12} = \frac{-0.69263\ (s+0.01995)\ (s+0.009479)(s+0.007273)}{(s+0.0724)(s+0.01678)(s+0.01119)}$$

$$q_{21} = \frac{-4.7336(s+0.05025)(s+0.03412)(s+0.01802)}{(s+0.0724)(s+0.01678)(s+0.01119)}$$

### 6.4.3) Ideal and Inverted Decoupling

Another two alternative decoupling designs are given in Figure 6-15 and Figure 6-16 [Gagnon et al, 1998]. These two decoupling techniques are known as inverted decoupling (Figure 6-15) and ideal or general decoupling (Figure 6-16).

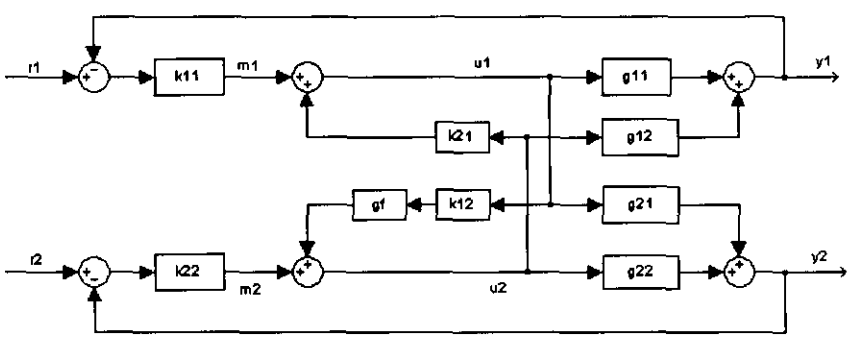


**Figure 6-15: Alternative inverted decoupling.**

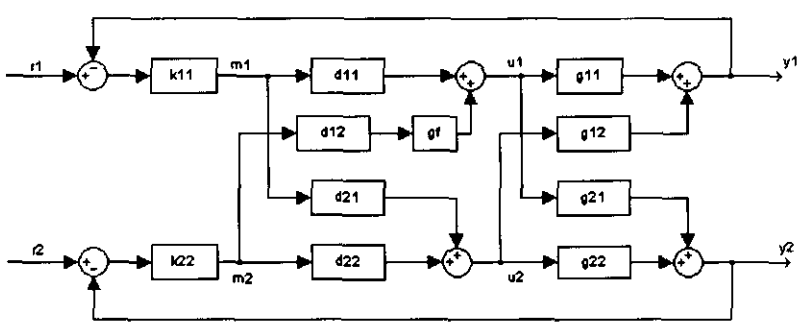


**Figure 6-16: Alternative ideal decoupling.**

As was the case with $k_{12}$, $d_{12}$ also needs to be filtered to prevent $u_1$ from hitting saturation limits.

It can be shown by substitution that the decoupling terms for ideal decoupling are given by:

$$d_{11} = d_{22} = \frac{g_{11}g_{22}}{g_{11}g_{22} - g_{12}g_{21}}$$
$$d_{12} = \frac{-g_{12}g_{22}}{g_{11}g_{22} - g_{12}g_{21}} \qquad (6.20)$$
$$d_{21} = \frac{-g_{21}g_{11}}{g_{11}g_{22} - g_{12}g_{21}}$$

The detail transfer functions are then:

$$d_{11} = \frac{2.3785(s+0.05025)(s+0.01802)(s+0.009479)}{(s+0.0724)(s+0.01678)(s+0.01119)}$$

$$d_{21} = \frac{-4.7336(s+0.05025)(s+0.03412)(s+0.01802)}{(s+0.0724)(s+0.01678)(s+0.01119)}$$

$$d_{12} = \frac{-0.69263(s+0.01995)(s+0.009479)(s+0.007273)}{(s+0.0724)(s+0.01678)(s+0.01119)}$$

$$d_{22} = \frac{2.3785(s+0.05025)(s+0.01802)(s+0.009479)}{(s+0.0724)(s+0.01678)(s+0.01119)}$$

Numerical values of all the decoupling transfer functions are summarised in Appendix B. Given all the decoupling designs above, the controller tuning was then done for the following PI controller structures.

1) PI controllers with no decouplers (Figure 6-4).
2) PI controllers with simplified decoupling (Figure 6-12).
3) PI controllers with only $k_{12}$ decoupling.
4) PI controllers with only $k_{21}$ decoupling.
5) PI controllers with $k_{12}$ and $q_{21}$ decoupling (Figure 6-13).

6) PI controllers with $k_{21}$ and $q_{12}$ decoupling (Figure 6-14).
7) PI controllers with inverted decoupling (Figure 6-15).
8) PI controllers with ideal decoupling (Figure 6-16).

### 6.4.4) PI Controller Tuning

One of the advantages of decoupling is the fact that, for a 2x2 system, the four process models are reduced to two more complex models that are completely decoupled and single loop controller design techniques could be applied to get optimum PI controller parameters. Ignoring the fact that $k_{12}$ requires a filter so that this term is physically achievable, just for now, the two single loop models and controllers were evaluated.

Setpoints are constant so a type I control law is required. This takes the form of a PID controller in industrial systems. The D term is often not used due to excess noise on the measurements so that a PI controller structure, the most commonly used in the mineral processing industry, is then the choice for the selected controller type, with the PI structure given by:

$$g_c = \frac{K_c(s + K_I)}{s} \tag{6.21}$$

Where $K_c$ is the controller gain and $K_I$ is the reciprocal of the controller time constant, $\tau_c$.

For simplified decoupling given in Figure 6-12, without $g_f$, the two decoupled process models are given by:

$$\begin{aligned} G_{pm1} &= g_{11} + g_{12}k_{21} \\ &= g_{11} - \frac{g_{12}g_{21}}{g_{22}} \\ &= \frac{0.00065678\,(s + 0.0724)\,(s + 0.01678)\,(s + 0.01119)}{(s + 0.05025)\,(s + 0.01995)\,(s + 0.01802)\,(s + 0.009479)} \end{aligned} \tag{6.22}$$

$$
\begin{aligned}
G_{pm2} &= g_{22} + g_{21}k_{12} \\
&= g_{22} - \frac{g_{12}g_{21}}{g_{11}} \\
&= \frac{0.00086985(s+0.0724)(s+0.01678)(s-0.01119)}{(s+0.05025)(s-0.03412)(s-0.01802)(s+0.009479)}
\end{aligned}
\tag{6.23}
$$

Where $G_{pm1}$ and $G_{pm2}$ are the process models for loop one ($u_1$-$y_1$, air addition and bubble velocity) and loop two ($u_2$-$y_2$, pulp level and blue bubble colour) respectively.

There is no RHP zeros or poles in the modified process transfer functions, which indicate minimal phase and stable plant models. Further evaluation of the Bode plots for $G_{pm1}$ and $G_{pm2}$ in Figure 6-17 and Figure 6-18 shows that both the process models, for the amplitude ratio and phase angle, exhibit first order dynamics. Selecting appropriate values for $K_c$ and $K_i$ for each loop is therefore not expected to be very difficult.

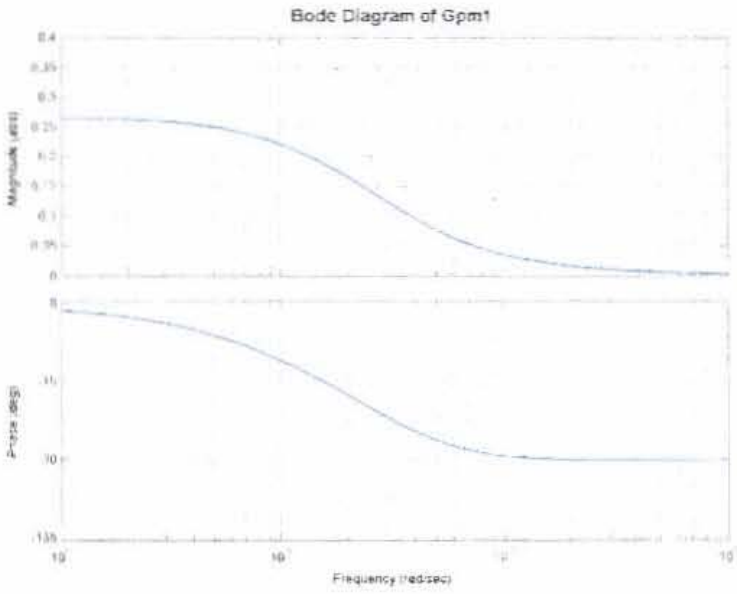


**Figure 6-17: Bode diagram for $G_{pm1}$.**

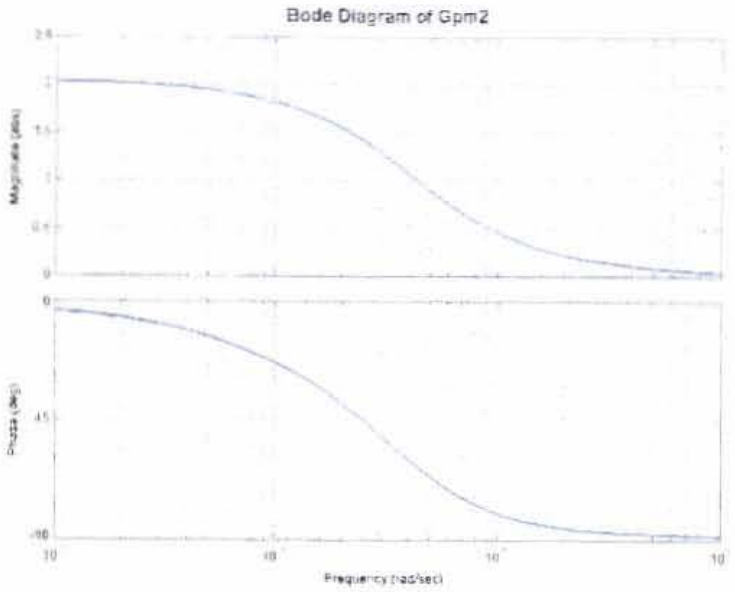


**Figure 6-18: Bode diagram for $G_{pm2}$.**

As was the case with the system identification, differential evolution was again used as the optimisation routine to find a minimum value of a constrained objective function based on $y_i$ with $K_{ci}$ and $K_{ii}$ as the independent inputs. The objective function was taken as the absolute integral between the output and its setpoint. The inputs were constrained by multiplying the same objective function with the integral between u and its constrained value when u exceeded this constrained value.

As a first attempt the initial constraints on the inputs were an order of magnitude bigger ($u_1$=50 $m^3$/min and $u_2$ = 500 %) than the constraints on the real plant. This was done to get a feel for the desired path of the inputs when the objective function is minimised. The setpoints of $y_1$ and $y_2$ (0.2085 pixels/s and 1.6148 RGB respectively) were selected such that specified final values of $u_1$ and $u_2$ (4 $m^3$/min and $u_2$ = 40 %) were obtained. Given in Figure 6-19 and Figure 6-20 are $y_1$-$u_1$ and $y_2$-$u_2$ closed loop responses where $K_{ci}$ and $K_{ii}$ have been optimised by minimising the absolute integral of the error (IAE) and the u values does not exceed their upper constraint.

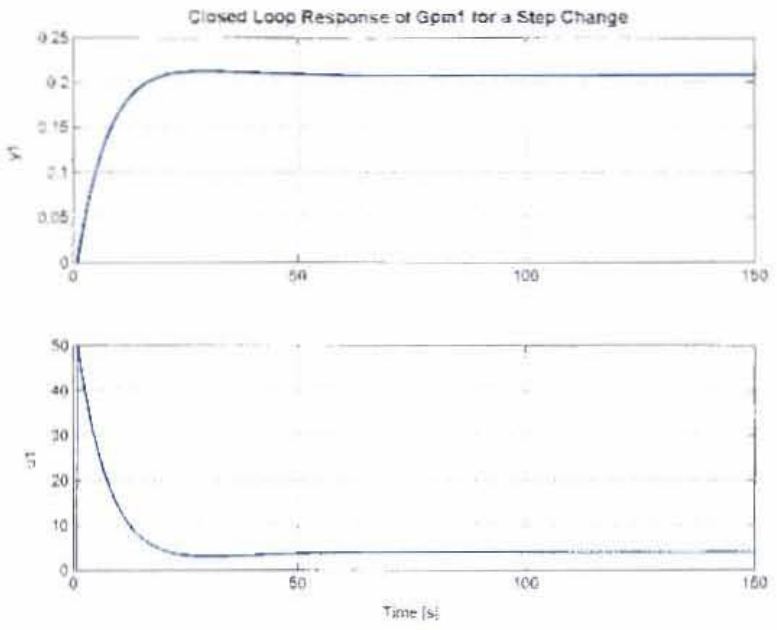


**Figure 6-19: Closed loop step response $G_{pm1}$, $u_1$ constraint to 50 $m^3$/min.**

Due to the first order nature of the $G_{pm1}$ and $G_{pm2}$ models it can be seen from Figure 6-19 and Figure 6-20 that the u values in both cases shoot up to their maximum allowed values in order to reduce the error between the setpoint and the output. It is therefore clear that the optimum controller gain would not be selected based on the performance of the output variables, but rather just on the u variables and their constraints.

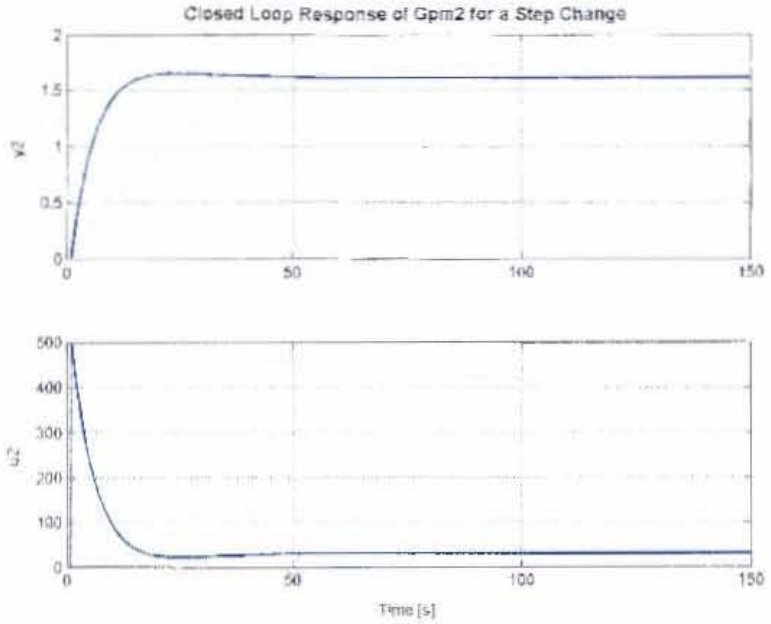


**Figure 6-20: Closed loop step response $G_{pm2}$, $u_2$ constraint to 500 %.**

It was decided to restrict the inputs to only overshoot the steady state u values by 25 %. Given in Figure 6-21 and Figure 6-22 are the optimally tuned (for the IAE case) closed loop responses where $u_1$ has been constrained to 5 $m^3$/min and $u_2$ to 50 %. The setpoints and steady state u values are the same as for the previously tuned two loops. From the given figures it is clear that there is a significant trade off between input constraints and output performance. For the two input constraint cases discussed, the output settling time is almost 400% more for the case where $u_1$ has been constrained to 5 $m^3$/min and $u_2$ to 50 %.

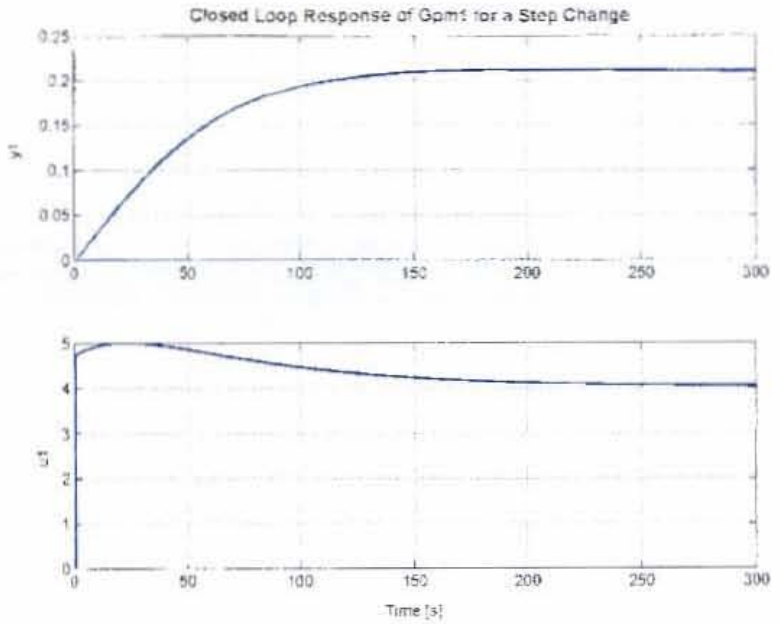


**Figure 6-21: Closed loop step response $G_{pm1}$, $u_1$ constraint to 5 $m^3$/min.**

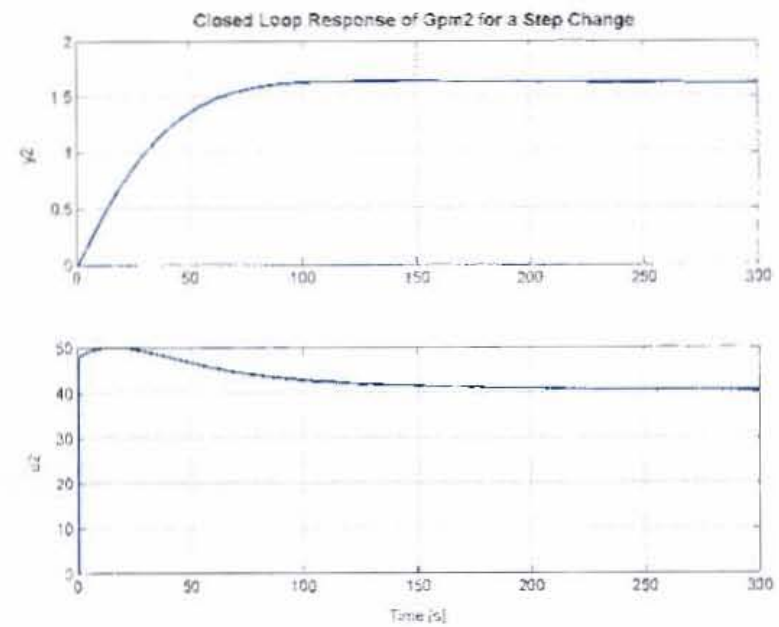


**Figure 6-22: Closed loop step response $G_{pm2}$, $u_2$ constraint to 50 %.**

Given in Table 6-3 are the optimum IAE PI controller parameters for the above given loops with their constraints. These controller settings are later on further evaluated in a regulatory control simulation with real process noise and disturbance data.

**Table 6-3: $K_c$ and $K_I$ values for $G_{pm1}$ and $G_{pm2}$.**

| Process Model | $K_c$ | $K_I$ | $u_1$ constriant | $u_2$ constraint |
|---|---|---|---|---|
| $G_{pm1}$ | 240 | 0.0161 | 50 | - |
| $G_{pm2}$ | 310 | 0.0253 | - | 500 |
| $G_{pm1}$ | 22.8 | 0.0209 | 5 | - |
| $G_{pm2}$ | 29.6 | 0.0329 | - | 50 |

The approach followed to determine a single objective function value from the two controlled variable outputs for the purpose of finding optimum PI controller settings for the different decoupling designs, given in section (6.4) above, was to normalise the error in both loops by dividing it with its corresponding setpoint. The normalised errors were then summed to give one value that would serve as the global objective function to tune both loops simultaneously. This tuning method (as apposed to the SISO tuning of $G_{pm1}$ and $G_{pm2}$ above) was necessary in all the decoupling cases as it was not possible to fully decouple any loop due to the filter that was added after the $k_{12}$ and $q_{12}$ decouplers as a result of their behaviour.

The controller tuning simulation was configured as given in Table 6-4 and was then run for 1000 seconds. The error for both outputs was computed over the whole range so that the error caused by interaction is also considered in the objective function.

**Table 6-4: Simulation step times and $u_i$ constraints.**

| Time | $y_1$ SP | $y_2$ SP | $u_1$ constraint | $U_2$ constraint |
|---|---|---|---|---|
| 1 | 0 to 0.2085 | 0 | -5 to 5 | -50 to 50 |
| 250 | 0.2085 to 0 | 0 | -5 to 5 | -50 to 50 |
| 500 | 0 | 0 to 1.615 | -5 to 5 | -50 to 50 |
| 750 | 0 | 1.615 to 0 | -5 to 5 | -50 to 50 |

Given in Figure 6-23 and Figure 6-24 are the tuning results for cases with no decoupling and with simplified decoupling. The rest of the graphical tuning results for the other decoupling structures are presented in appendix C, while a summary of all the results are given in Table 6-5.

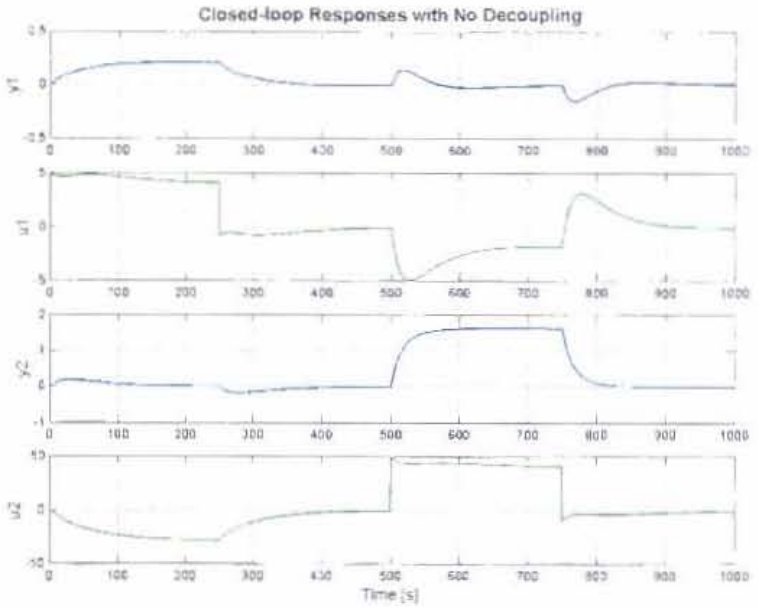


**Figure 6-23: Optimally tuned closed loop responses for the case with no decoupling.**

From Figure 6-23 it can be seen that the constraint of –5 $m^3$/min imposed on $u_1$ (just after 500 seconds), might have caused some restrictions on the closed loop response of loop two. This was the case for all given controller structures.

**Table 6-5: Tuning results of all the decoupling designs.**

| No | Structure | $K_{c1}$ | $K_{i1}$ | $K_{c2}$ | $K_{i2}$ | IAE 1 | IAE 2 |
|---|---|---|---|---|---|---|---|
| 0 | $G_{pm1}$ and $G_{pm2}$ | 22.8 | 0.0209 | 29.6 | 0.0329 | - | - |
| 1 | No decoupling | 23.9 | 0.0235 | 31.2 | 0.0504 | 34.0 | 99.6 |
| 2 | Simplified | 22.9 | 0.0209 | 10.4 | 0.0555 | 30.4 | 151 |
| 3 | Only $k_{12}$ | 24.0 | 0.0206 | 14.2 | 0.0439 | 23.7 | 251 |
| 4 | Only $k_{21}$ | 23.4 | 0.0190 | 31.4 | 0.0380 | 36.9 | 51.3 |
| 5 | $K_{12}$-$q_{21}$ | 17.2 | 0.0158 | 11.6 | 0.0504 | 31.7 | 176 |
| 6 | $K_{21}$-$q_{12}$ | 22.7 | 0.0217 | 6.8 | 0.0509 | 26.6 | 159 |
| 7 | Inverted | 17.1 | 0.0161 | 10.4 | 0.0357 | 31.3 | 147 |
| 8 | Ideal | 9.95 | 0.0331 | 5.44 | 0.0664 | 30.9 | 152 |

The restriction $u_1$ imposed on loop two is better quantified by evaluating the simplified decoupling structure (Figure 6-24), which represents $G_{pm1}$ and $G_{pm2}$, except for an additional filter. Comparing the controller parameters (no 0 and 2) in Table 6-5 reveals

that the controller gain for loop two has been reduced from 29.6 to 10.4 due to the constraint on $u_1$, while the parameters for loop one stayed the same as it was obtained for $G_{pm1}$. The constraint imposed on $u_2$ is also never reached due to $u_1$ requiring a slower reaction from $u_2$ so that it can recover from the gain of the $k_{12}$ decoupler. This shows that the individual loop tuning of $G_{pm1}$ and $G_{pm2}$ might be more difficult as this problem is not evident from the two single loop designs.

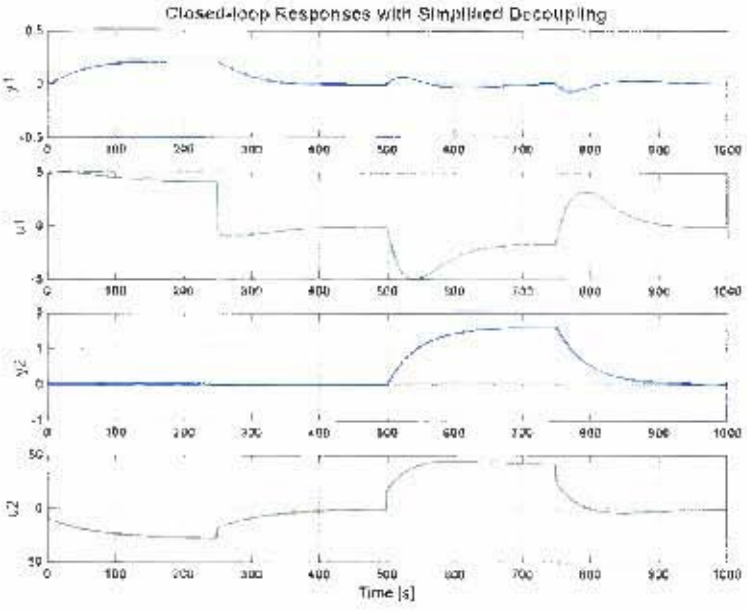


**Figure 6-24: Optimally tuned closed loop responses for the case with simplified decoupling.**

The degree of decoupling that was sacrificed by the additional filter, $g_f$, after $k_{12}$, can also be seen in the in Figure 6-24 at 500 and 750 seconds. The interaction of loop two on loop one is about half (comparing maximum peaks of $y_1$) compared to no decoupling. This indicates that there is some advantage to be gained from the decoupling, but the process interactions are not so significant that one loop struggles to recover, without decoupling, from an oscillation as a result of a setpoint change in the second loop. Keeping in mind that the better performance obtained with decoupling is based on simulation results with a constant process model and that the accuracy of the decoupling terms are highly dependant on an accurate and consistent process model, it could be considered not to make use of decoupling at all.

## 6.5) Linear Quadratic Gaussian Controller Design

Linear quadratic gaussian (LQG) control is a well-known state-space technique that achieves a required performance or robustness specification on the inputs or outputs of a system [Matlab, Control Systems Toolbox User's Guide, 2001]. Internal stability is also guaranteed [LaPlante, 1999; Maciejowski, 1989]. Closed loop performance ($y_i$) and control effort ($u_i$) are traded off, taking into account process disturbances and measurement noise [Braae, Maciejowski, 1989].

The plant model can be represented in state space form by:

$$\frac{dx}{dt} = Ax + Bu + \Gamma w$$
$$y = Cx + Du + v \qquad (6.24)$$

Where: $x$ → plant states
$u$ → plant inputs
$y$ → plant outputs
and $w, v$ are zero-mean gaussian noise of the plant.

The conversion of the dynamic models in the s-domain to state space was done by a Matlab function and the constants for the state space model parameters is given by:

$$A = \begin{bmatrix} -0.01995 & 0 & 0 & 0 & 0 \\ 0 & -0.009479 & 0 & 0 & 0 \\ 0 & 0 & -0.06827 & -0.02897 & 0 \\ 0 & 0 & 0.03125 & 0 & 0 \\ 0 & 0 & 0 & 0 & -0.03412 \end{bmatrix}$$

$$B = \begin{bmatrix} 0.03125 & 0 \\ 0.0625 & 0 \\ 0 & 0.03125 \\ 0 & 0 \\ 0 & 0.03125 \end{bmatrix}$$

$$C = \begin{bmatrix} 0.05 & 0 & 0.01456 & 0.003388 & 0 \\ 0 & 0.06588 & 0 & 0 & 0.06621 \end{bmatrix}$$

$$D = \begin{bmatrix} 0 & 0 \\ 0 & 0 \end{bmatrix}$$

The LQG control problem is then to devise a feedback-control law, which minimises the cost function given by [Maciejowski, 1989]:

$$J = \lim_{T \to \infty} E\left\{ \int_0^T (z^T Q z + u^T R u) dt \right\} \qquad (6.25)$$
$$z = Mx$$

Where: $Q$ is a weighting matrix for the states
$R$ is a weighting matrix for the outputs
and $z$ is some linear combination of the states.

Q and R are user-determined matrices that determine the trade off between output performance and control effort.

In order to solve Eq.(6.25) the inputs, u, are then defined as a linear function of the states, x, given by:

$$u = -K_c x \qquad (6.26)$$

$K_c$ is the optimal state-feedback gain given by:

$$K_c = R^{-1} B^T P_c \qquad (6.27)$$

Where $P_c$ satisfies the algebraic Riccatti equation given by:

$$A^T P_c + P_c A + P_c B R^{-1} B^T P_c + M^T Q M = 0 \qquad (6.28)$$

The states of the plant are required to implement the state-feedback control law, $K_c$. Many of these state variables are not measured on a real process and so a Kalman filter is used to estimate the states. The noise covariance data of the system states is used to determine the Kalman gain, also through an algebraic Riccati equation. A Kalman filter minimises the asymptotic covariance of the state estimation error given by:

$$E\left\{(x-\hat{x})^T(x-\hat{x})\right\} \tag{6.29}$$

The LQG controller is then a combination of the optimal feedback gain, the Kalman filter and an integrator as shown in the diagram of Figure 6-25. The integrator ensures asymptotic setpoint tracking for constant setpoint values. If omitted the LQG controller can only be used for disturbance rejection.

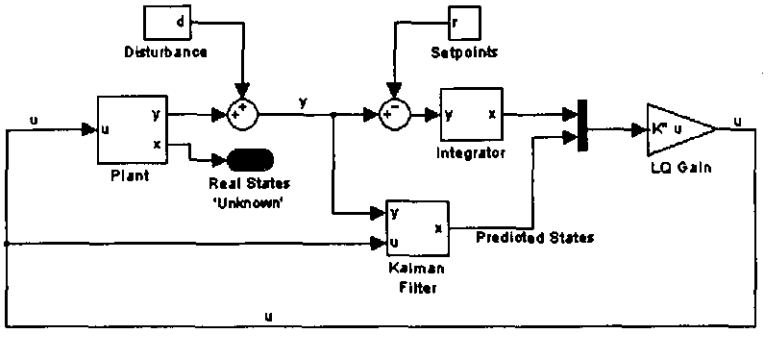


**Figure 6-25: LQG control system including the state observer.**

### 6.5.1) State Observer Design

Dutton [1997] recommends that the most accurate estimation of the Kalman filter parameters should be done under simulation with the inclusion of all known disturbances to the process. In order to simulate process conditions as realistically as possible a closed loop, PI controlled, simulation with real process noise (actuator and measurement noise) and with a square wave setpoint was constructed. A Kalman filter was put in parallel with the plant model so that states from the plant model and that of the Kalman filter could be compared.

The covariance matrices for a theoretical Kalman filter is given by:

$$Q_k = E[\mathbf{w}\mathbf{w}^T] \tag{6.30}$$

$$R_k = E[\mathbf{v}\mathbf{v}^T] \tag{6.31}$$

Where w is the system noise and v is the measurement noise.

Initial estimates for $Q_k$ and $R_k$ to determine whether these matrices would require non-diagonal elements, were obtained by running a regulatory closed loop control simulation (using two PI controllers with no decoupling). An initial assumption was that both matrices had dominant diagonal elements. The plant state and output signals from the simulation where then divided by their standard deviation so that the variances of these signals are equal to one. The cross correlation of these signals (states and measurements) were calculated so that the degree of correlation between the individual states and individual measurements could be determined. Given below are the correlation coefficient matrices for plant outputs and states.

$$\mathrm{cov}\left[\frac{\mathbf{y}(t)}{\sigma_{yi}}\right] = \begin{bmatrix} 1 & 0.0308 \\ 0.0308 & 1 \end{bmatrix}$$

$$\mathrm{cov}\left[\frac{\mathbf{x}(t)}{\sigma_{xi}}\right] = \begin{bmatrix} 1 & 0.9354 & 0.2285 & 0.1659 & 0.2561 \\ 0.9354 & 1 & 0.1731 & 0.2623 & 0.3113 \\ 0.2285 & 0.1731 & 1 & 0.0005 & 0.5028 \\ 0.1659 & 0.2623 & 0.0005 & 1 & 0.8640 \\ 0.2561 & 0.3113 & 0.5028 & 0.8640 & 1 \end{bmatrix}$$

Where $\sigma$ is the population standard deviation.

A correlation coefficient is considered to be significant for values above 0.6 (or below –0.6). From the cross correlation matrices given above it can be seen that the measurement noise signals are uncorrelated (correlation coefficient of 0.0308) and $R_k$ would therefore only contain diagonal elements. The correlation coefficients, for the Q

matrix, between the states indicate a strong correlation between $x_1$ and $x_2$ (0.9354), and between $x_4$ and $x_5$ (0.8640). $Q_k$ would therefore contain diagonal elements as well as $q_{12}$, $q_{21}$, $q_{45}$ and $q_{54}$ non-diagonal elements with the other elements set to zero.

A covariance matrix of the system noise ($Q_k$) was then estimated by minimising the error between the states from the plant model (before the noise is added) and the predicted states from the Kalman filter utilising differential evolution as the optimisation routine. Diagonal elements of the covariance matrix of the measurement noise ($R_k$) were estimated in the same manner.

The $R_k$ and $Q_k$ matrices were regressed on the data of the first 1000 seconds in Figure 6-32. Covariance for the $q_{11}$, $q_{22}$, $q_{12}$ and $q_{21}$ elements were negligible, resulting in zero values for these elements as well. Given in Figure 6-32 is the predicted vs. process model states. Judging by inspection on the graphs below the predicted states are almost exactly tracking the process model states with the actual states indicated in blue and the predicted states in red.

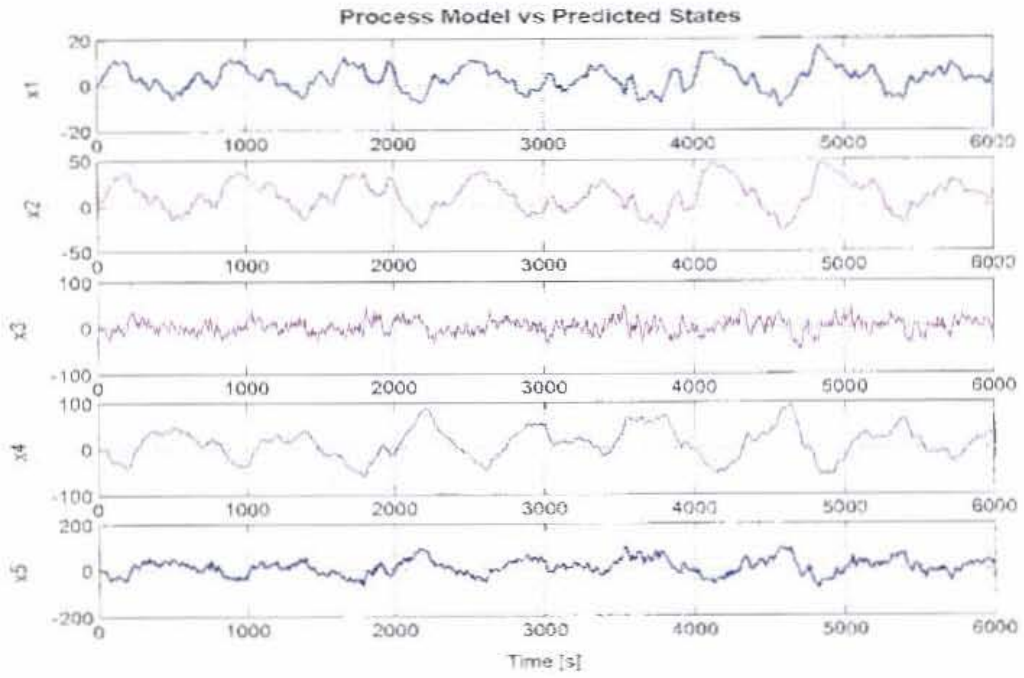


**Figure 6-26: Predicted vs. process model states.**

Variance on the prediction of the measurement signal by the Kalman Filter is given in Figure 6-27. The variance, by inspection of the graph below, of both measurements has been reduced.

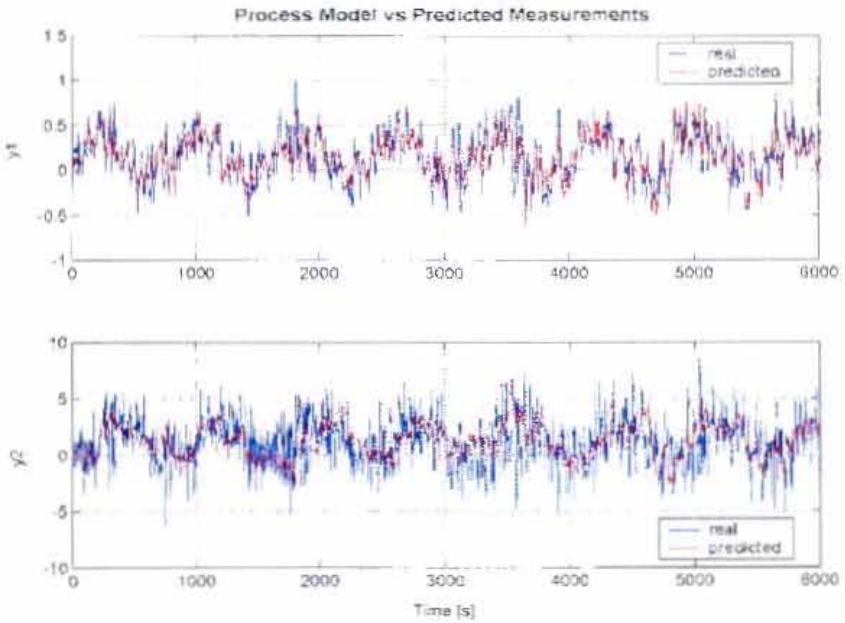


**Figure 6-27: Predicted vs. process model outputs.**

The $R_k$ and $Q_k$ matrixes obtained from the DE optimisation routine are given below.

$$R_k = \begin{bmatrix} 209 & 0 \\ 0 & 16954 \end{bmatrix}$$

$$Q_k = \begin{bmatrix} 0 & 0 & 0 & 0 & 0 \\ 0 & 0 & 0 & 0 & 0 \\ 0 & 0 & 259 & 0 & 0 \\ 0 & 0 & 0 & 718 & 187 \\ 0 & 0 & 0 & 187 & 540 \end{bmatrix}$$

### 6.5.2) LQ Gain Design

Equation (5.20) can be rewritten to represent the outputs rather than the states and is a special case of z=Mx given in Eq. (6.25).

$$y = Cx \tag{6.32}$$

so that the objective function is then given by:

$$J = \lim_{T\to\infty} E\left\{\int_0^T (x^T C^T Q C x + u^T R u)dt\right\} \tag{6.33}$$

A closed loop simulation was constructed, as given in Figure 6-25 with the same setpoints and step times as was used for the PI controller tuning simulations (Table 6-4). Integrators (as shown in Figure 6-25) were added to the error signal to enable servo setpoint tracking.

Initial optimisation attempts for Q and R assumed that these matrices contained non-diagonal elements as well. These eight variables were optimised with the differential evolution optimisation routine by minimising the sum of the integrals of the absolute errors, each divided by their own setpoint so that the IAE for both loops carry the same weight. From the initial optimisation it was shown that the non-diagonal entries tend to zero so that they were set to zero and both matrices only contained diagonal elements.

Given in Figure 6-28 are the closed loop responses for the LQG servo controller without process noise. The setpoints of $y_1$ and $y_2$ (0.2085 pixels/s and 1.6148 RGB respectively) were selected such that specified final values of $u_1$ and $u_2$ (4 $m^3$/min and $u_2$ = 40 %) were obtained. These are the same setpoints and step times that were used for the PI controller types earlier.

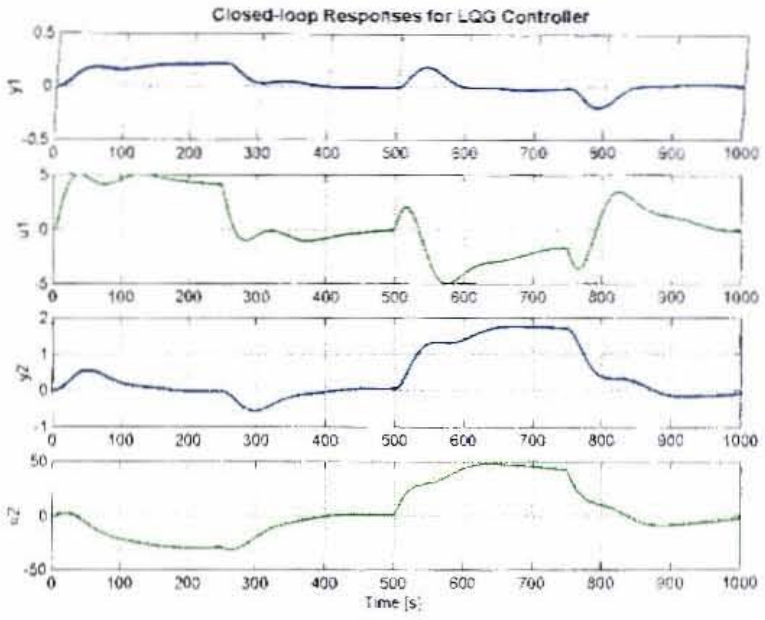


**Figure 6-28: Closed loop tuning results for LQG setpoint control.**

The LQG parameters obtained from the DE optimisation routine are:

$$\mathbf{Q} = \begin{bmatrix} 1144 & 0 \\ 0 & 37.7 \end{bmatrix} \text{ and } \mathbf{R} = \begin{bmatrix} 0.573 & 0 \\ 0 & 0.0665 \end{bmatrix}$$

while the optimal feedback gain matrix, **K**, is given by:

$$\mathbf{K} = \begin{bmatrix} 1.4006 & 0.1414 & 0.2792 & 0.0179 & 0.1160 & 0.0012 & 0.0004 \\ 1.4626 & 0.9711 & 0.4923 & 0.1409 & 0.6958 & -0.0013 & 0.0037 \end{bmatrix}$$

The closed loop poles of the LQC controller are the eigenvalues of the matrix A-BK, which is given by:

| No | Closed Loop Poles |
|---|---|
| 1 | -1.1477e-001 |
| 2 | -3.8830e-002 +8.592e-003i |
| 3 | -3.8830e-002 -8.592e-003 i |
| 4 | -1.7305e-002 |
| 5 | -1.1653e-002 |
| 6 | -1.3258e-004 |
| 7 | -1.9489e-005 |

From the closed loop poles above the system is stable with no RHP poles as expected with the internal stability of LQG controllers guaranteed [Maciejowski, 1989]. The dominant pole at -1.9489e-005 indicates a very slow response time of the MIMO controller. This however is not confirmed by the simulation responses obtained. It is therefore assumed that zeros cancel the two slow poles at -1.3258e-004 and -1.9489e-005. This could be problematic for the LQG controller robustness as any condition change (plant change or additional delay time for some reason) that might move these two cancelling zeros, would result in an extremely slow controller response. This also opens up the possibility of poor internal performance [La Plante, 1999].

Similarly, a regulatory LQG controller was designed. No setpoint changes were made but real process noise and disturbance data were included in the simulation. The objective function was also kept the same. Figure 6-29 shows the closed loop response for the LQG regulatory controller.

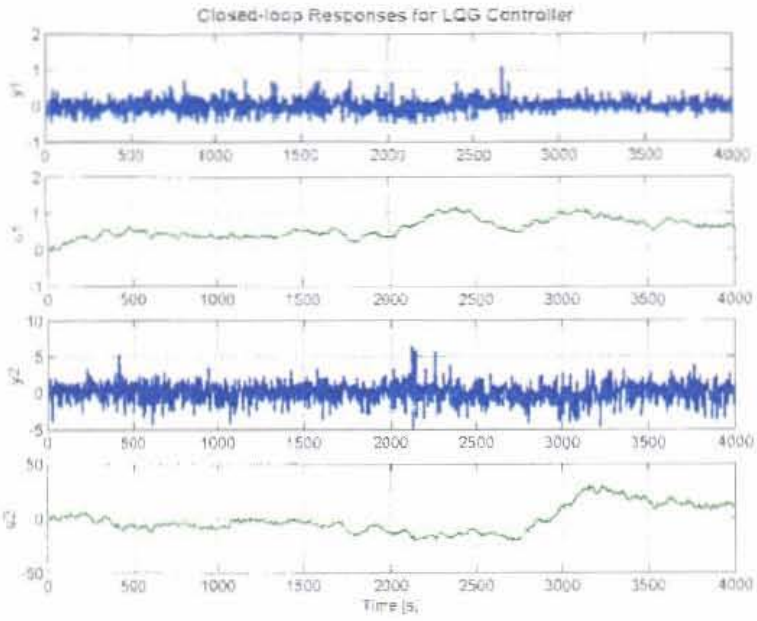


**Figure 6-29: Tuned regulatory control for LQG controller**

The LQG parameters obtained were:

$$\mathbf{R} = \begin{bmatrix} 0.3779 & 0 \\ 0 & 0.0018 \end{bmatrix} \text{ and } \mathbf{Q} = \begin{bmatrix} 9.6 & 0 \\ 0 & 0.0608 \end{bmatrix}$$

and the optimal feedback gain, **K**, obtained for the regulatory design was:

$$\mathbf{K} = \begin{bmatrix} 0.0447 & 0.0037 & 0.0056 & -0.0015 & 0.0014 & 0.0016 & 0.0004 \\ 1.0194 & 0.2273 & 0.2511 & 0.0432 & 0.1032 & -0.0055 & 0.0229 \end{bmatrix}$$

Closed loop LQG regulatory controller poles are all in the LHP and are given below.

| No | Closed Loop Poles |
|---|---|
| 1 | -0.0617 |
| 2 | -0.0351 |
| 3 | -0.0205 |
| 4 | -0.0162 |
| 5 | -0.0096 |
| 6 | -0.0014 |
| 7 | -0.0001 |

As was the case with the servo design, the regulatory design also has a very slow pole that corresponds to a settling time of 40 000 seconds. Again such slow responses are not evident in the simulations so that these poles must be cancelled by zeros and poor internal performance is a possibility.

## *6.6) Internal Model Control Design*

Internal model control [Seborg 1989, Ogunnaike 1994] involves inverting a stable plant model, $\hat{G}_P$, without inverting the unstable zeros and then to specify a transfer function, $G_{CL}$, such that the product of the inverted process model, $\hat{G}_P^{-1}$, and the closed loop transfer function is bi-proper (number of poles equal number of zeros). If the system is unstable it is first stabilised using an inner loop. The resulting stable, closed loop system is then invertible [Maciejowski, 1989]. This specified transfer function would then be the closed loop transfer function, as the product of the plant with its inverse would equate to the identity matrix. The plant model, $\hat{G}_P$, is then put in parallel with the plant so that any differences between the plant model and the real process is in feedback to account for modelling errors and output disturbances.

The internal model controller is given by:

$$G_c = G_{CL}\hat{G}_P^{-1} \tag{6.34}$$

And the closed loop transfer function is given by:

$$G_{CL} = \begin{bmatrix} \frac{1}{(\tau_{cl_1} s+1)^{n_1}} & 0 & 0 & 0 & 0 \\ 0 & \cdot & 0 & 0 & 0 \\ 0 & 0 & \cdot & 0 & 0 \\ 0 & 0 & 0 & \cdot & 0 \\ 0 & 0 & 0 & 0 & \frac{1}{(\tau_{cl_i} s+1)^{n_i}} \end{bmatrix} \quad (6.35)$$

Where n is equal to the difference between the poles and the zeros in $\hat{G}_P^{-1}$ and $\tau_{cl}$ is the closed loop time constant. The diagonal elements of $G_{CL}$ takes the form of a $n^{th}$ order filter and the tuning of the IMC controller then involves specifying $\tau_{cl}$. IMC automatically takes care of interactions. Given in Figure 6-30 is the IMC controller.

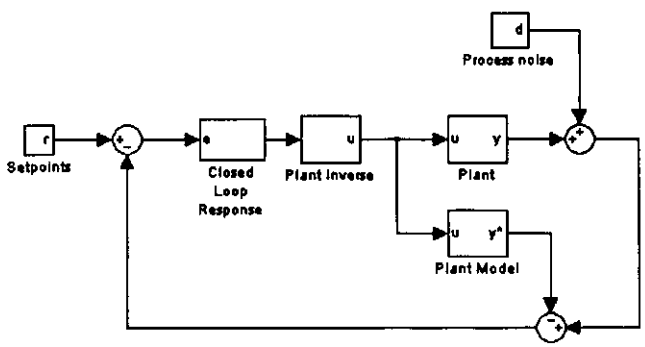


**Figure 6-30: Internal model controller.**

For the plant model, determined in section (6.1),

$$\hat{G}_P = \begin{bmatrix} \frac{0.07831}{(50.13s+1)} & \frac{0.003654(137.5s+1)}{(55.5s+1)(19.9s+1)} \\ \frac{0.4344}{(105.5s+1)} & \frac{0.06064}{(29.31s+1)} \end{bmatrix} \quad (6.36)$$

The plant inverse is:

$$\hat{G}_P^{-1} = \frac{1}{g_{11}g_{22} - g_{12}g_{21}} \begin{bmatrix} g_{22} & -g_{12} \\ -g_{21} & g_{11} \end{bmatrix} \quad (6.37)$$

$G_{CL}$ for both loops only needs to be first order (n=1) to make $\hat{G}_P^{-1}$ bi-proper. $G_{CL}$ is then given by:

$$G_{CL} = \begin{bmatrix} \frac{1}{\tau_{cl1}s+1} & 0 \\ 0 & \frac{1}{\tau_{cl2}s+1} \end{bmatrix} \qquad (6.38)$$

From the PI controller design it is known that the decoupling from loop two to loop one is too aggressive, causing $u_1$ to exceed its constraint and that a faster closed loop time constant for loop two can be obtained if $u_1$ is passed through a first order filter to damp out high frequency.

Given in Figure 6-31 is the closed loop tuned response for the IMC controller. The same setpoints, step times and $u_i$ constraints were applied as given in Table 6-4. Only 25 % overshoot for $u_1$ was allowed. The closed loop time constants are: $\tau_{cl}$ = 45 and $\tau_{cl}$ = 56, which was obtained from trial and error such that $u_1$ does not exceeds its constraint of 5 $m^3$/min.

The detailed transfer function for the IMC controller as given by Eq. (6.34) is then:

$$Gc_{11} = \frac{33.835\,(s+0.05025)\,(s+0.03412)\,(s+0.01995)\,(s+0.01802)\,(s+0.009479)}{(s+0.0724)\,(s+0.03412)\,(s+0.02222)\,(s+0.01678)\,(s+0.01119)}$$

$$Gc_{21} = \frac{-67.3379\,(s+0.05025)\,(s+0.03412)\,(s+0.01995)\,(s+0.01802)\,(s+0.009479)}{(s+0.0724)\,(s+0.02222)\,(s+0.01678)\,(s+0.01119)\,(s+0.009479)}$$

$$Gc_{12} = \frac{-5.9782\,(s+0.05025)\,(s+0.03412)\,(s+0.01995)\,(s+0.01802)\,(s+0.009479)\,(s+0.007273)}{(s+0.0724)\,(s+0.05025)\,(s+0.01802)\,(s+0.01786)\,(s+0.01678)\,(s+0.01119)}$$

$$Gc_{22} = \frac{20.5289\,(s+0.05025)\,(s+0.03412)\,(s+0.01995)\,(s+0.01802)\,(s+0.009479)}{(s+0.0724)\,(s+0.01995)\,(s+0.01786)\,(s+0.01678)\,(s+0.01119)}$$

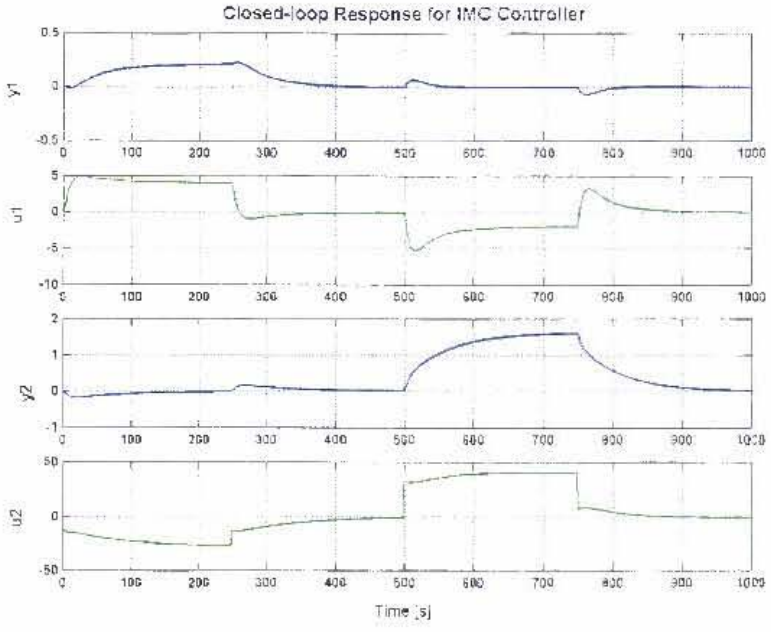


**Figure 6-31: IMC closed loop response.**

From Figure 6-31 it can be seen that the two loops are not fully decoupled. $u_1$ was filtered with a first order filter with a time constant of 10 seconds. Given in Figure 6-32 is the filtered $u_1$ from Figure 6-31 as well as the unfiltered $u_1$. The sharp spikes in $u_1$, especially from the decoupling of loop two to loop one at times 500 and 750 seconds, gets reduced by 50 %. The 10 second time constant in the low pass filter with a pole at -0.1, is non-dominant with respect to the dominant process pole of -0.0095 calculated in section (6.3.1).

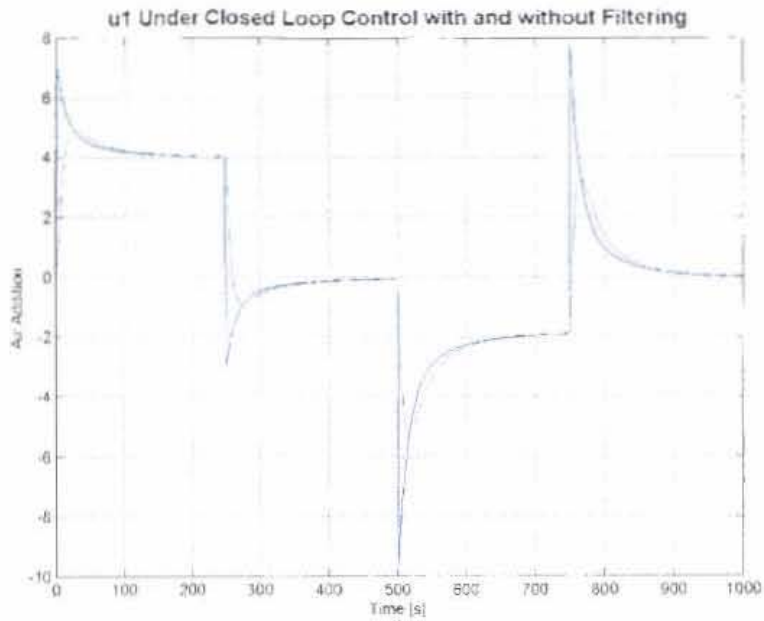


**Figure 6-32: $u_1$ Under closed loop response: with and without a filter.**

## *6.7) Controller Comparison and Evaluation by Simulation*

A 16-hour disturbance and actuator noise data set was collected to evaluate the controllers designed in section 5.6. The data set consisted of three smaller sets of data that were collected during nighttime on the plant. The controllers that were simulated are given below:

1. No decoupling.
2. Simplified decoupling.
3. $k_{12}$ Decoupling.
4. $k_{21}$ Decoupling.
5. $k_{12}$ & $q_{21}$ Decoupling.
6. $k_{21}$ & $q_{12}$ Decoupling.
7. Inverted decoupling.
8. Ideal decoupling.
9. LQG servo controller.
10. LQG regulator.

11. IMC.

The noise that was used in the simulations was real process noise with the mean removed. The resulting noise signal for velocity and colour is shown in Figure 6-33 and Figure 6-34 (the raw signals indicated in blue).

The simulated closed loop controller output values that were obtained, were put through a forward and backward moving average filter (100 second window) so that the high frequency noise was filtered with no phase lag [Matlab's users guide (filtfilt)].

Given in Figure 6-33 and Figure 6-34 are the filtered and unfiltered bubble velocity and bubble colour noise signals for a period of 10000 seconds. Filtered values were only used to evaluate and compare the outputs from the different controller simulations.

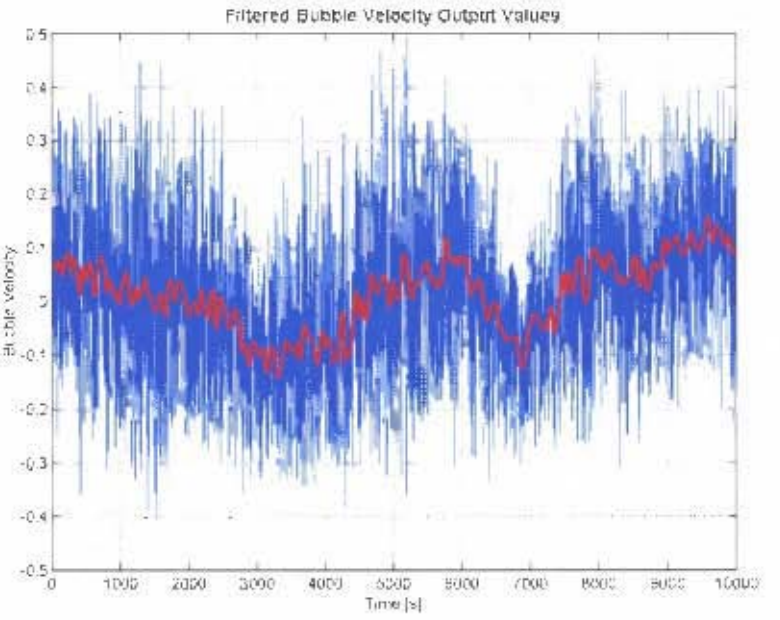


**Figure 6-33: Forward and backward filtering of bubble velocity.**

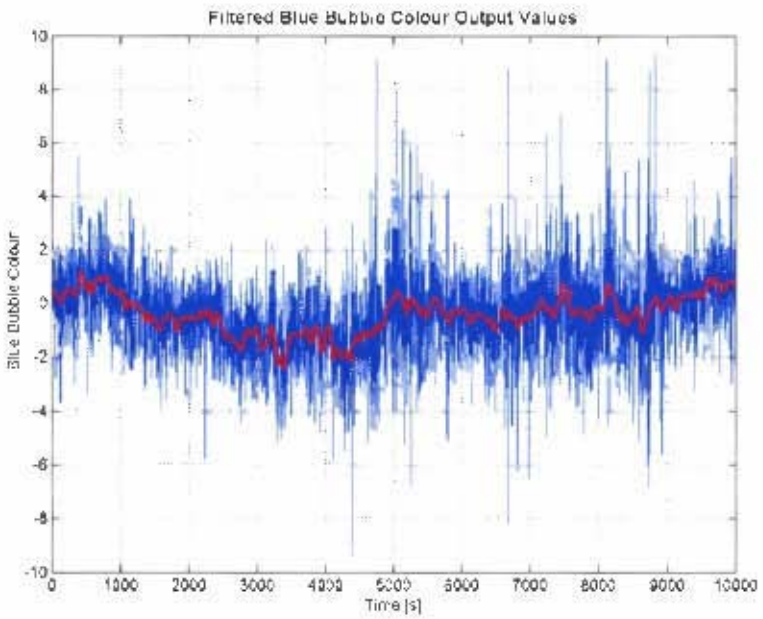


**Figure 6-34: Forward and backward filtering of blue bubble colour.**

Given in Figure 6-35 to Figure 6-38 are the comparative histograms for the open loop (indicated in red) and closed loop (indicated in blue) data sets for the bubble velocity and bubble colour with no decoupling and simplified decoupling control loops. The design objective of the closed loop control was to reject the noise by maintaining the setpoint at a constant value (in the simulator this was zero as the mean was removed from the data). The simplified decoupler controller (Figure 6-36) has slightly more values around zero for bubble velocity control, while the opposite is true for the bubble colour control.

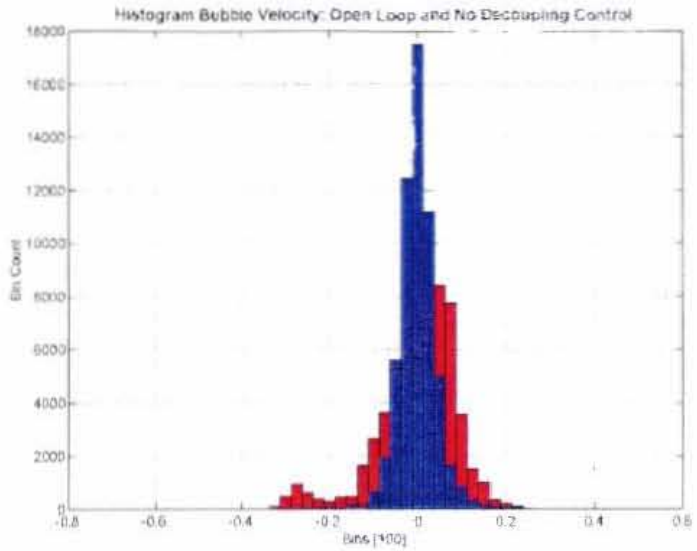


**Figure 6-35: Comparative histogram of bubble velocity regulatory control with no decoupling and open loop data.**

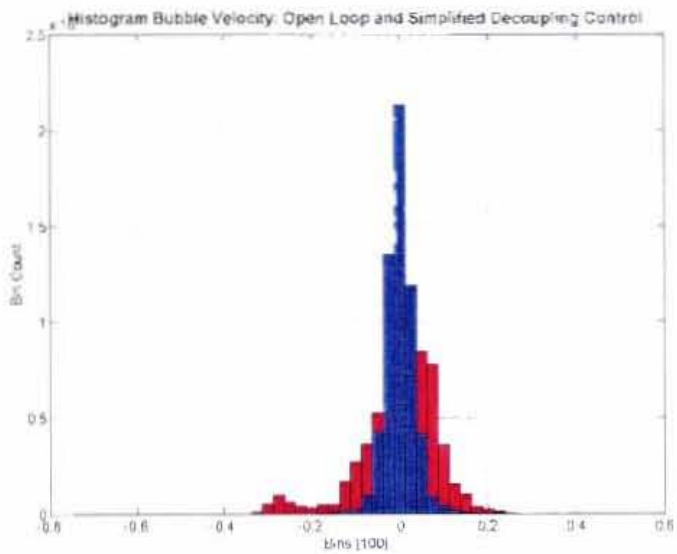


**Figure 6-36: Comparative histogram of bubble velocity regulatory control with simplified decoupling and open loop data.**

The improvement of closed loop control for the outputs is more pronounced for the bubble colour output compared to the bubble velocity output.

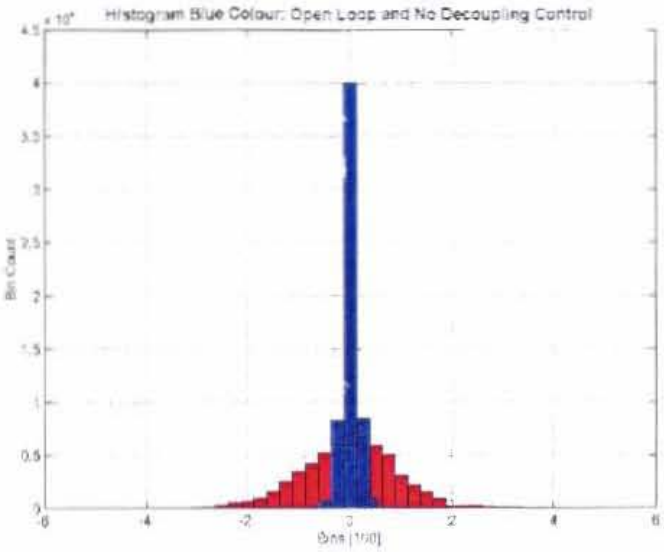


**Figure 6-37: Comparative histogram of bubble colour regulatory control with no decoupling and open loop data.**

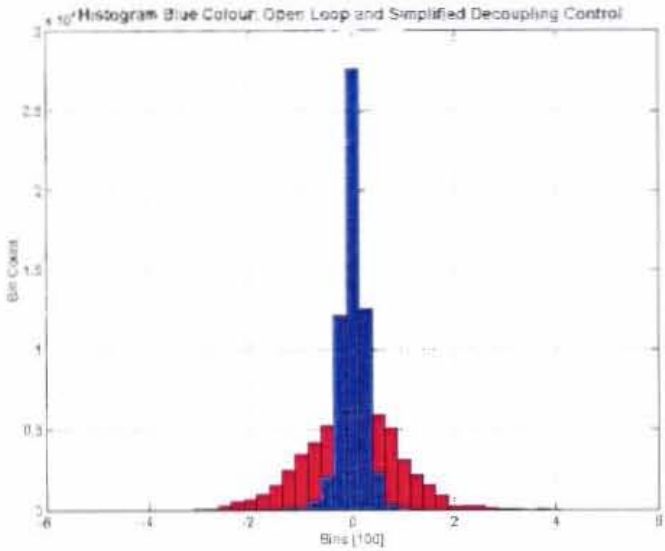


**Figure 6-38: Comparative histogram of bubble colour regulatory control with simplified decoupling and open loop data.**

A more visual comparison of all the controller outputs (the setpoint was zero) are given in Figure 6-39 to Figure 6-44 where open loop and closed loop filtered data are

presented for a duration of a 1000 seconds. From Figure 6-39 it can be seen that the "no decoupling" and "k12 decoupling" controllers follow each other closely.

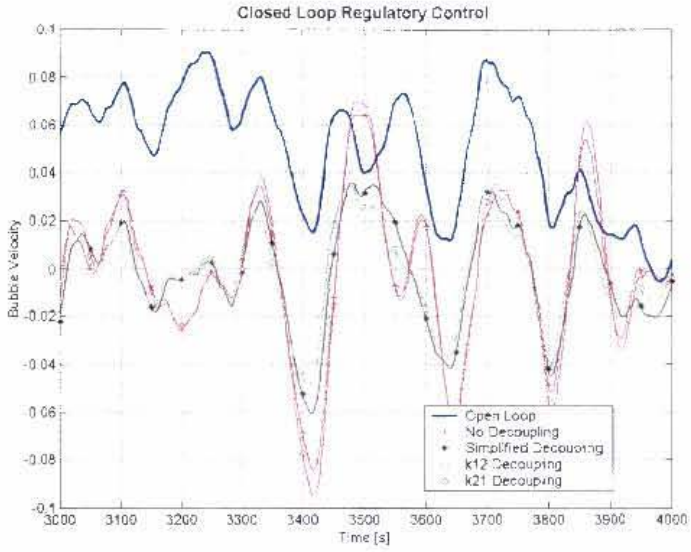


**Figure 6-39: Closed loop bubble velocity regulatory control; graph one.**

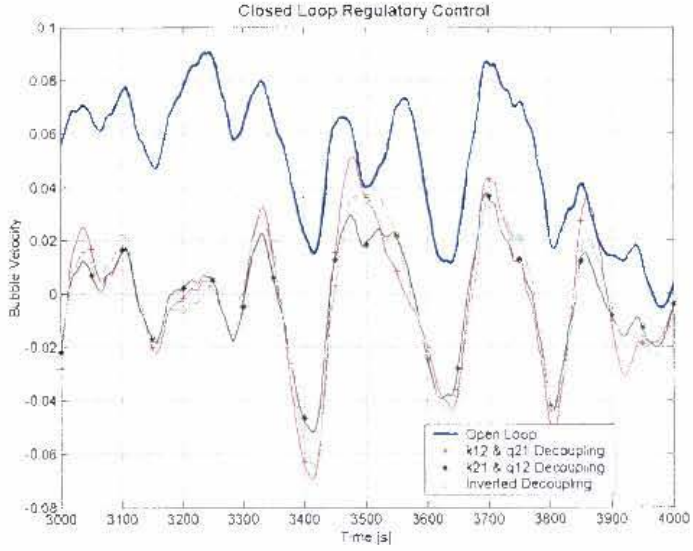


**Figure 6-40: Closed loop bubble velocity regulatory control; graph two.**

Figure 6-40 shows how closely the controllers with decoupling to both loops, follow each other.

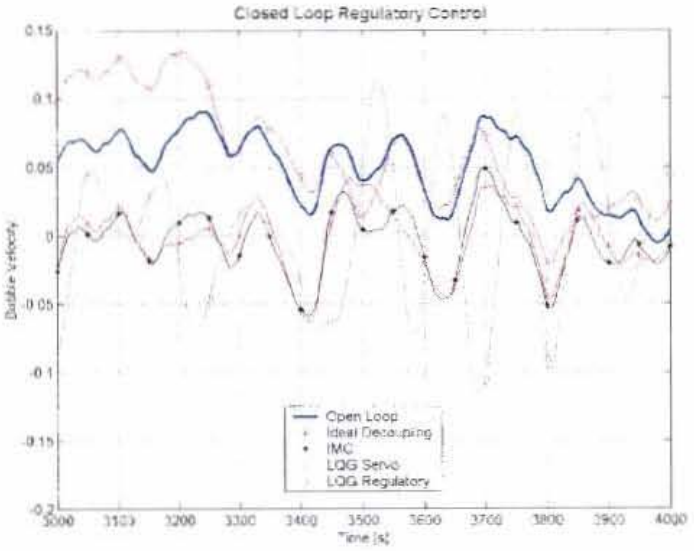


**Figure 6-41: Closed loop bubble velocity regulatory control; graph three.**

The integral values of the absolute error that is presented later showed that the LQG servo and regulatory controllers performed the worst based on only the output values. Figure 6-41 shows how the LQG servo controlier tends to oscillate, while the LQG regulatory controller are so slow to react, that the output for the first 400 seconds in Figure 6-41 are further away from zero than the open loop data. The poor performance from the LQG controllers might be as a result of the pole placements as discussed in section (6.5.2). The Q and R matrices of the LQG controller were adjusted to try and improve the performance output performance. This was achieved but at the expense of the input variables exceeding their constraint limits. As mentioned earlier the input constraints are vital so that this could not be accepted. The exact theoretical reason for the poor performance needs a further and more detailed investigation. Since this project has already identified and designed controllers that can be used for implementation, the more detailed investigation towards a critical analysis of the LQG controller performance in comparison to PI control is left as a recommendation.

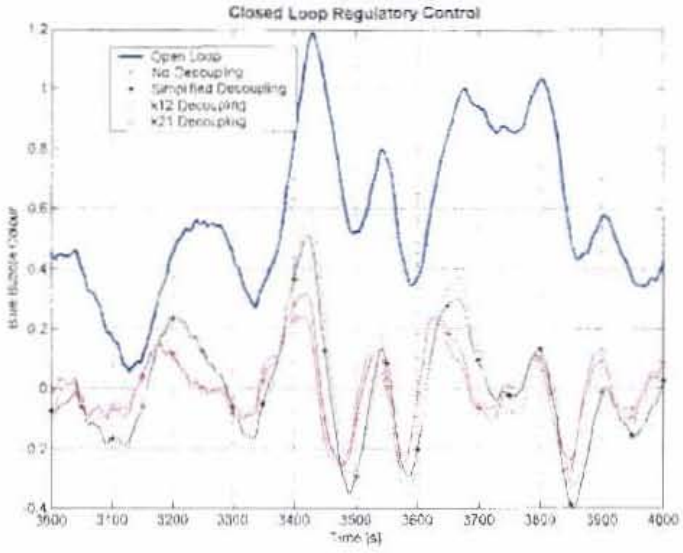


**Figure 6-42: Closed loop bubble colour regulatory control; graph one.**

The closed loop control for the blue colour follows more or less in the same pattern as the bubble velocity control. From Figure 6-43 it can be seen how strongly the outputs for the given controllers follow each other.

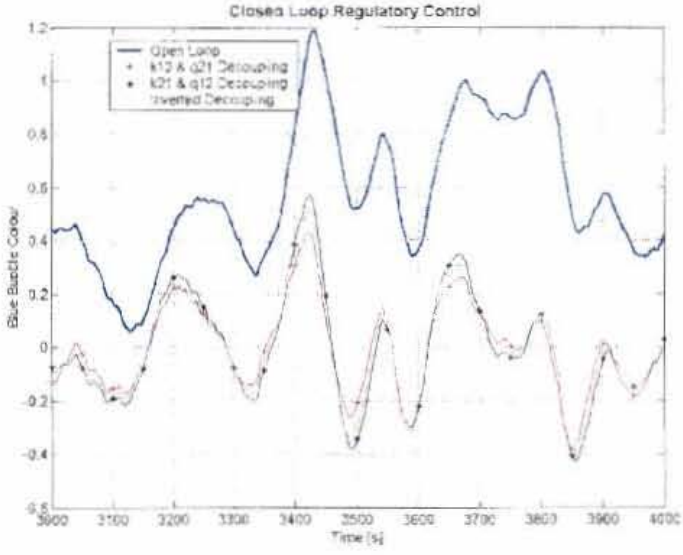


**Figure 6-43: Closed loop bubble colour regulatory control; graph two.**

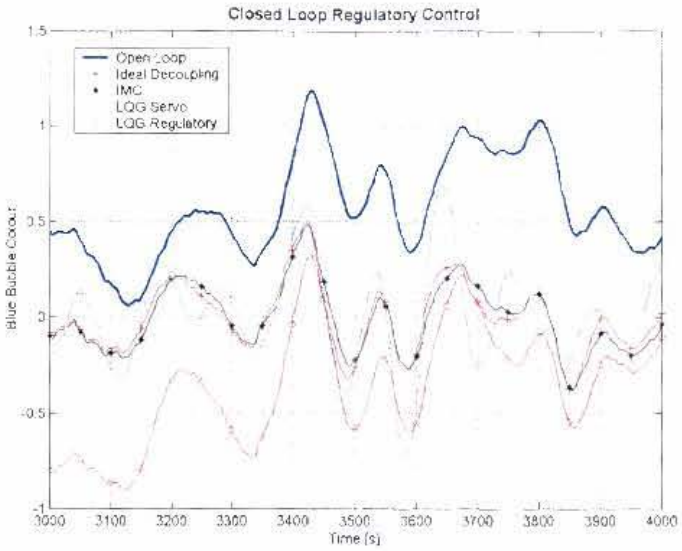


**Figure 6-44: Closed loop bubble colour regulatory control; graph three.**

As was the case for the bubble velocity LQG control, the same response goes for the blue colour control from Figure 6-44.

From the figures given above it was shown that some controllers give more or less the same output results. In order to identify and group similar controllers the correlation coefficients between the outputs were calculated and are given in Table 6-6 (velocity output values) and Table 6-7 (blue colour output values).

**Table 6-6: Correlations between controller outputs for velocity control.**

| No | Controller | 1 | 2 | 3 | 4 | 5 | 6 | 7 | 8 | 9 | 10 | 11 | 12 |
|---|---|---|---|---|---|---|---|---|---|---|---|---|---|
| 1 | Open Loop | 1.00 | | | | | | | | | | | |
| 2 | No Decoupling | 0.10 | 1.00 | | | | | | | | | | |
| 3 | Simplified Decoupling | 0.15 | 0.90 | 1.00 | | | | | | | | | |
| 4 | k12 Decoupling | 0.11 | 0.92 | 0.96 | 1.00 | | | | | | | | |
| 5 | k21 Decoupling | 0.11 | 0.99 | 0.91 | 0.91 | 1.00 | | | | | | | |
| 6 | k12 & q21 Decoupling | 0.14 | 0.89 | 0.98 | 0.96 | 0.92 | 1.00 | | | | | | |
| 7 | k21 & q12 Decoupling | 0.16 | 0.83 | 0.99 | 0.95 | 0.85 | 0.97 | 1.00 | | | | | |
| 8 | Inverted Decoupling | 0.15 | 0.88 | 1.00 | 0.95 | 0.90 | 0.97 | 0.98 | 1.00 | | | | |
| 9 | Ideal Decoupling | 0.14 | 0.91 | 1.00 | 0.97 | 0.92 | 0.98 | 0.98 | 0.99 | 1.00 | | | |
| 10 | IMC | 0.23 | 0.74 | 0.88 | 0.83 | 0.76 | 0.86 | 0.93 | 0.88 | 0.88 | 1.00 | | |
| 11 | LQG Servo | 0.07 | 0.61 | 0.61 | 0.52 | 0.55 | 0.61 | 0.55 | 0.58 | 0.58 | 0.44 | 1.00 | |
| 12 | LQG Regulatory | 0.55 | 0.10 | 0.19 | 0.12 | 0.13 | 0.19 | 0.25 | 0.20 | 0.17 | 0.42 | 0.14 | 1.00 |

**Table 6-7: Correlations between controller outputs for bubble colour control.**

| No | Controller | 1 | 2 | 3 | 4 | 5 | 6 | 7 | 8 | 9 | 10 | 11 | 12 |
|---|---|---|---|---|---|---|---|---|---|---|---|---|---|
| 1 | Open Loop | 1.00 | | | | | | | | | | | |
| 2 | No Decoupling | 0.09 | 1.00 | | | | | | | | | | |
| 3 | Simplified Decoupling | 0.21 | 0.83 | 1.00 | | | | | | | | | |
| 4 | k12 Decoupling | 0.20 | 0.80 | 0.94 | 1.00 | | | | | | | | |
| 5 | k21 Decoupling | 0.05 | 0.94 | 0.73 | 0.62 | 1.00 | | | | | | | |
| 6 | k12 & k21 Decoupling | 0.21 | 0.82 | 0.98 | 0.91 | 0.76 | 1.00 | | | | | | |
| 7 | k21 & k12 Decoupling | 0.22 | 0.79 | 1.00 | 0.95 | 0.67 | 0.97 | 1.00 | | | | | |
| 8 | Inverted Decoupling | 0.22 | 0.83 | 1.00 | 0.94 | 0.73 | 0.98 | 1.00 | 1.00 | | | | |
| 9 | Ideal Decoupling | 0.23 | 0.83 | 1.00 | 0.93 | 0.74 | 0.99 | 0.99 | 1.00 | 1.00 | | | |
| 10 | IMC | 0.26 | 0.73 | 0.97 | 0.90 | 0.65 | 0.97 | 0.97 | 0.97 | 0.97 | 1.00 | | |
| 11 | LQG Servo | 0.13 | 0.76 | 0.73 | 0.80 | 0.66 | 0.73 | 0.71 | 0.73 | 0.70 | 0.68 | 1.00 | |
| 12 | LQG Regulatory | 0.41 | 0.46 | 0.70 | 0.71 | 0.35 | 0.70 | 0.71 | 0.70 | 0.70 | 0.73 | 0.48 | 1.00 |

The controllers that could be grouped together for achieving the same output values are all the controllers with decoupling in the same loop. The correlation between these controllers is more than 0.98. IMC also correlates strongly (correlation coefficient of 0.97) to these controllers for the blue colour output, but to a lesser extent for the velocity control (correlation coefficient of 0.88).

The integral of the absolute difference between the setpoints and the outputs were calculated and are given in Table 6-8. From this table the best controller structure for the bubble velocity regulatory control is the decoupling system with only the $k_{12}$ decoupler. For the bubble colour control the best structures were the controller with no decoupling closely followed by the controller with only the $k_{21}$ decoupler. These two controller structures were considerably better than the other controllers for the blue colour regulation.

Table 6-8: IAE values of controller outputs under regulatory control.

| Controller Structure | Bubble Velocity | | Blue Colour | |
|---|---|---|---|---|
| | Filtered | Unfiltered | Filtered | Unfiltered |
| Open Loop | 4 042 | 7 383 | 42 602 | 81 598 |
| No Decoupling | 1 768 | 6 962 | 6 174 | 70 508 |
| Simplified Decoupling | 1 380 | 6 329 | 10 212 | 69 450 |
| k12 Decoupling | 1 332 | 6 329 | 10 740 | 69 539 |
| k21 Decoupling | 1 980 | 7 007 | 6 296 | 70 679 |
| k12 & q21 Decoupling | 1 573 | 6 448 | 9 718 | 69 553 |
| k21 & q12 Decoupling | 1 230 | 6 245 | 11 343 | 69 474 |
| Inverted Decoupling | 1 469 | 6 348 | 10 242 | 69 455 |
| Ideal Decoupling | 1 424 | 6 356 | 9 719 | 69 444 |
| IMC | 1 318 | 6 270 | 10 366 | 69 413 |
| LQG Servo | 3 106 | 8 218 | 13 500 | 71 927 |
| LQG Regulatory | 2 620 | 6 609 | 18 109 | 70 638 |

The worst performance was from the LQG controllers as noted earlier.

Given in Table 6-9 are the standard deviations for the different controller outputs. The minimum standard deviations for each output correspond to the minimum integral values given in Table 6-8. This was expected as a smaller absolute integral of a signal means that the signal had a smaller cumulative error so that it moved within a narrower band around the setpoint and therefore a smaller standard deviation.

Table 6-9: Standard deviation of controller outputs under regulatory control.

| Controller Structure | Bubble Velocity | | Blue Colour | |
|---|---|---|---|---|
| | Filtered | Unfiltered | Filtered | Unfiltered |
| Open Loop | 0.0909 | 0.1607 | 0.9348 | 1.9098 |
| No Decoupling | 0.0423 | 0.1553 | 0.1487 | 1.7189 |
| Simplified Decoupling | 0.0330 | 0.1405 | 0.2438 | 1.6991 |
| k12 Decoupling | 0.0268 | 0.1404 | 0.2578 | 1.7015 |
| k21 Decoupling | 0.0474 | 0.1565 | 0.1507 | 1.7218 |
| k12 & q21 Decoupling | 0.0373 | 0.1433 | 0.2306 | 1.7007 |
| k21 & q12 Decoupling | 0.0294 | 0.1385 | 0.2704 | 1.6999 |
| Inverted Decoupling | 0.0351 | 0.1409 | 0.2443 | 1.6992 |
| Ideal Decoupling | 0.0340 | 0.1411 | 0.2321 | 1.6989 |
| IMC | 0.0321 | 0.1392 | 0.2496 | 1.6990 |
| LQG Servo | 0.0706 | 0.1829 | 0.3129 | 1.7458 |
| LQG Regulatory | 0.0598 | 0.1462 | 0.4200 | 1.7217 |

The corresponding input values for the given outputs above are provided in Figure 6-45 to Figure 6-50 given below. The different controller inputs for the bubble velocity control strongly correlates except for the LQG inputs.

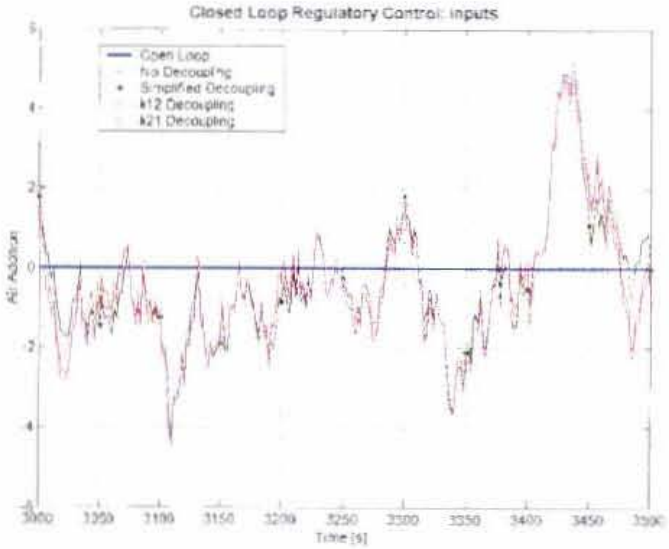


**Figure 6-45: Air addition for closed loop regulatory control; graph one.**

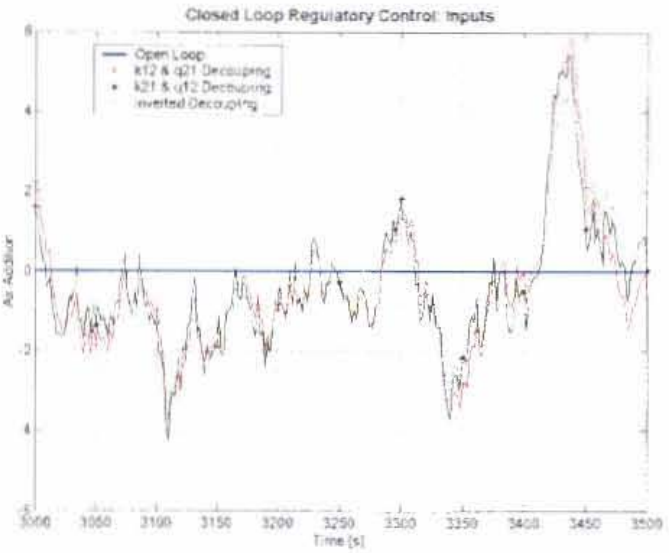


**Figure 6-46: Air addition for closed loop regulatory control; graph two.**

Figure 6-47 shows the slow response of the LQG regulatory input control. The LQG controllers also have the least amount of variance. The poor performance from the LQG controllers might be a result of the tuning method that was not appropriate for this controller type. The IMC controller output in Figure 6-47 does not exhibit high frequency due to the filter that was put on it.

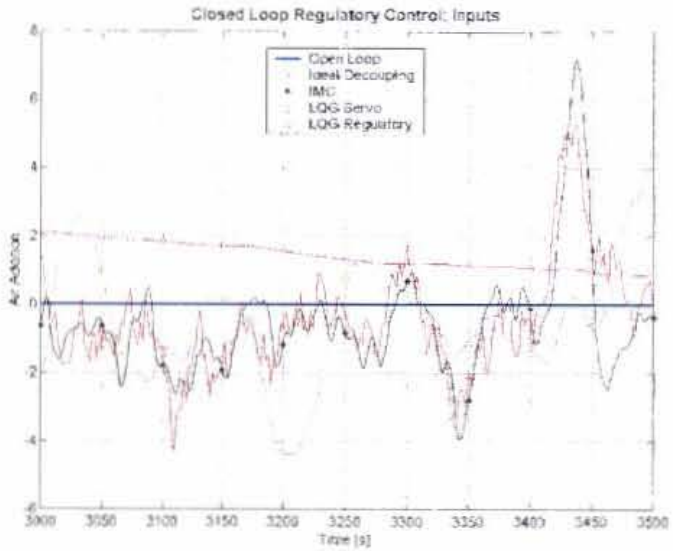


**Figure 6-47: Air addition for closed loop regulatory control; graph three.**

The controllers for which the filter, gf, was included to filter the high frequency of $u_1$, are correlated while the controllers without the filter are following each other, except for the LQG controllers. From Figure 6-48 the "no decoupling" and "$k_{21}$ decoupling" (controllers without gf) have more high frequency than the other two controller presented in this graph. The high frequency is a result of the decoupling from loop two to loop one that is absent causing the level to react only in a feedback manner compared to the feed forward control that is supplied by a decoupler.

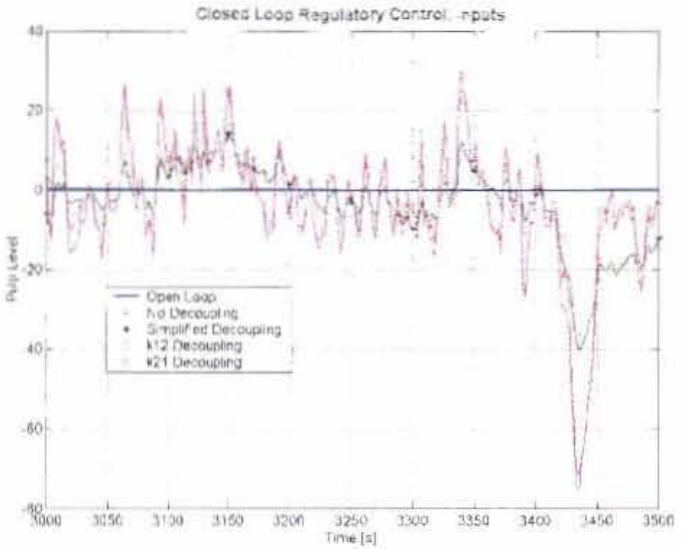


**Figure 6-48: Pulp level for closed loop regulatory control; graph one.**

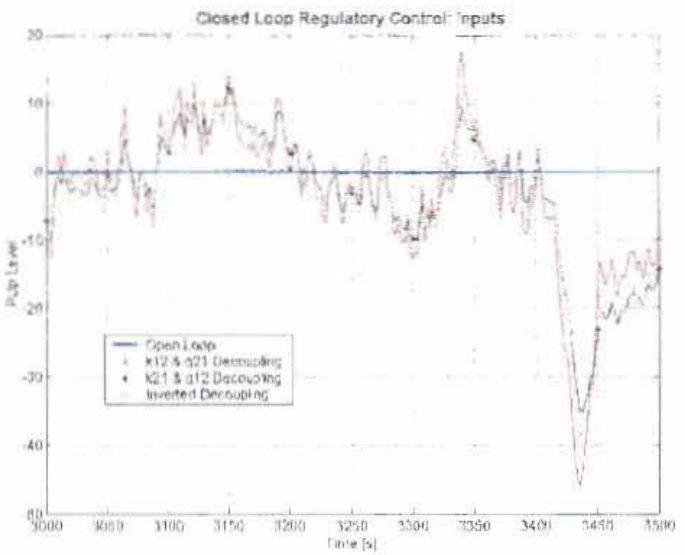


**Figure 6-49: Pulp level for closed loop regulatory control; graph two.**

Figure 6-49 again shows the strong correlation between the controllers with decoupling in the same loop.

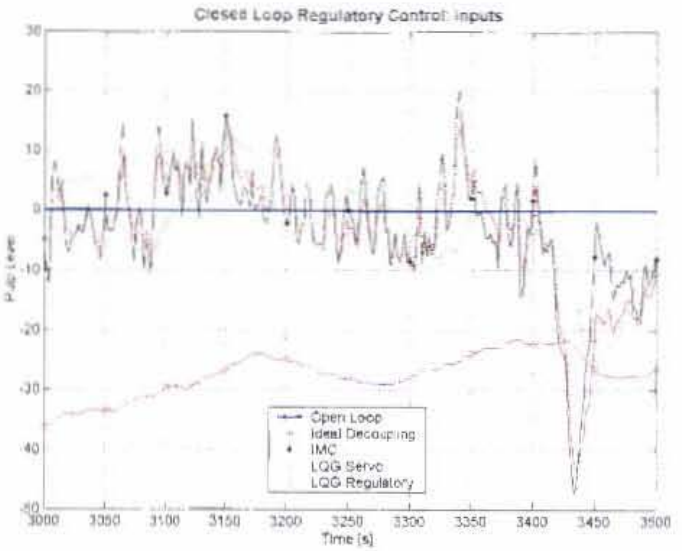


**Figure 6-50: Pulp level for closed loop regulatory control; graph three.**

Figure 6-50 shows the minimum variance control from the LQG controllers and the strong correlation between the IMC and simplified decoupling controller outputs.

## *6.8) Controllers Sensitivity to Modelling Errors*

Controller sensitivity to modelling errors was tested by running simulations where the plant model gains were increased and decreased by 20% keeping all the controller parameters the same. None of the controllers became unstable when the plant models were changed. Given in Table 6-10 are the IAE values for the bubble velocity and blue bubble colour outputs for the simulations with:

- Normal plant models.
- Plant models with all the model gains increased by 20%.
- Plant models with all the model gains decreased by 20%.

**Table 6-10: IAE values for modified plant models to test controller sensitivity.**

| Controller Structure | Bubble Velocity | | | Blue Bubble Colour | | |
|---|---|---|---|---|---|---|
| | Normal | + 20 % | -20 % | Normal | + 20 % | -20 % |
| No Decoupling | 34.0 | 30.7 | 38.3 | 99.6 | 86.2 | 119 |
| Simplified Decoupling | 30.4 | 27.6 | 34.3 | 151 | 128 | 185 |
| k12 Decoupling | 23.7 | 22.0 | 26.0 | 251 | 215 | 299 |
| k21 Decoupling | 36.9 | 32.9 | 42.5 | 51.3 | 44 | 62 |
| k12 & q21 Decoupling | 31.7 | 28.5 | 35.9 | 176 | 153 | 209 |
| k21 & q12 Decoupling | 26.6 | 24.2 | 30.1 | 159 | 136 | 196 |
| Inverted Decoupling | 31.3 | 28.9 | 35.7 | 147 | 124 | 181 |
| Ideal Decoupling | 30.9 | 28.6 | 34.2 | 152 | 129 | 186 |
| IMC | 30.7 | 35.9 | 34.9 | 195 | 216 | 237 |
| LQG Servo | 42.6 | 35.1 | 59.2 | 253 | 232 | 329 |

For all the controllers, except for IMC, the IAE decreased when the process models gains were increase by 20 %. The poorer performance of the IMC controller was expected as its design is based on the inverse of the plant model and the assumption that the plant model is accurate. All the IAE values were increased for the case where the plant model gains were decreased. As pointed out in section (6.4) an increase in the controller gain (which has the same effect as an increase in the process model gain) would increase the output performance, but the constraints on the inputs prevent this.

From the observations above it seems that all the controllers are reasonably robust for changes up to 20 % in the plant model based on the IAE values.

## *6.9) Controllers Sensitivity to Noise Disturbances*

Another important consideration when evaluating controllers is to test for internal stability and the response time of the controller to recover from this [Laplante, 1999; Braae]. Given in Figure 6-51 below is a standard closed loop control diagram.

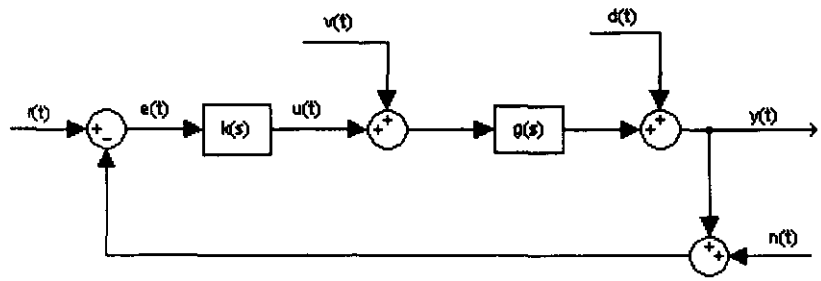


**Figure 6-51: Standard closed loop control diagram.**

Indicated on this diagram are the actuator noise, v(t), process disturbance, d(t) and measurement noise, n(t). Robustness of the controllers to process actuator and disturbance noise signals has already been tested, as these were included in the simulated controller evaluation in section (6.7). More information about the controller stability for the individual noise and disturbance signals can be obtained by stepping these signals at different times and monitoring the speed of response from the controllers. This would enable the separate identification of controller sensitivity to each disturbance and to noise signals.

A simulation was constructed as indicated in Figure 6-51 above. Given in Table 6-11 is the simulation information with the time intervals and step change sizes that was used. The step changes to the setpoints, r(t), remained the same as during the controller evaluation earlier and the step sizes of the noise and disturbance signals (v(t), d(t) and n(t)) were calculated as 20% of the nominal signals to which it was added.

**Table 6-11: Simulation step times and magnitudes for internal stability tests.**

| No | Signal | Velocity Loop Values | Colour Loop Values | Time [s] |
|---|---|---|---|---|
| 1 | $r(t)_1$ | 0 → 0.2085 | - | 0 |
| 2 | $v(t)_1$ | 0 → 1.0 | - | 250 |
| 3 | $d(t)_1$ | 0 → 0.0416 | - | 500 |
| 4 | $n(t)_1$ | 0 → 0.0416 | - | 750 |
| 5 | $r(t)_2$ | - | 0 → 1.615 | 1000 |
| 6 | $v(t)_2$ | - | 0 → 10 | 1250 |
| 7 | $d(t)_2$ | - | 0 → 0.323 | 1500 |
| 8 | $n(t)_2$ | - | 0 → 0.323 | 1750 |

The simulation results for simplified decoupling, IMC and LQG servo controllers are shown in Figure 6-52, Figure 6-53 and Figure 6-54 respectively. Simulations results of the other controllers are given in appendix E.

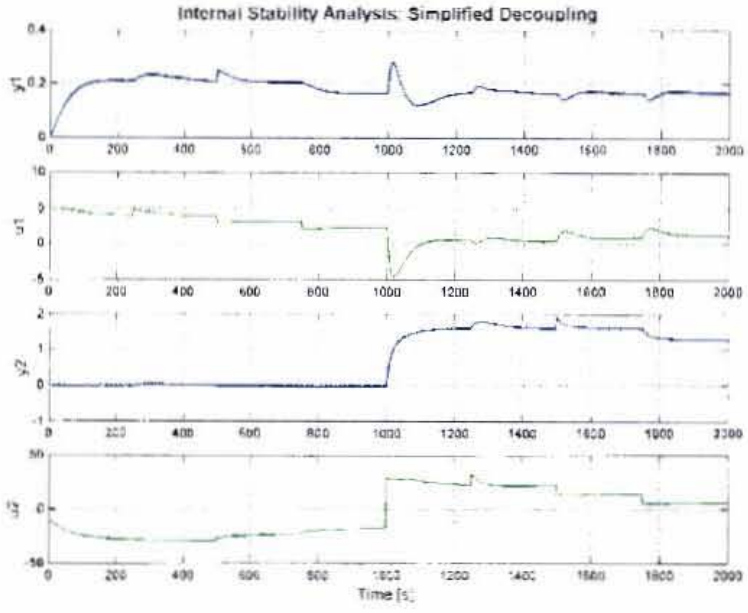


**Figure 6-52: Internal stability analysis of simplified decoupling.**

Figure 6-52 shows that PI control with simplified decoupling are robust and recovers quickly from disturbance and noise step changes. The step change from the measurement noise signal causes a bias in the controller outputs ($y_1$ at t = 750s and $y_2$ at t = 1750). Settling time of the outputs to these step changes is about 200 seconds.

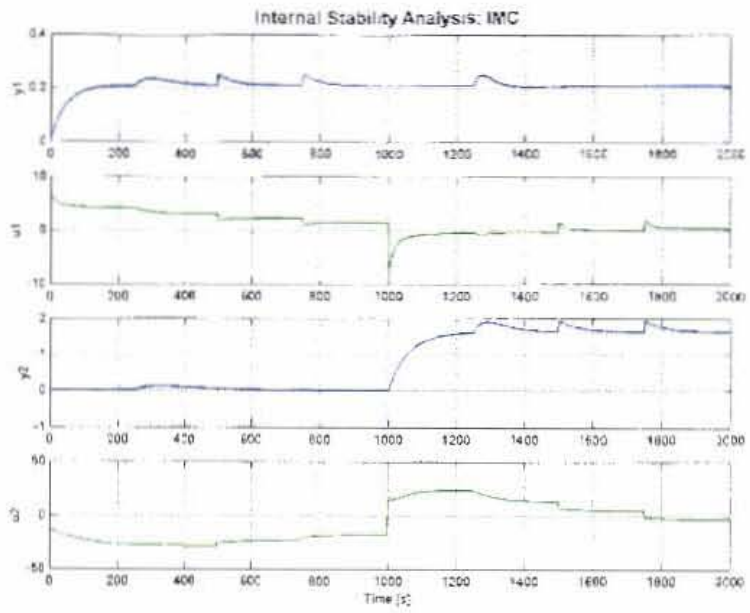


**Figure 6-53: Internal stability analysis for IMC.**

Settling time of the IMC controller, for both outputs (about 120 seconds), to the disturbance, d(t) and the measurement noise, n(t) signals are less than for the PI controlled outputs as shown in Figure 6-52 and Figure 6-53.

The LQG servo controller, shown in Figure 6-54, initially seems to have the shortest recovery time of 50 seconds for both outputs out of all the controllers. By closer evaluation of the output signals it can be seen that the outputs quickly recovers to slightly above their setpoint values, after which it slows down considerable to only reach the setpoints at a total of slightly more than 200 seconds settling time.

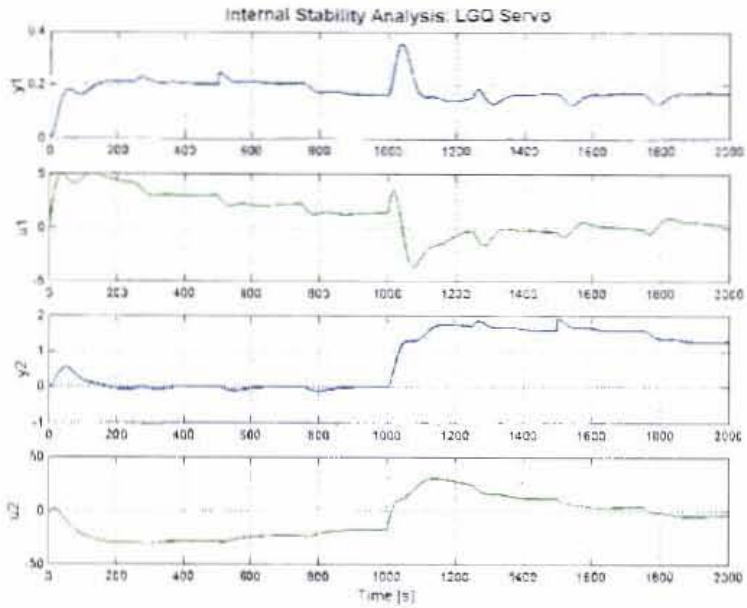


**Figure 6-54: Internal stability analysis of LQG servo controller**

## *6.10) Discussion on Controller Design*

There is a clear distinction between stabilisation and optimisation flotation control. In reviewing what has been done up to now, only certain areas of stabilisation control around one flotation has been addressed in a simulation environment. Different controller types and structures have been simulated so that the best ones can be selected for implementation on the process. The three controllers that performed the best under simulation were:

- Two PI controllers with no decoupling.
- Two PI controllers with decoupling from the bubble colour loop to the bubble velocity loop.
- Internal model controller

None of the controllers were such that it outperformed the others in both loops. The PI controllers with no decoupling had the best IAE value for the colour output with a

reduction in the open loop IAE from 42 602 to 6 174. Unfortunately this controller was one of the worst performers in the reduction of the bubble velocity output with a reduction of the open loop IAE from 4 042 to 1 768.

The controller with decoupling from the colour loop to the velocity loop was the best performer in the velocity control loop and reduced the IAE to 1 132, while it reduced the blue output IAE to 10 740.

The IMC controller on average performed well in both loops and reduced the IAE in the colour loop to 10 366 and in the velocity loop to 1 318. The simplified decoupling was in the same type of range as the IMC controller.

Further in general in can be said that the blue output considerably benefited more from closed control than the bubble velocity output with much bigger percentage reductions in from the open loop IAE to the closed loop IAE.

# 7. Controller Implementation

The controllers that were shown by simulation to give the best performance were implemented on the plant. These are:

- PI control without decoupling.
- PI control with only the $k_{12}$ decoupler.
- IMC

Prior to controller implementation some process changes were made and come about. It was suspected that these changes might have an influence on the performance of the controllers that would be tested. More about these process changes is said later on in this section.

## *7.1) Controller Coding and Implementation Environment.*

A soft PLC (WonderWare's InControl) was used for the implementation. One advantage of the soft PLC that was used, is that it could be used as a simulator as well. This made the checking and validating of the controller coding to correspond to simulation results obtained from Matlab an easy task.

A standard PI control block of the soft PLC was used and only the controller's time constants required conversion. The soft PLC also had a transfer function block that allows a maximum of two poles and one zero. This was used to configure the $k_{12}$ decoupler as well as the plant model that is used by the IMC controller.

Implementation of the Matlab s-domain IMC controller was more difficult. Given below is the step-by-step procedure that was used to get the Matlab controller coded in the soft PLC.

- The IMC controller as given by Eq. (6.34) was simplified using pole-zero cancellation with an absolute tolerance of 0.001 in Matlab. This reduced the size of the controller transfer functions from a total of 21 to 15 poles and zeros. The simplified controller was checked by visual inspection to

have a minimal effect on the closed loop performance by comparing simulation results from the original and simplified controller. When the tolerance on pole-zero proximity is increased to 0.002 the cancellation start to have a significant effect on the controller performance as dominant poles are cancelled.

- The reduced s-domain controller transfer functions are then converted to the z-domain using zero order hold with a 1 second sampling interval (scan time of the soft PLC was set at 1 second).
- From the z-domain transfer functions the difference equations of the controller outputs are derived as given for the general case in Eq. (7.1) and (7.2).

$$k(z) = \frac{b_0 + b_1 z^{-1} + b_2 z^{-2} + b_3 z^{-3} + \ldots}{1 - a_1 z^{-1} - a_2 z^{-2} - a_3 z^{-3} - \ldots} \tag{7.1}$$

$$u_{[k]} = a_1 u_{[k-1]} + a_2 u_{[k-2]} + a_3 u_{[k-3]} + \ldots \\ b_0 e_{[k]} + b_1 e_{[k-1]} + b_2 e_{[k-2]} \ldots \tag{7.2}$$

where u is the controller output and e is the error signal.

- As stated earlier the dynamic process model used by the IMC controller was build-up from InControl transfer function blocks.
- All the signals originating from transfer blocks as given by Figure 6-30 are then known and the remaining unknown signals are just a subtraction of two known signals.
- Clamps, using if statements, was put on the u signals to prevent the process inputs from going outside operating ranges.
- In order to make the transfer of control bumpless, a bias was added to the u values of the IMC controller so that these values correspond to the u values of the process just before the controller was switched on.
- "Switching on" the IMC controller only entailed starting to write the IMC u values back to the plant as the IMC controller was already getting data from the process so that the transfer functions were continuously tracking

the process. While the controller was in off mode the velocity and colour setpoints was calculated as a filtered value of the velocity and colour PVs. This ensured that the controller transfer functions were not trying to make big process changes prior to switching the controller on.

- A first order filter with a 10 second time constant was used on the raw bubble velocity and blue bubble colour signals. This was necessary as the measurement signals were very noisy.

## *7.2) Controller Testing*

Communications to and from the plant PLC to the soft PLC was done with OPC (Open Protocol Connection), which is the standard for real time Ethernet communications in the process industry. The soft PLC runs from a normal PC.

### 7.2.1) Initial Implementation

After system identification was performed on the plant and prior to the design of the multivariable controllers, two PI control loops with small gains and long integral time constants were implemented on bubble velocity and blue colour signals running simultaneously. This was done before any process changes occurred. The closed loop responses for these loops are given in Figure 7-1. Both the velocity and blue colour signals were filtered after control for presentation in the graph. From this figure it can be seen that the level control loop is having difficulty in maintaining the level to its changing setpoint. Possible reasons for this are the continual change in the pressure at the cell outlet due to changes in the air addition and pulp level. This effect is looked at and discussed in more detail in Appendix F.

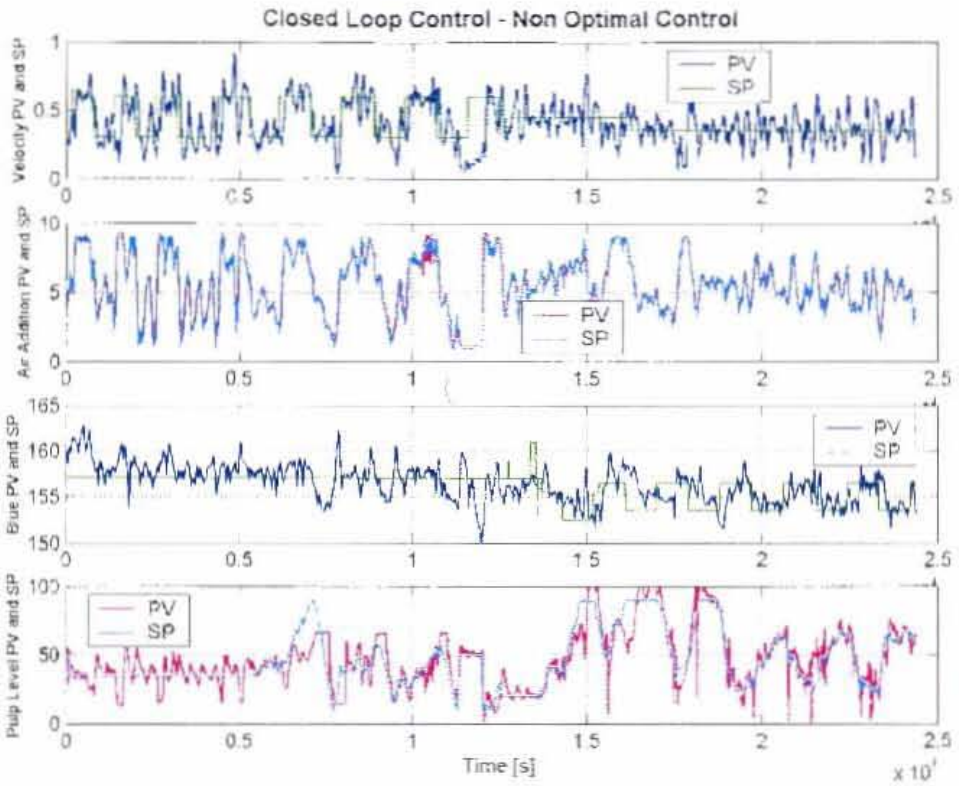


**Figure 7-1: Non-optimal no decoupling closed loop control.**

From Figure 7-1 it can be seen that only the bubble velocity control loop was operational for the first 5 500 seconds after which the bubble colour control loop was switched on. For the first 12 500 seconds the bubble velocity setpoint was stepped up and down every 900 seconds while blue colour setpoint was kept constant from 5 500 to 12 500 seconds. After 12 500 seconds the velocity setpoint was kept constant and the blue colour setpoint was stepped up and down every 1100 seconds.

### Setpoint selection

From a metallurgical point of view it was relatively easy to select an operating range within which the bubble velocity setpoint should be (The velocity setpoint was stepped between the limits of this range in the above closed loop experiment.). This was done by running the velocity control loop at different setpoints and then by visual inspecting of the flotation cell, checking whether the mass pull obtained was within conditions that

experience operators would run the plant at. There was no procedure or method by which metallurgically acceptable ranges for the blue colour setpoints could be selected. The reason for this is that bubble colour, in the case of PGM froths has not been related to metallurgical performance yet. Furthermore the colour measurement, besides having day-night correlated fluctuations, as a result of light changes, was also slowly drifting in its measurement over time. This was probably a result of degrading of the light source. This meant that the absolute measurement of colour was also not reliable in terms of relating a measured value to metallurgical performance. Consequently the colour setpoints for the specific period during which the colour controller was tested, was selected by taking the value of the blue measurement at the minimum and maximum pulp levels.

In summary of the given implementation, the following can be concluded:

- Both the bubble velocity and blue colour can be controlled independently.
- Pulp level seems to be less stable with changes in air addition and pulp level setpoints.
- A velocity setpoint can be selected based on operator experience while the same could not be done for the colour measurement.
- The interaction between the measurements does not seem to be significant enough to make the control loops oscillate so as to necessitate multivariable control.

### 7.2.2) Process Changes

Due to continual development of Anglo Platinum's machine vision (SmartFroth) system various upgrades are done on the system from time to time. The major upgrades of the camera system since the system identification was software upgrades that gave more refined measurements and a major hardware upgrade. The hardware upgrade included the installation of new cameras on every cell in the primary rougher bank each with a hood that prevented direct sunlight from shining on the froth. A different kind of spotlight to that of the previous installation was installed.

The other major process change that BRPM went through was a gradual ore type change. BRPM is a very young plant and the mining operation is continually being developed and expanded. During system identification and the initial implementation a major part of the feed to BRPM consisted of open cast material. This gradually changed until most of the feed became fresh underground ore. A change in ore type is the single biggest disturbance to a flotation plant.

Unfortunately the camera system was upgraded before the designed controllers could be tested. It was therefore anticipated that the designed controllers might not perform according to their designs.

### 7.2.3) Designed PI Control

#### No decoupling PI control

The parameters determined in section 6.4 were used for the bubble velocity control loop while the bubble colour loop was given a small gain (10 % of the optimally determined value) and a long integral time constant (4 times longer then the optimal value). Given in Figure 7-2 is the closed loop bubble velocity response. It can be seen that from 7900 seconds onwards the velocity loop seems to start oscillating as the air addition PV moved further away from its setpoint. As a result the gain of the velocity controller was reduced from 24 to 15. This reduced the aggressiveness of the controller and the air addition control loop was then almost able to maintain the air PV at its set point. Both the control loop gains were then further adjusted until the air addition and pulp level loops were able to maintain the changing setpoints. The final controller settings were $K_{c1}$=12, $K_{c2}$= 10, $K_{i1}$=0.021 and $K_{i2}$=0.028, while the optimal values were $K_{c1}$=24, $K_{c2}$= 31, $K_{i1}$=0.0235 and $K_{i2}$=0.0504. It can be concluded from this that the speed of the bubble velocity and bubble colour controllers is restricted by the speed of the air addition and pulp level control loops. The dynamics of the air addition and pulp level control loops should therefore be included in future machine vision controller designs.

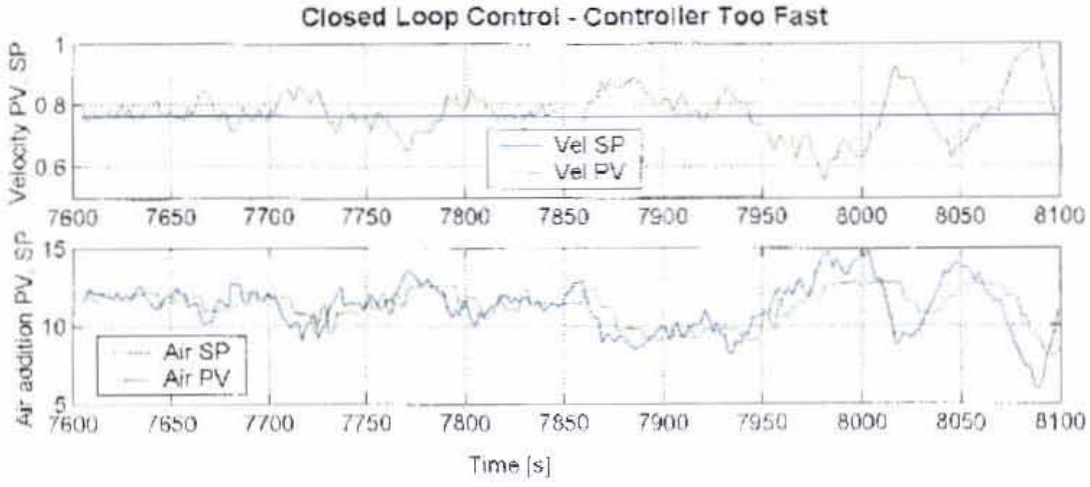


**Figure 7-2: Simulation determined optimal PI controllers parameters to fast.**

The controllers with these settings were left running and changes were made to the bubble velocity and colour setpoints. From Figure 7-3 it can be seen that the velocity control loop is well tuned and controlled closely around its setpoint. The same cannot be said for the blue control loop. The problems for this loop starts with the level control loop that only maintains the level PV to its setpoint during certain periods. Also the blue colour does not seem to respond to level changes as well as it did earlier in the project as shown in Figure 7-1.

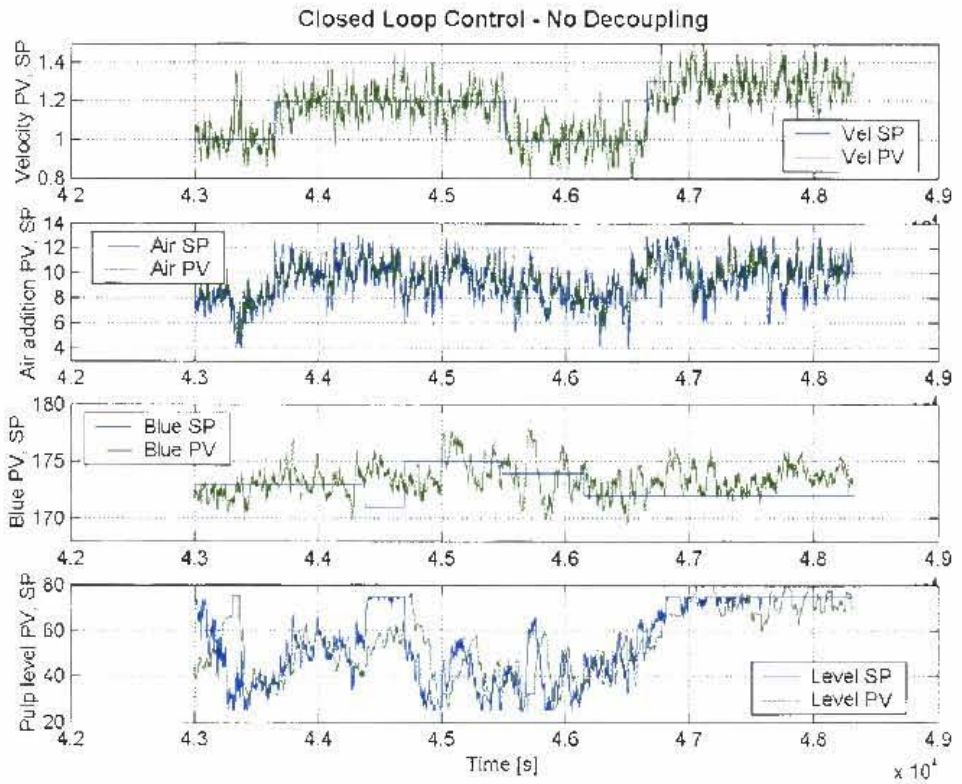


**Figure 7-3: Closed loop control with detuned PI controller parameters.**

The fact the blue colour response worsened could possibly be attributed to the process conditions that changed since the initial test work was done. The fact that a different spotlight was installed had an influence on the average value of colour. A stronger light source would increase the average colour measurement while a weaker light would decrease the average colour measurement. It might be that there exists an optimal light strength at which relative changes in colour as a result of input perturbations would be at a maximum. Since the average, night, blue colour measurement is different now compared to when the initial test work was done, might mean that the light source is not optimal for maximum relative changes in colour for input changes.

The new camera that was installed had a different fixed zoom to that of the previous installation and since the bubble velocity is measured pixels/s, this would have changed the measured bubble velocity gain. From plant data it was estimated that the gain has

increased by ±30%. Any future machine vision modelling should use an absolute measure of velocity.

In order to make an estimate of how much the plant models have changed, a comparison of plant and simulation responses was done. The air addition and pulp level setpoints, as well as the actual air addition and pulp level values from the above implementation was put through the plant model. The results are shown in Figure 7-4. The model would not account for any process disturbances so that this might have caused some bias in the model outputs.

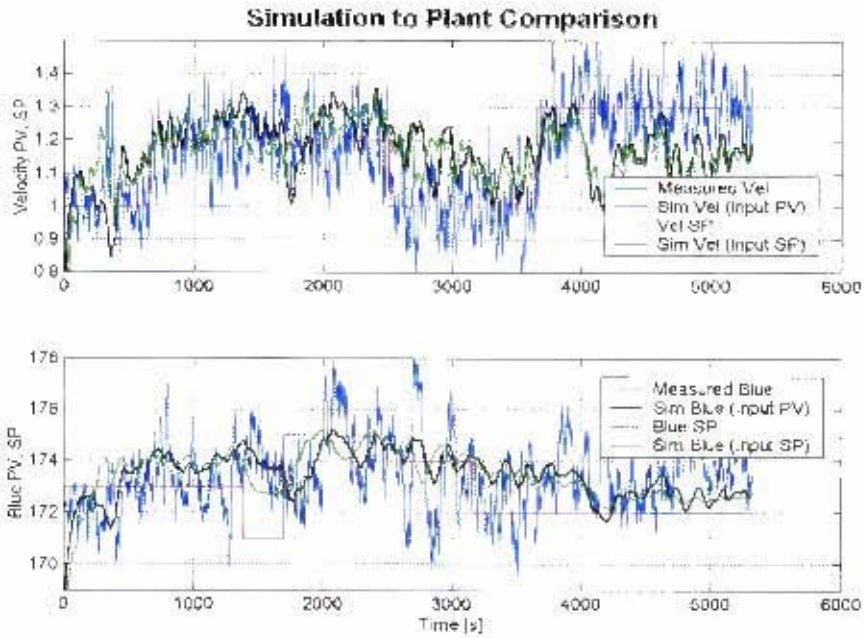


**Figure 7-4: Comparison of plant to simulation results.**

From this comparison it can be seen that the velocity gain of the process has increased, as the model outputs are not changing by the same magnitude as that of the process for the same input changes. The bubble colour model appears to be tracking the actual measurement better over certain ranges. It also seems that the bubble colour gain has increased, as changes in the bubble colour measurement are smaller in magnitude to the measured signal. There are irregular, sudden movements in the measured blue signal that is not described by the model so that this can only be attributed to disturbances. In conclusion it can be said that the process gains as measured by the

sensor have changed, but not by a significant amount such that the designed controller would not function anymore. From Figure 7-3 it can be seen that the velocity loop is functioning properly and that there is a problem with the colour loop. The sudden changes in the blue colour from Figure 7-4 that is not captured by the plant model and therefore assumed to be disturbances might be the reason for the poor performance of the colour loop. If the colour is subjected to excessive disturbances it can result in poor controller performance.

**$k_{12}$ decoupling control**

The $k_{12}$ decoupling controller was briefly implemented with the same, slower PI parameters as used previously or the PI controller with no decoupling. The results were worst compared to those obtained without the decoupling controller. This was attributed to the changes in the process model and it was decided not to refine this decoupling controller since its $k_{12}$ block is derived from the old plant models.

### 7.2.4) Internal Model Control (IMC)

In section (6.8) it was determined that the IMC controller performance (compared to the other controllers) was the most sensitive to changes in the plant model. It was therefore suspected that the IMC controller would not perform well for the changes in process conditions that occurred.

Closed loop results for the IMC controller is given in Figure 7-5. The control on both loops is poor as a result of the following reasons:

1) The model used to derive the controller does not represent the process very well anymore.
2) IMC parameters have been tuned to be as fast as possible within input constraints so that the air addition and pulp level control loops cannot maintain the setpoints.
3) The colour signal seems to be less responsive to level changes as originally determined by the system identification.

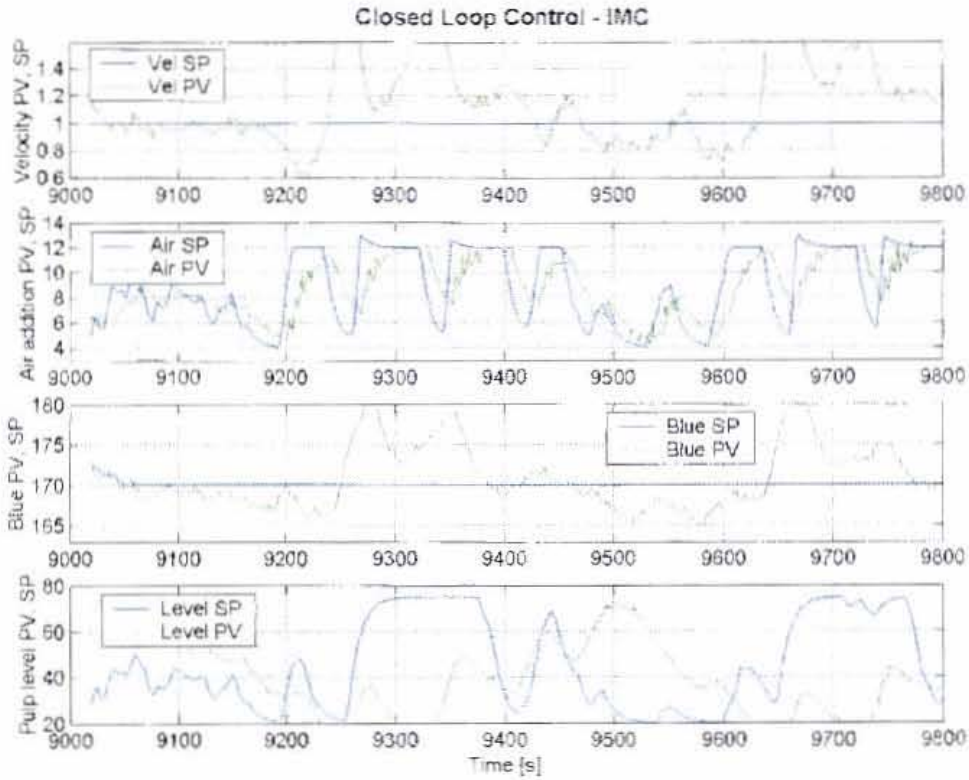


**Figure 7-5: Closed loop control – IMC.**

### 7.2.5) Discussion on Controller Implementation Results

Under circumstances where the process experience major changes the system identification should be repeated, new plant models should be obtained and a new controller must be designed. It was decided not to do this for the following reason: Since the start of this project other machine vision projects was initiated. One of these focussed on relating bubble velocity and the bubble colour measurements to metallurgical performance. From this test work (Anglo Platinum internal project) bubble velocity are being related to concentrate mass pull while the colour measurement could not be related to the metallurgical performance of the cell. Further more the colour measurement was also very sensitive to external light changes and did not always seem to be consistent in its responses to air addition and pulp level changes. A decision was made that the colour measurement is therefore not suitable for industrial implementation.

This meant that the industrial implementation of camera control over the short term would only be concerned with bubble velocity and it's inferential to mass pull. It was therefore not worth putting any more effort, time and money into refining the multivariable control of bubble velocity and bubble colour.

In summary the following control issues and metallurgical topics have been identified as important considerations for the implementation of machine vision outputs.

- Bubble velocity is a stable and reliable output, which can be effectively controlled to a setpoint by manipulating the air addition, while bubble colour is not yet suited for industrial implementation.
- Manipulation of the air addition and pulp level setpoints continually changes the pressure drop between two cells. This makes efficient control of the pulp level difficult. A gain scheduling type pulp level controller might improve pulp level control under such conditions.
- Relating machine vision outputs in terms of metallurgical performance is essential for optimal setpoint selection.
- Machine vision controllers that changes either the air addition or pulp level setpoints can only be as fast as what the air addition and pulp level controllers can maintain the changing setpoint.

# 8. Discussion and Conclusions

From the literature, not much is published on automated flotation control using machine vision outputs. Of the two publications that do cover the topic, both controller implementations were sub optimal as the control actions only consisted of an if-then rule base that made fixed incremental percentage changes to the manipulated variables. From the lack of information in the literature on this topic, it was concluded that the research and implementation on the application of machine vision is still in its early developing phases.

A system identification exercise showed that machine vision outputs of SmartFroth were linearly related to air addition, pulp level, initial concentrate grade, initial concentrate flow rate, initial concentrate % solids and flotation feed dry tonnage so that linear control theory could be applied. This linear relationship only applied to two machine vision outputs namely bubble velocity and bubble colour. The average bubble area also seemed to have a linear increase in its gain for step changes to the pulp level.

Linear dynamic models of the machine vision outputs were analysed and it was determined that the biggest operating region for MIMO control exists when the air addition is manipulated to control the bubble velocity and the pulp level is manipulated to control the blue bubble colour. The multivariable controller was relatively simple as there was not much interaction between the two loops, as shown by the relative gain array with a relative gain of 1.49. Different decoupling structures were tested in a simulation environment and it was found that the difference between the decoupling structures were small with no single decoupling structure outperforming any of the other structures. Other control techniques that were applied included internal model control (IMC) and LQG. The IMC controller performance was in line with the PI controllers with the decoupling structures. LQG control performed poorly in comparison with the other controllers so that this type of control is not recommended in this application. The three controllers that performed best under simulation based on IAE values were:

- PI control without decoupling.
- PI control with only the $k_{12}$ decoupler.

change in sensor type seemed to have altered the originally obtained process gains as measured by the new machine vision system.

- BRPM went through a gradual ore type change. During system identification and the initial implementation a major part of the feed to BRPM consisted of open cast material. This gradually changed until most of the feed became fresh underground ore. A change in ore type is the single biggest disturbance to a flotation plant.

As a result of the difficulties experienced with the colour measurement and its control it was decided that the measurement was not suitable for industrial implementation. The bubble velocity on the other hand showed great potential as a controllable machine vision measurement. SISO control of the bubble velocity to air addition currently seems to hold the biggest potential for online machine vision control.

# 9. Recommendations

The financial benefits of machine vision cannot be determined on only one flotation cell (or would be very difficult to do), since flotation profit is dependant on the performance of a whole flotation stage or circuit that consists of many flotation cells. It is recommended to expand the machine vision system from one cell to a whole flotation stage. From this project it is known that bubble velocity can be controlled to a setpoint and colour or bubble area could not. The expansion of the camera system to the whole rougher stage could then be used to determine if there is any financial benefits or ease of operation incentive with closed loop velocity control.

Further and more detailed recommendations on work that needs to be done towards an overall flotation control strategy would be:

- More research on relating machine vision outputs to metallurgical performance with specific reference to bubble velocity and colour is required.
- Gain scheduling may be of use as it might improve pulp level control (see appendix A).
- System identification was done but not applied in a controller design for OSA measurements. The dynamic models for the OSA system could be used to design a stabilisation controller for OSA measurements.
- The simulation that was used for this controller design can be improved by including the dynamics of the air addition and pulp level sensors and as well as their controllers.

# 10. List of References


1. Aldrich C, Moolman DW, Bunkell SJ, Harris MC and Theron DA.

   *Relationship between surface froth features and process conditions in the batch flotation of a sulphide ore.*
   Minerals Engineering Vol. 10, Elsevier Science Ltd, 1998.

2. Banford AW, Aktas Z and Woodburn ET.

   *Interpretation of the Effect of Froth Structure on the Performance of Froth Flotation using Image Analysis.*
   Powder Technology 98, Elsevier Science Ltd, 1998.

3. Bazin C, Trusiak AR and Hodouin D.

   *Application of a dynamic material balance program to an industrial flotation plant.*
   Minerals Engineering, Vol. 12, Elsevier Science Ltd, 1999.

4. Bezuidenhout M, Moolman DW and Van Deventer JSJ.

   *The Identification of Perturbations in a Base Metal Flotation Plant using Computer Vision of the Froth Surface.*
   Minerals Engineering, Vol. 10, 1997

5. Bergh LG, Yianatos JB, Acuna CA, Perez H and Lopez F.

   *Supervisory Control at Salvador Flotation Columns.*
   Minerals Processing, CIM Bulletin, 1995.

6. Bonifazi G, Massacci P and Meloni A.

   *Prediction of Complex Sulphide Flotation Performances by a Combined 3D Fractal and Colour Analysis of the Froths.*
   Minerals Engineering, Vol. 13, Elsevier Science Ltd, 2000.

7. Braae M

   *Multivariable Feedback Control*
   University of Cape Town, Postgraduate class notes.

8. Cipriano A, Guarini, M, Soto A, Briceno H and Mery D

   *Expert Supervision of Flotation Cells using Digital Image Processing*
   Proceedings of the XX IMPC – Aachen, pp. 281 – 292, September 1997.

9. Cipriano A, Guarini M, Vidal R, Soto A, Sepulveda C, Mery D and Briseno H

   *A Real Time Visual Sensor for Supervision of Flotation Cells*
   Miner. Eng., Vol. 11, No 6, pp. 489 - 499,1998.

10. De Never N

    *Fluid Mechanics for Chemical Engineers*
    McGraw-Hill, Inc, 1991.

11. Dutton K, Thompson S and Barraclough B

*Control Engineering*
Addison Wesley Longman Ltd., 1997.

12. Gagnon E, Pomerleau and Desbiens A.

*Simplified, ideal or inverted decoupling?*
ISA Transactions 37, Elsevier Science Ltd., 1998

13. Hargrave JM and Hall ST

*Diagnosis of Concentrate Grade and Mass Flowrate in Tin Flotation from Colour and Surface Texture Analysis.*
Minerals Engineering, Vol. 10, Elsevier Science Ltd., 1997

14. Hargrave JM, Miles NJ and Hall ST

*The use of grey level measurement in predicting coal flotation performance.*
Minerals Engineering, Vol. 9, Elsevier Science Ltd., 1996

15. Hodouin D, Jamsa-Joulena SL, Carvalho MT and Bergh L

*State of the art and challenges in mineral processing control.*
Control Engineering Practice, Vol 9, Elsevier Science Ltd, 2001.

16. Holtham PN and Nguyen KK

*On-line analysis of froth surface in coal and mineral flotation using JKFrothCam.*
Mineral Processing 64, Elsevier Science Ltd., 2002

17. Hyotyniemi H and Ylinen R.

*Modeling of Visual Flotation Froth Data .*
Control Engineering Practice 8, Elsevier Science Ltd., 2000

18. Hyotyniemi H, Ylinen R and Miettunen J.

*AI in Practice: Case Study on a Flotation Plant*
Helsinki University of Technology, Control Engineering Laboratory Report, 2001

19. Kittel S, Galleguillos P and Urtubia H.

*Rougher Automation in Escondida Flotation Plant*
Minera Escondida, BHP Copper, Antofagasta, Chile.

20. LaPlante PA

*Comprehensive dictionary of electrical engineering*
CRC Press & IEEE Press, 1999.

21. Ljung L

*Linear System Identification User's Guide*
The Mathworks, Inc., 2001.

22. Lynch AJ, Johnson NW, Manlapig EV and Thorne CG

*Mineral and Coal Flotation Circuits – Their Simulation and Control*

Elsevier Scientific Publishing Company, Amsterdam and New York, 1981.

23. Lynch AJ and McKee DJ

*The Modelling and Control of Mineral Processing Plants*
Plenary Lecture: Proceedings of MINTEK 50, International Conference on Mineral Science and Technology (ed. Haughton LF) Sandton, South Africa, 1984.

24. Maciejowski JM

*Multivariable feedback design.*
Addison-Wesley Publishers Ltd., 1989.

25. Manlapig EV, Thornton AJ and Gonzalez G.

*Application of Adaptive Control in the Copper Concentrator, Mount Isa Mines.*
Process Development Department Mount Isa Mines, Mount Isa.

26. McKee DJ

*Case Studies of Flotation Control*
In "Innovations in Flotation Technology" Editors Mavros P and Matis KA, pp 235 – 262, Kluwer Academic Publishers, Netherlands, 1992.

27. Moolman DW, Aldrich C, Schmitz GPJ and Van Deventer JSJ

*The Interrelationship between Surface Characteristics and Industrial Flotation Performance*
Minerals Engineering, Vol. 9, No. 8, pp. 837 – 854, 1996a.

28. Moolman DW, Eksteen JJ, Aldrich C and Van Deventer JSJ

*The Significance of Flotation Froth Appearance for Machine Vision Control*
Int. J. Miner. Process., Vol. 48, pp. 135 – 158, 1996b.

29. Napier-Munn TJ

*An Introduction to Comparative Statistics and Experimental Design for Minerals Engineers*
Course Notes, 2nd Edition, Version 2.2, The University of Queensland, 1996.

30. Niemi AJ, Ylinen R and Hyotyniemi

*On characterization of pulp and froth in cells of flotation plant*
Int. J. Miner. Process. 51, Elsevier 1997

31. Ogunnaike BA and Ray WH

*Process Dynamics, Modeling and Control.*
Oxford University Press, New York and Oxford, 1994.

32. Seborg DE, Edgar TF and Mellichamp DA

*Process Dynamics and Control.*
Johnson Wiley & Sons, New York, 1989.

33. Smar VD, Klimpel RR and Aplan FF

*Evaluation of chemical and operational variables for the flotation of a copper ore Part I.*
Minerals Processing, Vol 42, Elsevier, 1994.

34. Storn R

*On the Usage of Differential Evolution for Function Optimization.*
Siemens AG, Germany, storn@icsa.berkeley.edu.

35. Suichies M, Leroux D, Dechert C and Trusiak A.

*An implementation of generalized predictive control in a flotation plant.*
Control Engineering Practice 8, Elsevier, 1999.

36. Sweet CG

*The Application of a Machine Vision System to Relate Froth Surface Characteristics to the Metallurgical Performance of a PGM Flotation Process.*
MSc, Chemical Engineering Department, University of Cape Town, 2000

37. Ventura E and Cilliers JJ

*A model to describe flotation performance based on physics of foams and froth image analysis.*
Minerals Processing, 1574, Elsevier, 2002

38. Ventura E

*Flotation froth structure and performance*
PHD, University of Manchester, Department of Chemical Engineering, 2000

39. Wills BA

*Mineral processing technology.*
Pergamon Press Ltd, Oxford, England, 1992.

34. Storn R

*On the Usage of Differential Evolution for Function Optimization.*
Siemens AG, Germany, storn@icsa.berkeley.edu.

35. Suichies M, Leroux D, Dechert C and Trusiak A.

*An implementation of generalized predictive control in a flotation plant.*
Control Engineering Practice 8, Elsevier, 1999.

36. Sweet CG

*The Application of a Machine Vision System to Relate Froth Surface Characteristics to the Metallurgical Performance of a PGM Flotation Process.*
MSc, Chemical Engineering Department, University of Cape Town, 2000

37. Ventura E and Cilliers JJ

*A model to describe flotation performance based on physics of foams and froth image analysis.*
Minerals Processing, 1574, Elsevier, 2002

38. Ventura E

*Flotation froth structure and performance*
PHD, University of Manchester, Department of Chemical Engineering, 2000

39. Wills BA

*Mineral processing technology.*
Pergamon Press Ltd, Oxford, England, 1992.

# Appendix A

# Step Test Plots and System Identification Graphs

Given in this section are the responses of the outputs that was not used in the controller design. The first set of plots show the raw data with an average value and the second set of plots shows the dynamic model that was fit to the average value. The parameters for the dynamic models are given in Table (5-6). The time axis units for the machine vision outputs (average bubble area) are 20 seconds per axis unit and that of the OSA outputs are given in minutes.

The dynamic models fitted to the OSA responses are given as it was obtained from the DE optimisation routine. Some of these responses does not seem to have reached steady state, however the residence time of the flotation cell is about 4 minutes and the process was given at least 16 minutes before a next step change was made. The process should therefore have reached steady state (at least four times the residence time) so that the assumption can be made that any drift or deviation was as a result of feed disturbance changes and not input changes. Some of these models can be refined by fixing the process gain based on a visual observation and then only regress for the time constants.

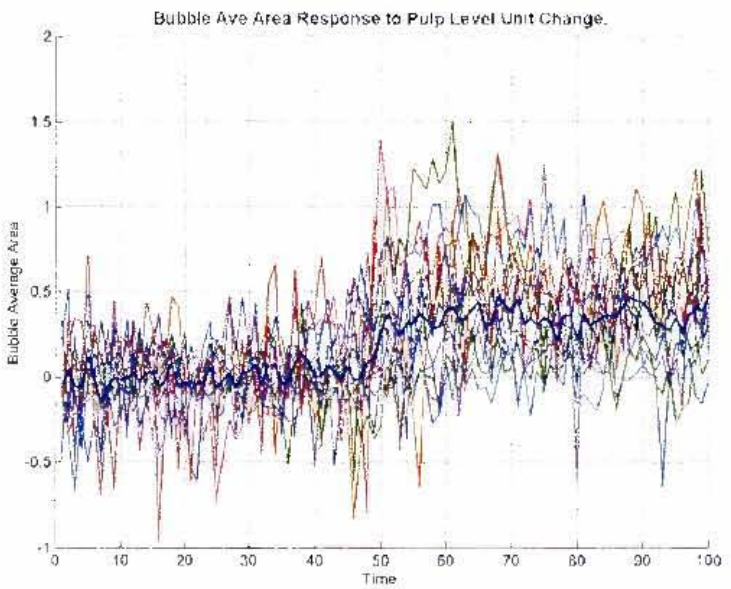


**Figure A.1: Average bubble area responses for pulp level step changes.**

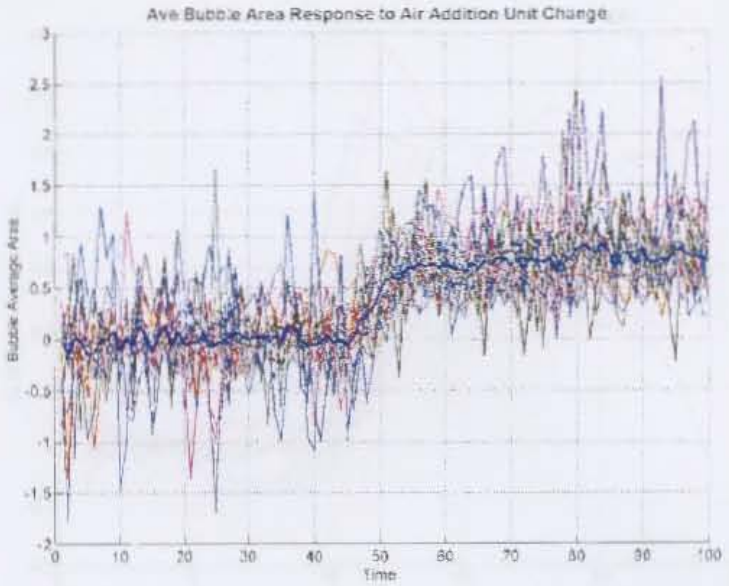


Figure A.2: Average bubble area responses for air addition step changes.

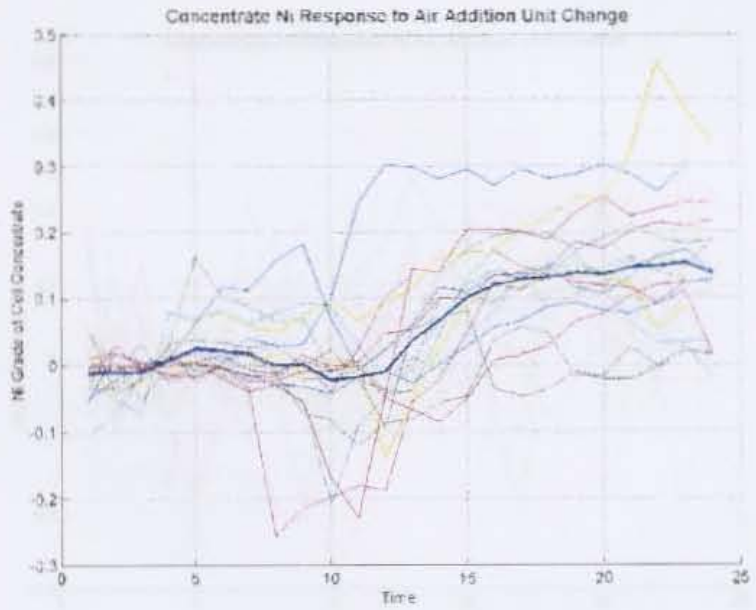


Figure A.3: Ni concentration responses for air addition step changes.

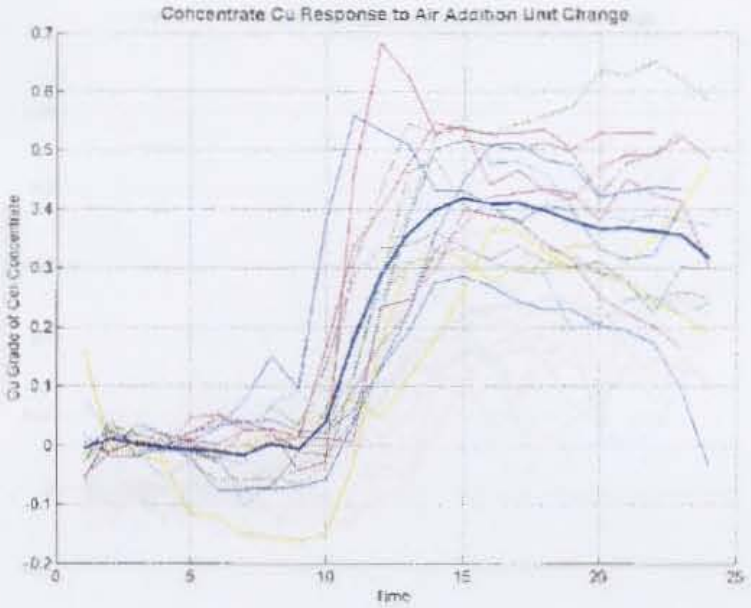


Figure A.4: Cu concentration responses for air addition step changes.

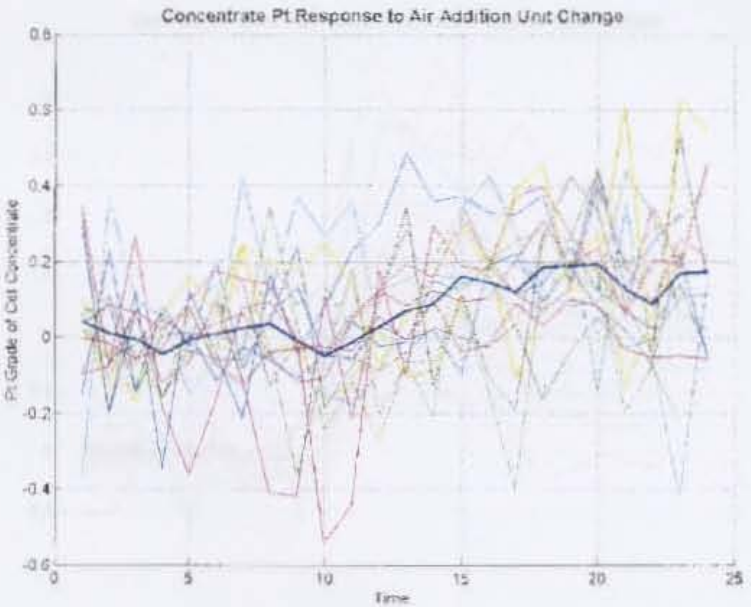


Figure A.5: Pt concentration responses for air addition step changes.

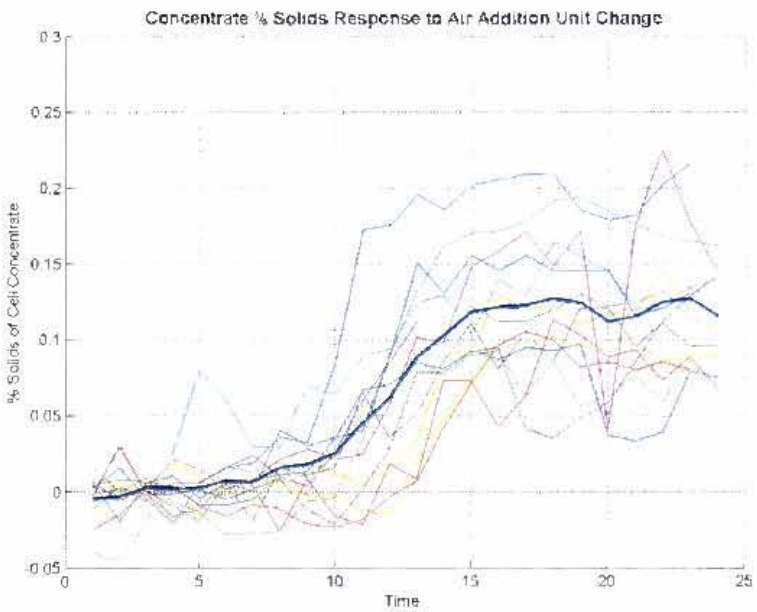


Figure A.6: % Solids responses for air addition step changes.

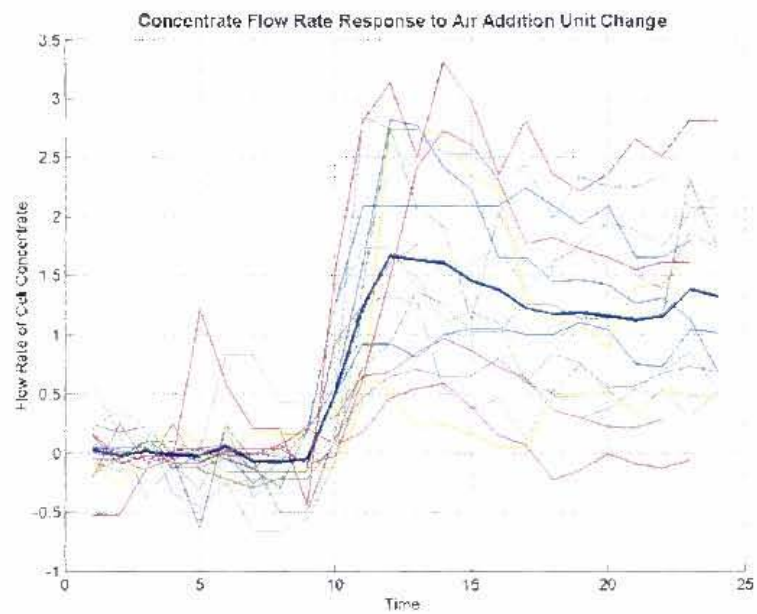


Figure A.7: Concentrate flow rate responses for air addition step changes.

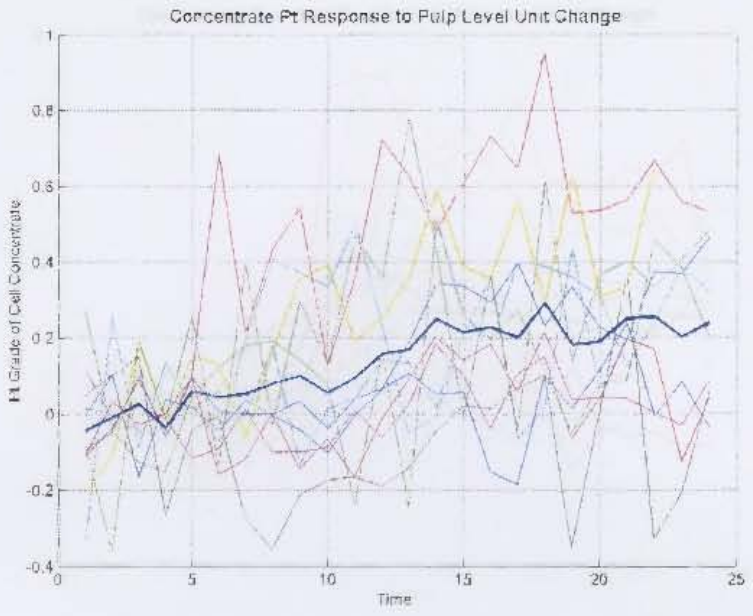


Figure A.10: Pt concentration responses for pulp level step changes.

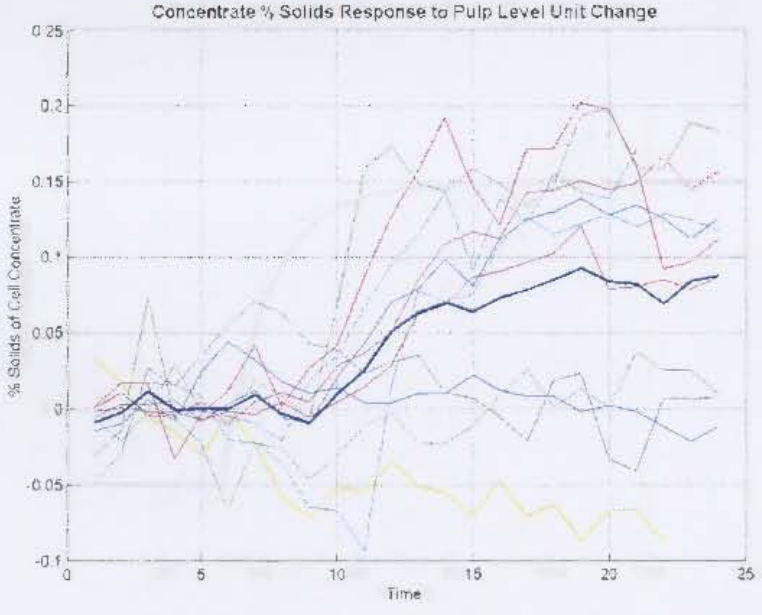


Figure A.11: Concentrate % solids responses for pulp level step changes.

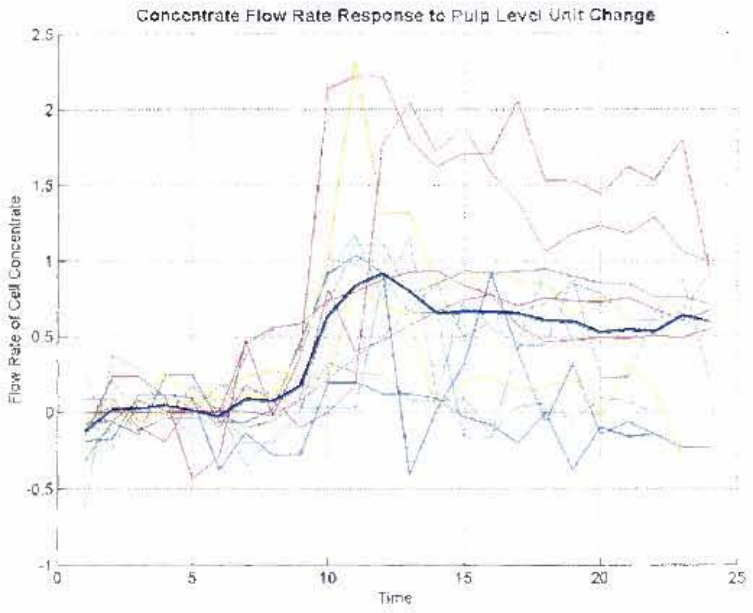


Figure A.12: Concentrate flow rate responses for pulp level step changes.

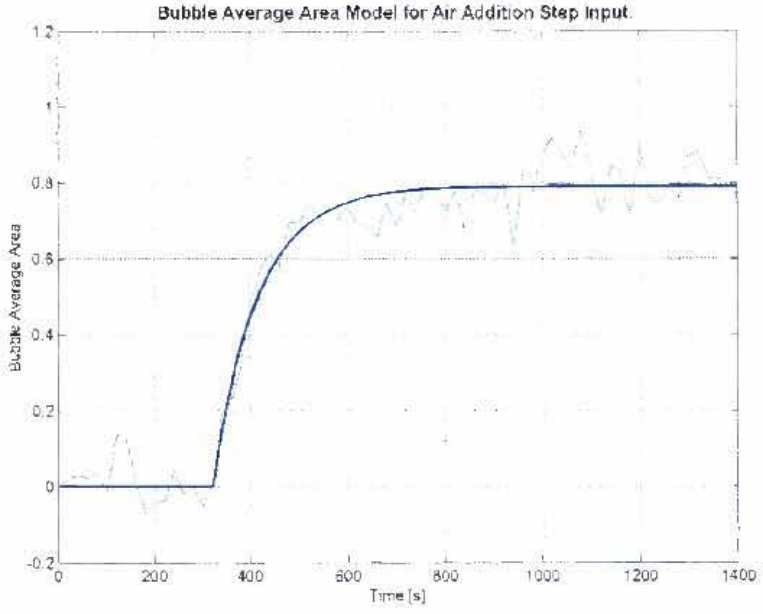


Figure A.13: Average bubble area response to a unit air addition step change.

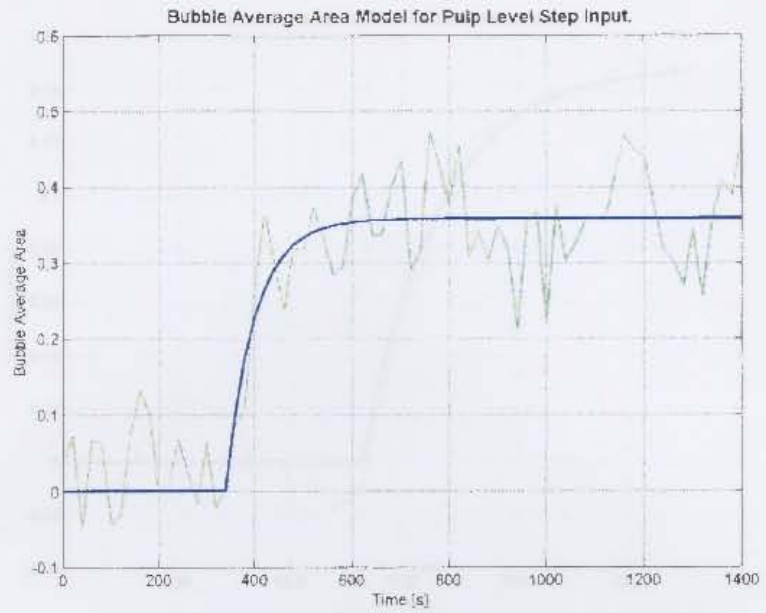


Figure A.14: Average bubble area response to a unit pulp level step change.

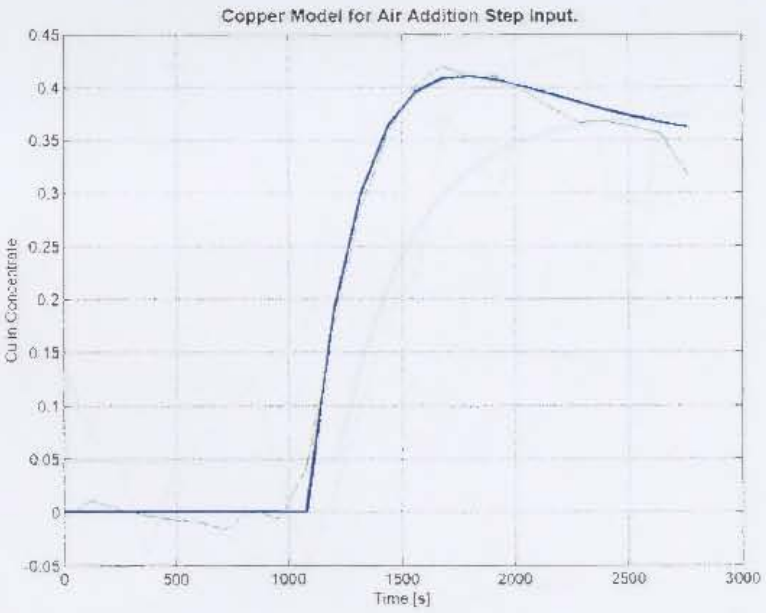


Figure A.15: Average Cu concentration response to a unit air addition step change.

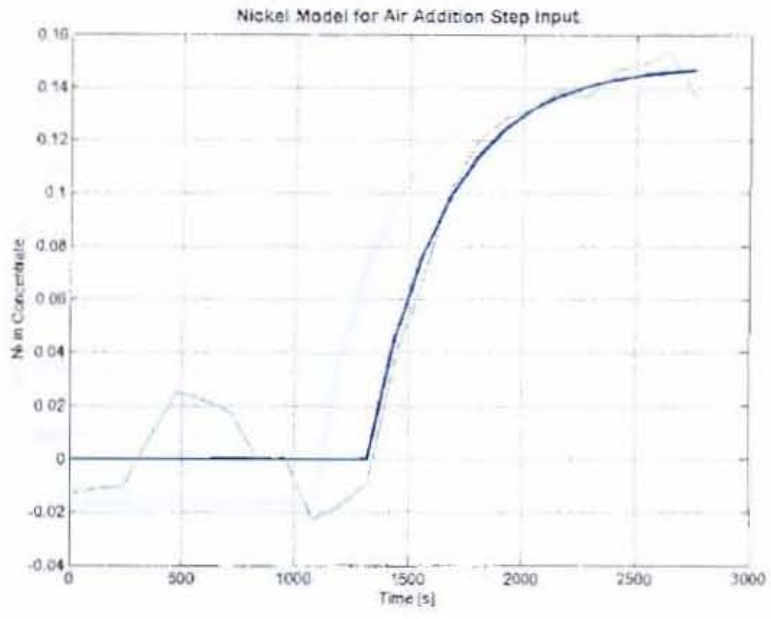


**Figure A.16: Average Ni concentration response to a unit air addition step change.**

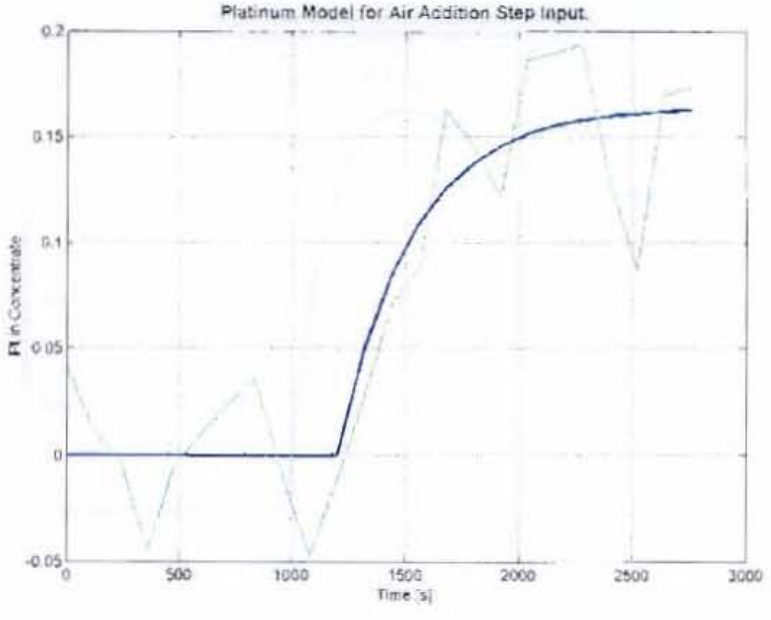


**Figure A.17: Average Pt concentration response to a unit air addition step change.**

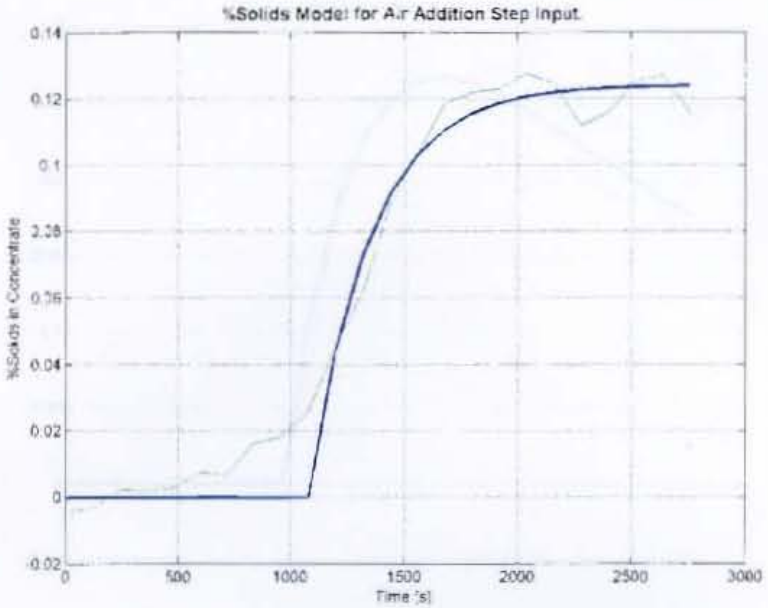


**Figure A.18: Average % solids response to a unit air addition step change.**

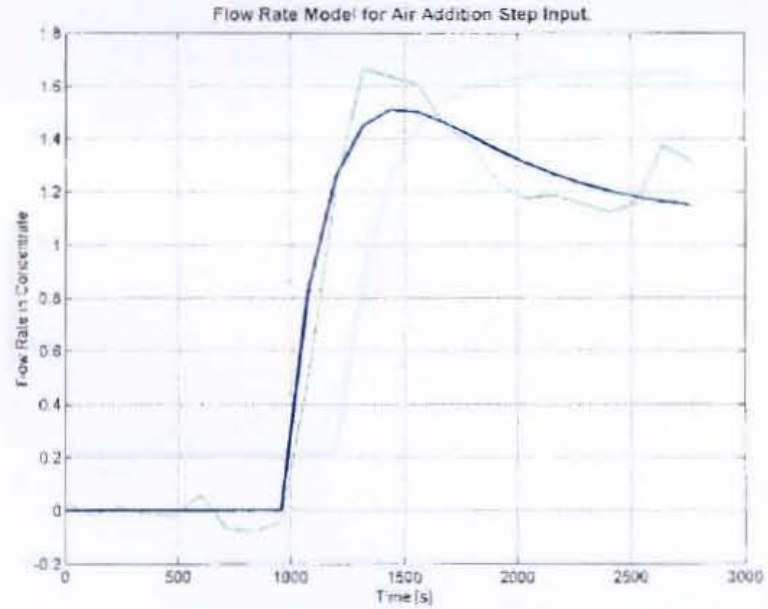


**Figure A.19: Average concentrate flow rate response to a unit air addition step change.**

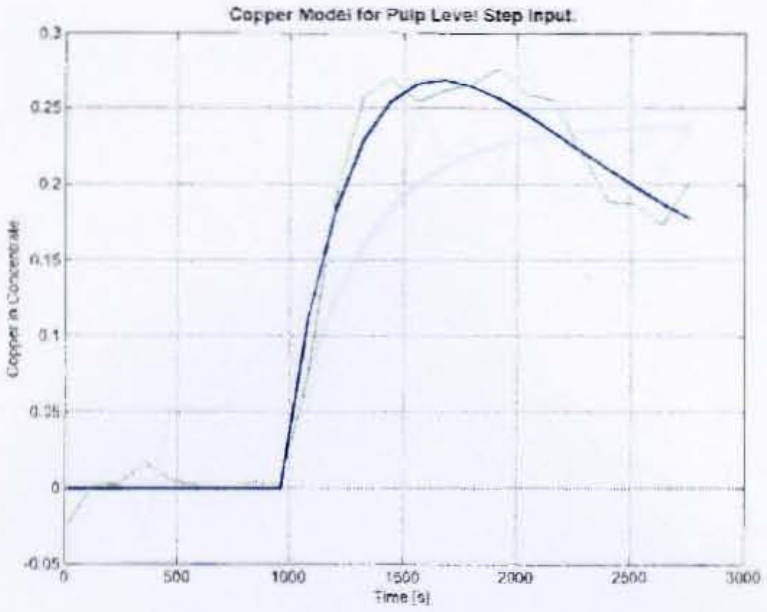


**Figure A.20: Average Cu concentration response to a unit pulp level change.**

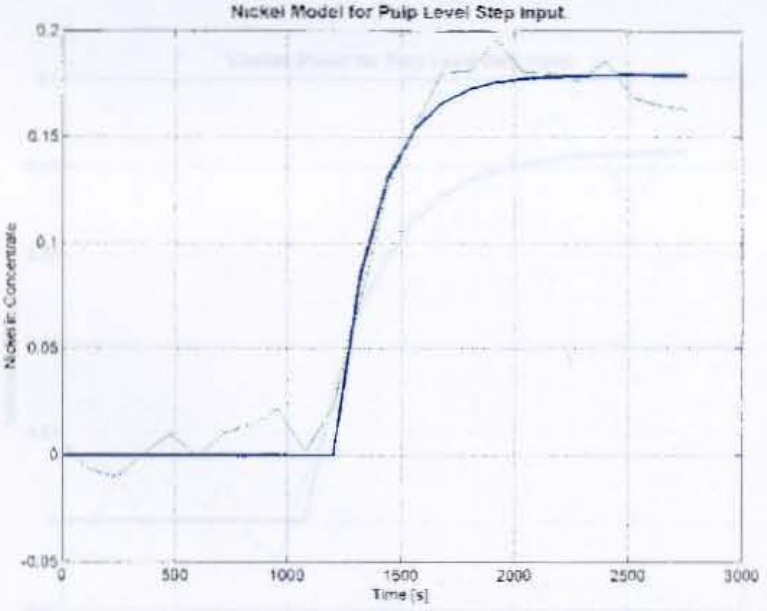


**Figure A.21: Average Ni concentration response to a unit pulp level change.**

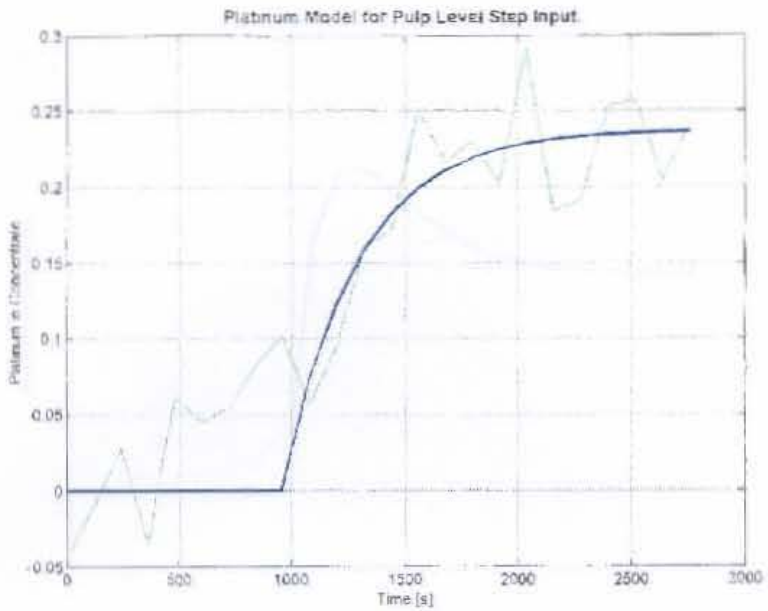


Figure A.22: Average Pt concentration response to a unit pulp level change.

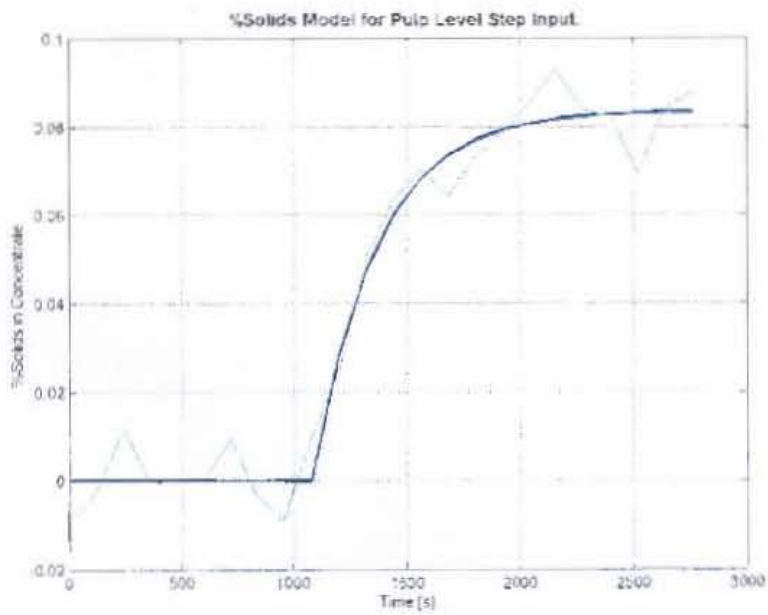


Figure A.23: Average % solids response to a unit pulp level change.

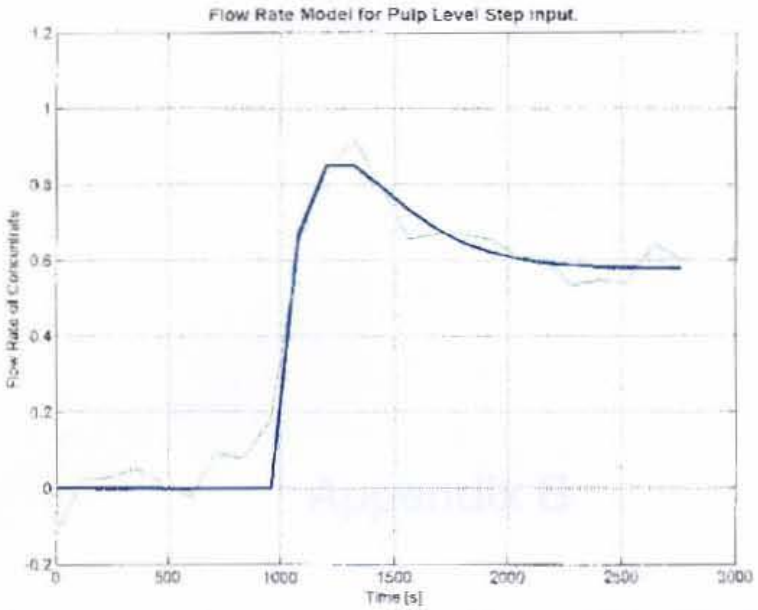


Figure A.24: Average concentrate flow rate response to a unit pulp level change.

# Appendix B

# Numerical Controller Transfer Functions

As a quick reference the numerical controller parameters and transfer functions are provided in this section.

**Tuning results of all the decoupling designs.**

| No | Structure | $K_{c1}$ | $K_{I1}$ | $K_{c2}$ | $K_{I2}$ | IAE 1 | IAE 2 |
|---|---|---|---|---|---|---|---|
| 0 | $G_{pm1}$ and $G_{pm2}$ | 22.8 | 0.0209 | 29.6 | 0.0329 | - | - |
| 1 | No decoupling | 23.9 | 0.0235 | 31.2 | 0.0504 | 34.0 | 99.6 |
| 2 | Simplified | 22.9 | 0.0209 | 10.4 | 0.0555 | 30.4 | 151 |
| 3 | Only $k_{12}$ | 24.0 | 0.0206 | 14.2 | 0.0439 | 23.7 | 251 |
| 4 | Only $k_{21}$ | 23.4 | 0.0190 | 31.4 | 0.0380 | 36.9 | 51.3 |
| 5 | $K_{12}$-$q_{21}$ | 17.2 | 0.0158 | 11.6 | 0.0504 | 31.7 | 176 |
| 6 | $K_{21}$-$q_{12}$ | 22.7 | 0.0217 | 6.8 | 0.0509 | 26.6 | 159 |
| 7 | Inverted | 17.1 | 0.0161 | 10.4 | 0.0357 | 31.3 | 147 |
| 8 | Ideal | 9.95 | 0.0331 | 5.44 | 0.0664 | 30.9 | 152 |

Plant models used for controller design

$$g_{11} = \frac{0.07831}{50.13\,s + 1}$$

$$g_{21} = \frac{0.4344}{105.5\,s + 1}$$

$$g_{12} = \frac{0.00045491\,(s + 0.007273)}{(s + 0.05025)\,(s + 0.01802)}$$

$$g_{22} = \frac{0.06064}{29.31\,s + 1}$$

$$G_{pm1} = \frac{0.00065678\,(s + 0.0724)\,(s + 0.01678)\,(s + 0.01119)}{(s + 0.05025)\,(s + 0.01995)\,(s + 0.01802)\,(s + 0.009479)}$$

$$G_{pm2} = \frac{0.00086985\,(s + 0.0724)\,(s + 0.01678)\,(s + 0.01119)}{(s + 0.05025)\,(s + 0.03412)\,(s + 0.01802)\,(s + 0.009479)}$$

Numerical values for the decouplers

$$k_{12} = \frac{-0.29121(s+0.01995)(s+0.007273)}{(s+0.05025)(s+0.01802)}$$

$$k_{21} = \frac{-1.9902(s+0.03412)}{(s+0.009479)}$$

$$q_{12} = \frac{-0.69263(s+0.05025)(s+0.01995)(s+0.01802)(s+0.009479)(s+0.007273)}{(s+0.0724)(s+0.05025)(s+0.01802)(s+0.01678)(s+0.01119)}$$

$$q_{21} = \frac{-4.7336(s+0.05025)(s+0.03412)(s+0.01802)(s+0.009479)}{(s+0.0724)(s+0.01678)(s+0.01119)(s+0.009479)}$$

$$d_{11} = \frac{2.3785(s+0.05025)(s+0.03412)(s+0.01995)(s+0.01802)(s+0.009479)}{(s+0.0724)(s+0.03412)(s+0.01995)(s+0.01678)(s+0.01119)}$$

$$d_{21} = \frac{-4.7336(s+0.05025)(s+0.03412)(s+0.01995)(s+0.01802)(s+0.009479)}{(s+0.0724)(s+0.01995)(s+0.01678)(s+0.01119)(s+0.009479)}$$

$$d_{12} = \frac{-0.69263(s+0.05025)(s+0.03412)(s+0.01995)(s+0.01802)(s+0.009479)(s+0.007273)}{(s+0.0724)(s+0.05025)(s+0.03412)(s+0.01802)(s+0.01678)(s+0.01119)}$$

$$d_{22} = \frac{2.3785(s+0.05025)(s+0.03412)(s+0.01995)(s+0.01802)(s+0.009479)}{(s+0.0724)(s+0.03412)(s+0.01995)(s+0.01678)(s+0.01119)}$$

IMC with no pole zero cancellations

$$Gc_{11} = \frac{33.835(s+0.05025)(s+0.03412)(s+0.01995)(s+0.01802)(s+0.009479)}{(s+0.0724)(s+0.03412)(s+0.02222)(s+0.01678)(s+0.01119)}$$

$$Gc_{21} = \frac{-67.3379(s+0.05025)(s+0.03412)(s+0.01995)(s+0.01802)(s+0.009479)}{(s+0.0724)(s+0.02222)(s+0.01678)(s+0.01119)(s+0.009479)}$$

$$Gc_{12} = \frac{-5.9782(s+0.05025)(s+0.03412)(s+0.01995)(s+0.01802)(s+0.009479)(s+0.007273)}{(s+0.0724)(s+0.05025)(s+0.01802)(s+0.01786)(s+0.01678)(s+0.01119)}$$

$$Gc_{22} = \frac{20.5289(s+0.05025)(s+0.03412)(s+0.01995)(s+0.01802)(s+0.009479)}{(s+0.0724)(s+0.01995)(s+0.01786)(s+0.01678)(s+0.01119)}$$

# Appendix C

# Controller Evaluation Graphs

This section gives the closed loop responses of the controller designs not shown in the main document.

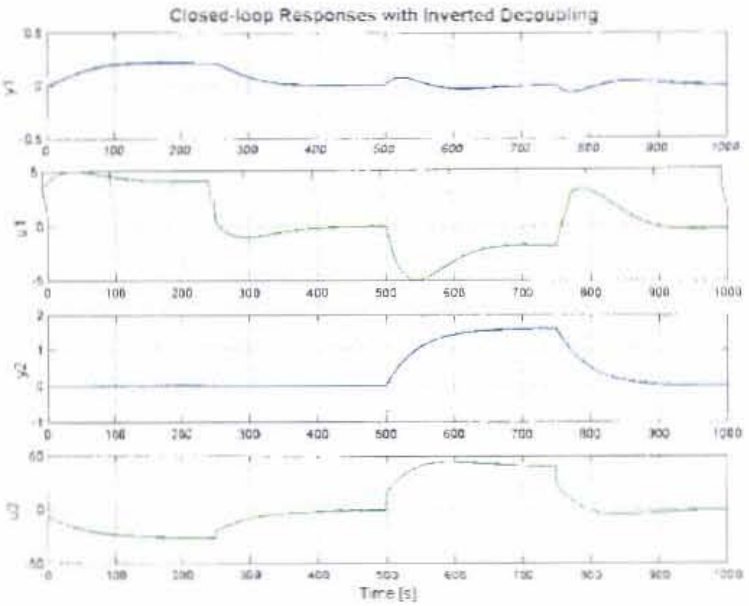


**Figure C.1: Optimally tuned closed loop responses for inverted decoupling.**

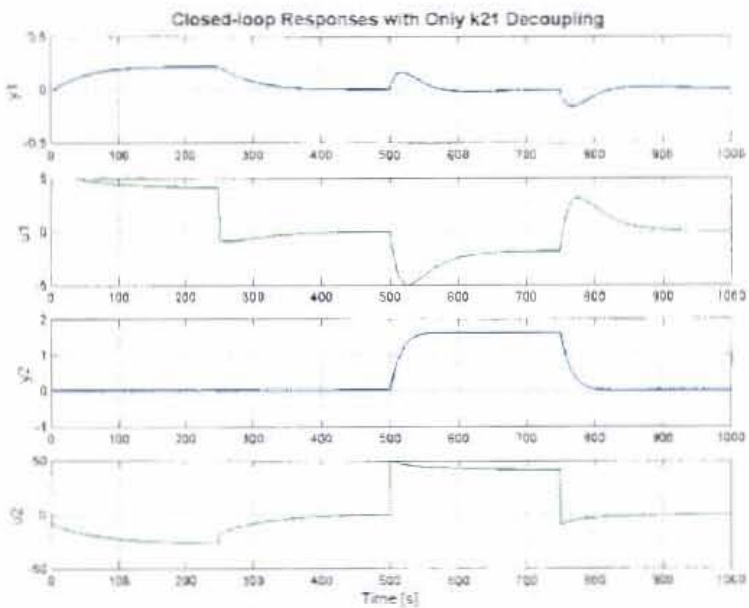


**Figure C.2: Optimally tuned closed loop responses for k21 decoupling.**

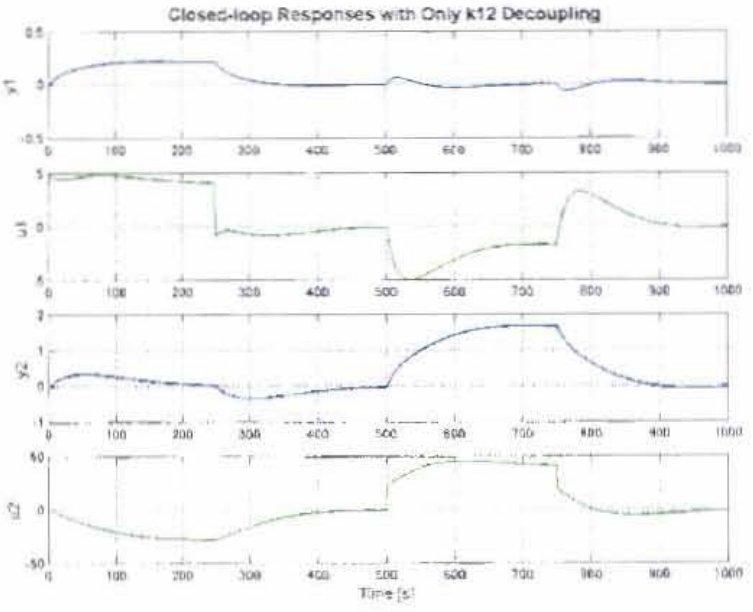


Figure C.3: Optimally tuned closed loop responses for k12 decoupling.

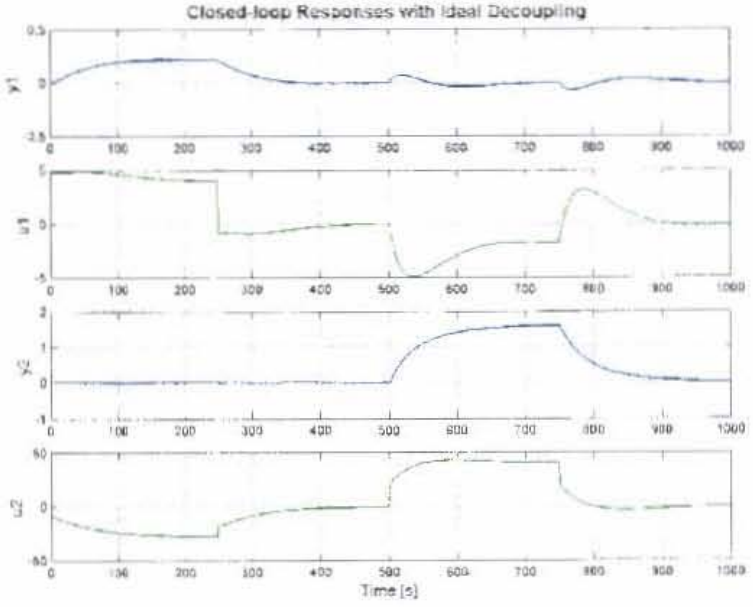


Figure C.4: Optimally tuned closed loop responses for ideal decoupling.

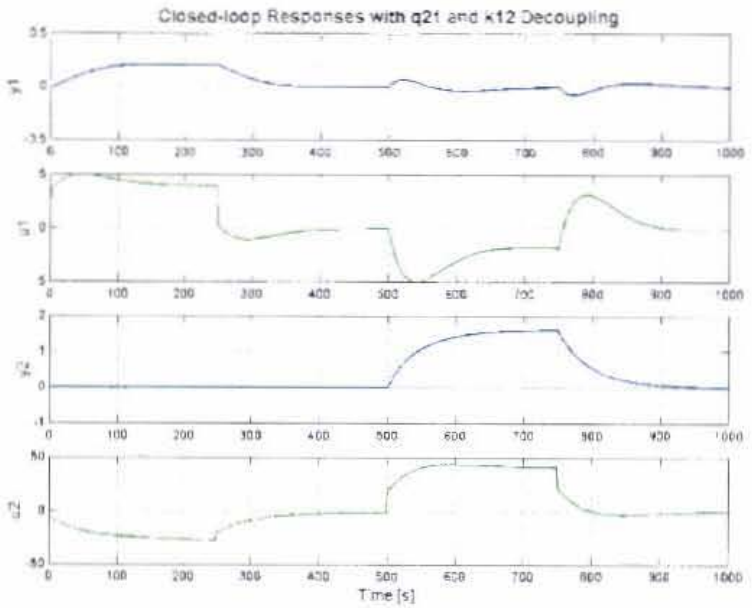


Figure C.5: Optimally tuned closed loop responses for q21 and k12 decoupling.

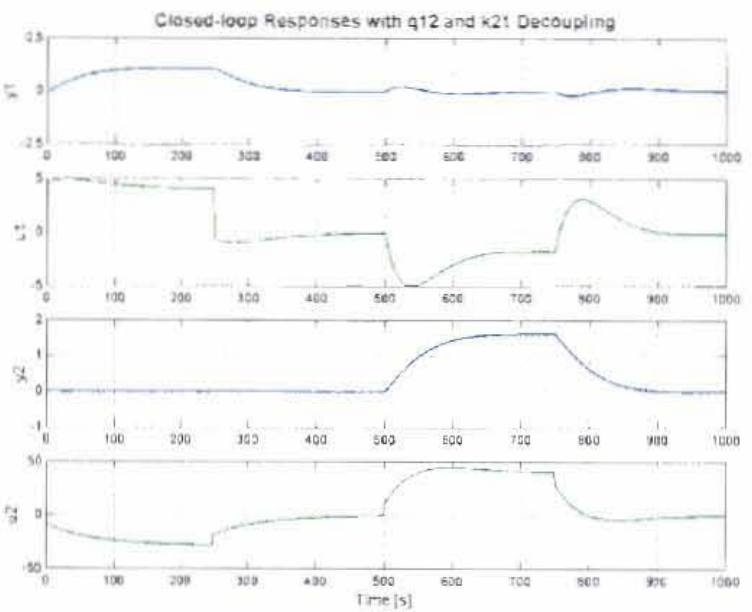


Figure C.6: Optimally tuned closed loop responses for q12 and k21 decoupling.

All the optimisation routines for this project were solved using Differential Evolution. All the optimisation problems were time series so that IAE (integral of the absolute error) could be used as the objective function. In many cases the optimised variables needed to be constraint within certain ranges. This was done by multiplying the IAE objective function by the magnitude of the deviance of the constraint variable outside the specified operating region. Such an objective function is extremely nonlinear, but DE handles this very well.

As an example the MIMO objective function is given.

The signals obtained from simulation:

$y_1$
$y_2$
$u_1$
$u_2$

with $r_1$ and $r_2$ as the output setpoints and $u_i$ constraint values is given by $u_{iuc}$ (upper constraint) and $u_{ilc}$ (lower constraint).

The variables that are optimised:

$K_{c1}$
$K_{c2}$
$K_{i1}$
$K_{i2}$

For a sampling interval of 1 second the integral is approximated by the sum of the error signal. The error in each loop is normalised such the loops are weighted equally in their contribution to the objective function. The objective function is then given by:

$$J = \frac{\sum |r_1 - y_1|}{r_1}(u_{1J} + 1) + \frac{\sum |r_2 - y_2|}{r_2}(u_{2J} + 1)$$

where $u_{IJ} = \sum |u_i - u_{iuc}| \Big\}_{u_i > u_{iuc}}^{where} + \sum |u_{ilc} - u_i| \Big\}_{u_i < u_{ilc}}^{where}$

Refinements to the objective function for MIMO controller tuning would be to include the following:

- Parameters to change the error weighting between the loops for the cases where the performance of one loop is more important than another.
- Add additional weight to some ranges of the output variables where deviations occurred as a result of a step change in another loop. This would minimise the interaction, should it be important, by giving some loops larger closed loop time constants than others.
- Disturbance and noise plant data can also be added.
- Different options for the objective function could be included like:
    - Integral of the squared error (ISE)
    - Integral time-weighted absolute error (ITAE)
    - Integral time-weighted squared error (ITSE)

# Appendix E

# Controllers Sensitivity to Noise Disturbances Graphs

This section gives the controller sensitivity graphs of the analysis that was performed in section 6.9 of the main document. See Figure 6-51 for the signals that was stepped and Table 6-11 for the signal step sizes.

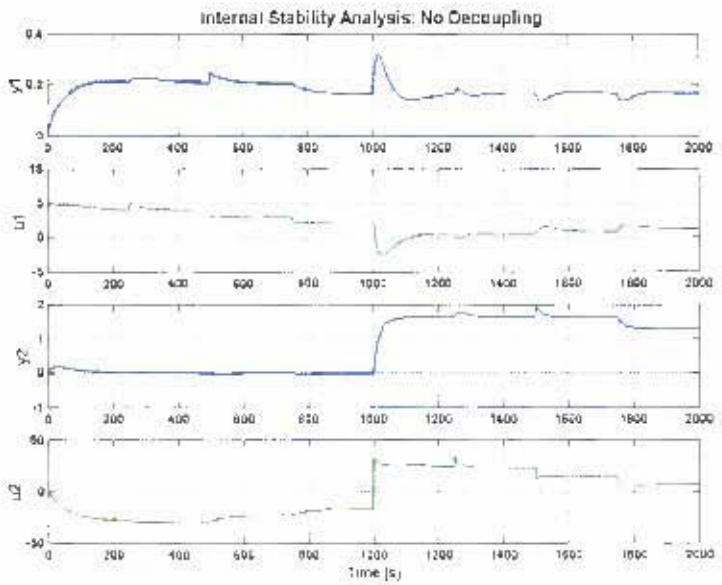


**Figure E.1: Internal stability analysis for the case with no decoupling.**

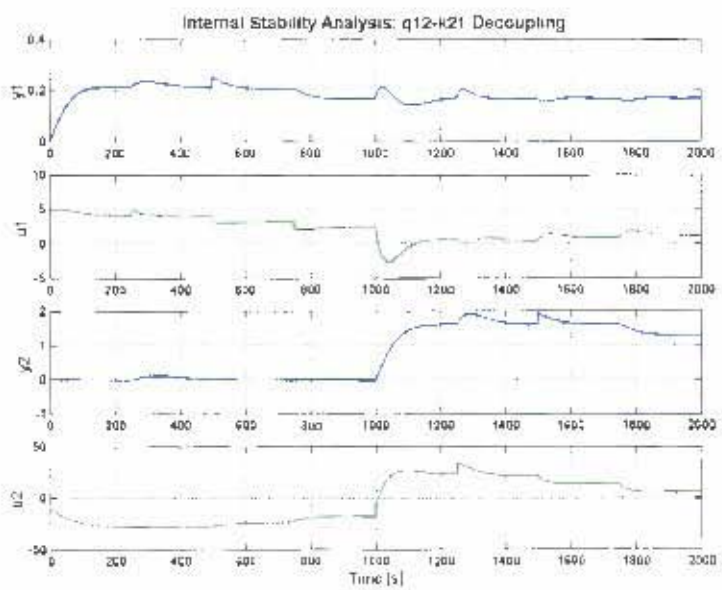


**Figure E.2: Internal stability analysis for the case with q12-k21 decoupling.**

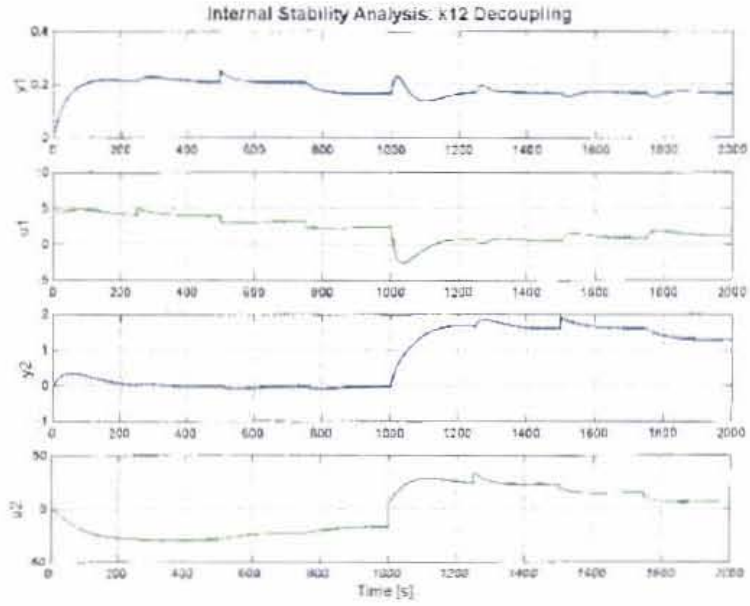


Figure E.3: Internal stability analysis for the case with only k12 decoupling.

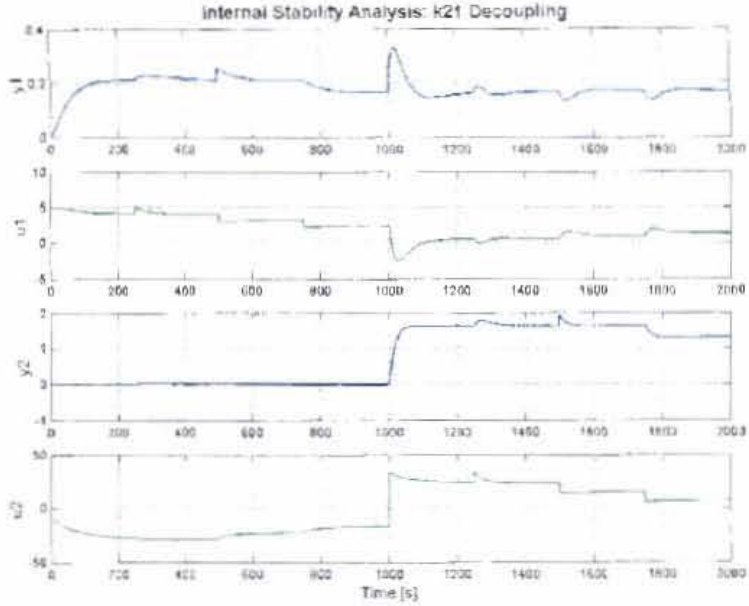


Figure E.4: Internal stability analysis for the case with k21 decoupling.

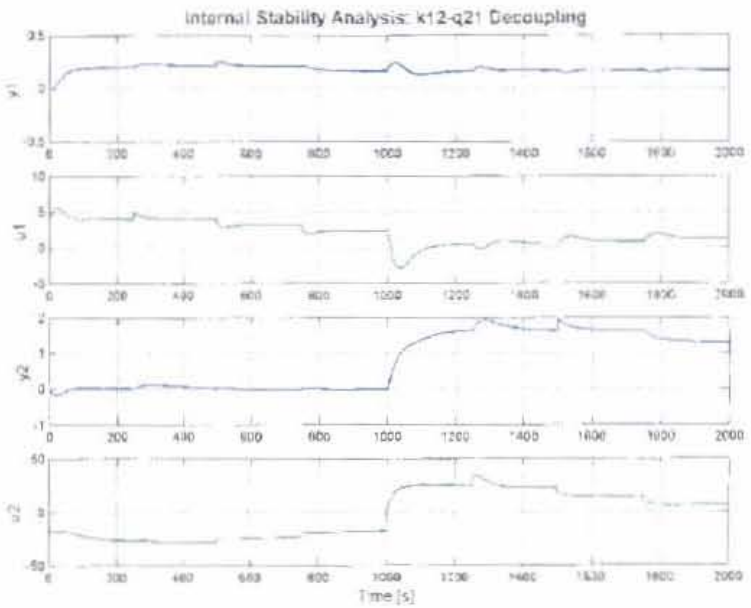


Figure E.5: Internal stability analysis for the case with k12-q21 decoupling.

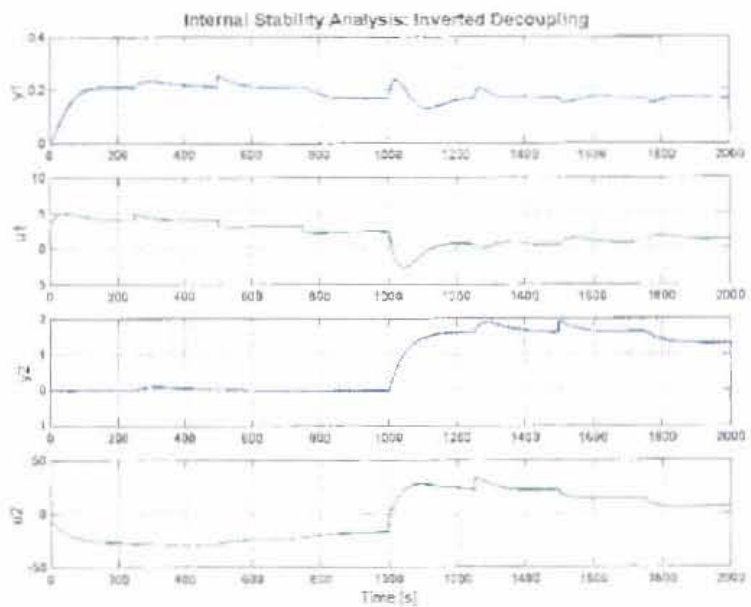


Figure E.6: Internal stability analysis for the case with inverted decoupling.

# Appendix F

# Further Discussion on Rougher Control

# Pulp Level Modelling and Control Suggestions.

It was realised during the step test exercises and implementation of the controllers that air addition and pulp level control cannot be done in isolation to the surrounding flotation cells. Sometimes when rougher cell one was under automated control the level PV became unstable so that the level control loop experienced difficulty in maintaining the level PV close the SP supplied by the bubble colour control loop. At other times the PV would start to increase above its setpoint so that the level control valve would respond until it reached 100%, at this point the cell starts to slime (slurry and not only the froth reports to the concentrate) and the MIMO controller (velocity and colour) is switched off with nominal setpoints given to both the air addition and the pulp level setpoint controllers. Soon after this the level PV would recover and reach its setpoint again. Initially this seemed strange as the same flow rate that passed through cell one also passed through cell two and the level control valve output of cell two rarely went above 50%. Flow rate fluctuations to the rougher cell from the milling section could therefore not the cause of these phenomena. It was soon realised that this only happened when the air addition setpoints were at high values. The cause of this was identified as the result of the hydrodynamic pressure difference between the cells that changes with changes in the air addition and pulp level. The explanation for level instability and the cell sliming is best described by a fundamental flow analysis on the system.

Consecutive rougher cell heights at BRPM differ with 600 mm down the bank to allow gravity flow from one cell to the next. Consider the diagram shown in Figure F.1 where h3 = 600 mm, the flow rate from the first to the second cell would be governed by the value of P1, P2 and the valve position.

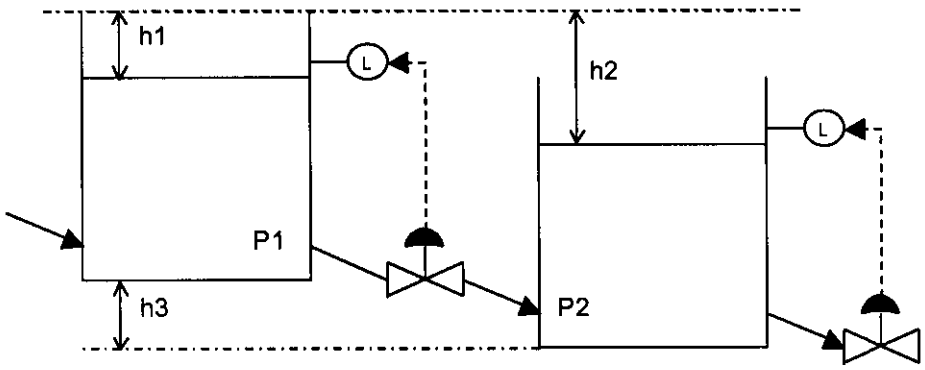


**Figure F.1: Diagram of two rougher cells indicating gravity flow.**

Fundamentally the flow rate can be modelled by the Bernoulli flow equation given by:

$$\Delta\left(\frac{P}{\rho}+g\cdot h+\frac{V^2}{2}\right)=-\Im \qquad \text{(F.1)}$$

The Bernoulli equation is reduced to the equation below which is used for valve sizing.

$$q = Cv\sqrt{P_1 - P_2} \qquad \text{(F.2)}$$

Where:

Cv ➔ valve coefficient that depends on the valve size

q ➔ flow rate

$P_1$ ➔ upstream pressure

$P_2$ ➔ downstream pressure

The upstream and down stream pressure difference is a function of both the pulp level as well as the air addition. Pressure difference is calculated from:

$$P_1 - P_2 = \rho_1 g h_1 - \rho_2 g h_2 \qquad \text{(F.3)}$$

Where:

$\rho_i$ ➔ bulk density of material in cell i

g ➔ 9.81 m/s$^2$

$h_i$ ➔ pulp height of cell i to a fixed reference height.

$h_x$ is measured by the pulp level sensors while $\rho_x$ would be affected by the air addition according to an empirical *gas hold up* correlation that is mainly a function of the pulp density, grind and air flow rate.

Gas hold up is defined by volume of pulp that is replaced by the induced air into the pulp phase. The two factors that determine how much pulp is replaced by the air addition are the amount of air induced and well as the residence time of the air in the pulp phase, which is strongly influenced by the viscosity of the pulp. A higher viscosity causes a higher friction between the rising bubbles and the surrounding pulp so that the bubble is subjected to a longer rise time and consequently resides longer in the pulp. Pulp viscosity in turn is mostly influenced by slurry density and particle size distribution.

The bulk density of the material in a flotation cell would be calculated as the total pulp mass divided by the sum of the pulp volume and the gas hold up volume. An increase in the gas hold up volume at a constant pulp level would therefore significantly reduce the bulk density, which would have a pronounced effect on the pressure difference between to cells so that the flow rate, as indicated in Eq. (F.2) would change.

Quantifying the effect of gas hold up in terms of the pressure difference between two cells, from test work done at BRPM, it was determined that the equivalent height of pulp replaced by the air induced, is given by the following linear relationship at a pulp density of 1.34 kg/l:

$$h_a = 0.047 \cdot a \qquad \text{(F.4)}$$

Where $h_a$ [m] is the pulp replaced by the air addition flow rate, $a$ [$m^3$/min].

Given the pressure difference calculation in Eq. (F.3), this could be simplified by replacing the pulp density terms with the equivalent heights of only the pulp by subtracting the gas hold up (calculated in term of height, Eq. (F.4)) from the level measured by the pulp level sensor:

$$P_1 - P_2 = \rho(gH_1 - gH_2) \qquad \text{(F.5)}$$

Where ρ is now given as the density of the pulp that passes through both cells and $H_i = h_i - h_{ia}$.

The maximum pulp level range that it can be controlled in on the rougher cells at BRPM is about 500 mm and the range of the air addition is between 0 and 12 $m^3$/min. Consider the operating condition case where the first cell has a froth depth from the cell lip of 400 mm with an air addition of 11 $m^3$/min and the second cell has a froth depth of 100 mm with an air addition of 4 $m^3$/min (which could be considered to be normal operating conditions for the individual cells since a deep froth bed would require a higher air addition rate and visa versa) then, according to Eq. (F.5) the pressure difference that would govern the flow rate can be calculated as:

$$\begin{aligned} P_1 - P_2 &= \rho g(H_1 - H_2) \\ &= \rho g((h_{ref} - h_1 - h_{a1}) - (h_{ref} - h_2 - h_{a2})) \\ &= \rho g((0 - 400 - 0.047 \cdot 10^3 * 11) - (-600 - 100 - 0.047 \cdot 10^3 * 4)) \\ &= -29\rho g \end{aligned}$$

Corresponding heights to the calculation above are indicated in the figure below.

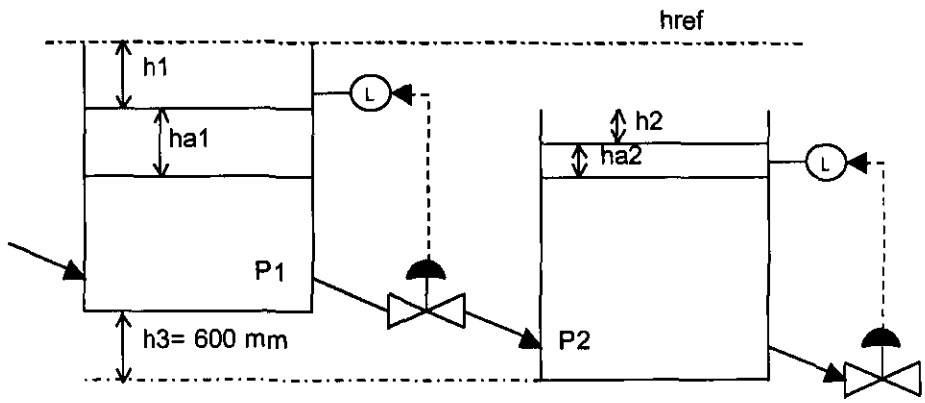


**Figure F.2: Heights used for calculation of the pressure difference.**

This shows that theoretically it is possible to have a negative pressure difference between two cells by the separate manipulation of the air addition and pulp level so that

the flow rate would flow from cell two to cell one. Practically this cannot happen due to fact that the first cell has a feed stream so that when the pulp flow is restricted as described above, the level in the first cell would start to decrease until the cell starts to slime. Traditional operator control ensured that both the air addition and pulp level of consecutive cells was more or less the same. With automated control of the pulp level and air addition this is however not the case.

The phenomena described above has pronounced implications for the automation of air addition and pulp level control as well as for the control loop parameters that maintains the level PV to its setpoint. As was the case for the description above, going the other way and supplying cell two with a froth depth of 400 mm and air addition of 11 $m^3$/min, and cell one with a froth depth of 100 mm and air addition of 4 $m^3$/min, the pressure difference between cells would be $1229 \cdot \rho g$. The significance of this for the pulp level controller is that the corresponding gain in the pulp level for a step change in the control valve output (that alters the flow rate between the cells as described by Eq. (F.2)) can be an order of magnitude (theoretically from $-Cv\sqrt{29\rho g}$ /(unit change in valve OP) to $Cv\sqrt{1299\rho g}$ /(unit change in valve OP)) different for different operating conditions of the air addition and pulp level of the cells before and after the control valve. Besides this effect, the dynamics of the control valve (pinch valve) is also non-linear.

It is therefore recommended that the controller developed in this project should be assisted with an upgrade of the PI pulp level controller. A possible controller upgrade could be the implementation of a gain-scheduling type of controller where the controller gain is a function of the calculated pressure difference between two cells.

As a short-term solution the bubble velocity and bubble colour controller outputs should be dynamically clamped, depending on the absolute values of the air addition and pulp level so that the pressure difference between two cells is never less than some calculated minimum.

# Optimisation Control

Automated control of flotation can be split up in two categories, stabilisation control and optimisation control. This project mainly focussed on the stabilisation control of froth image analysis outputs. Optimisation of these outputs and other measured outputs has not been analysed or discussed in the main document. This section gives a discussion on optimisation control with the objective to supply more information on the broader topic of rougher flotation control and to recommend further work on this topic.

Online flotation optimisation entails running the process under such conditions that the final process outputs are optimal [Lynch et al, 1981]. Given that the performance of the flotation process is mainly only measured by two quantities, namely the final recovery and concentrate grade of a flotation circuit [Hodouin et al, 2000], optimisation of a single flotation cell would be sub optimal done in isolation to the rest of the flotation circuit. The different flotation stages should be operated under conditions that would achieve maximum overall plant performance. Identifying what these conditions are would require process modelling of the effect the different flotation stages has on each other.

Since the scope of this project focuses on only one flotation cell, not much can be done with regard to the implementation of optimisation flotation control, but as one of the research objectives, this topic is researched and briefly discussed as optimisation control forms an integral part towards the development of an overall automated flotation control strategy.

The structure in which online flotation optimisation is further discussed, is to focus on the manipulated variables that is available for this purpose. Manipulated variables of the flotation process can be categorised in three components:

- Hydrodynamic variables that is applied to every flotation cell.
    - Air addition
    - Pulp level
- Chemical or reagent variables that generally applies to a flotation stage, which consists of a few flotation cells.

- Collector (i.e. xanthate)
- Frother
- Depressant
- Activator (i.e. copper sulphate)

- Mechanical variables that enables online altering of the circuit configuration that would be generally applied to a whole flotation circuit.

## *Hydrodynamic variables.*

Air addition and pulp level are the only variables that could possibly be applied to just a single flotation unit for local optimisation. Both these variables have an effect on the concentrate grade and recovery from a cell. Consider the scenario where the concentrate grade from a flotation cell with a deep froth bed and high air addition would give the same concentrate grade as a shallow froth bed and a low air addition. Taking this concept one step further, there exist infinite ratios between air addition and pulp level of a cell that would produce the same concentrate grade. For all air addition to pulp level ratios that produce the same concentrate grade of the same ore there must exist an optimum ratio or a range of ratios where the recovery of the cell is at a maximum. Given in Figure F.3 below is a graphical description of the concept described above.

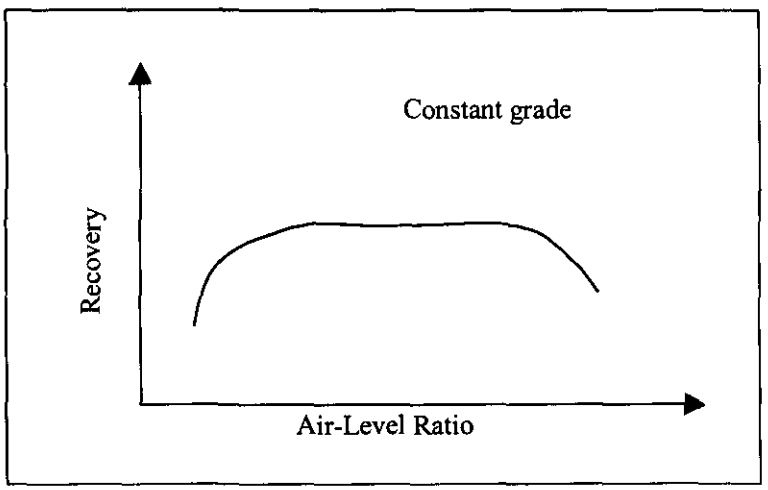


**Figure F.3: Optimisation of air addition and pulp level ratio to achieve maximum recovery**

Information required to determine the optimal recovery at a specified concentrate grade for the manipulation of air addition and pulp level can only be done through extensive metallurgical test work as the curve, indicated in Figure F.3 would be different under different operating conditions of the process. An additional requirement would be the online detection of the difference between a change in air addition and pulp level. As shown during the output selection of this project two such measurements might already be available namely the bubble velocity and bubble colour. An optimum recovery at a specified grade might therefore also be specified in terms of an optimum ratio between bubble velocity and bubble colour. Two of the obstacles that need to be overcome with such an optimisation routine are that bubble velocity and colour needs to be related to the metallurgical performance of a flotation cell. The second is that bubble colour is strongly influenced by ambient light and this needs to be eliminated. Hyotyniemi and Ylinen [2001] report on a hood that was installed over the froth image camera and its light source so that the froth surface area on which the camera focuses was shaded and protected from other direct light sources.

### *Chemical Variables*

Reagent optimisation on PGM ores is mostly done in an offline manner, except for frother addition that is controlled by the operator. Lynch et al [1981] and others report on the online manipulation of xanthate addition on coppers ores with the use of OSA measurements. The approach followed in the PGM flotation industry, where recovery is considerably more important than grade, with regard to xanthate control is to rather slightly over dose xanthate to ensure that there is always enough. Costs associated with additional xanthate dosage are almost negligible compared to recovery losses as a result of xanthate under dosage so that online xanthate control, within the platinum industry, is not really an option [Sweet, 2000].

As mentioned earlier reagent optimisation involves responsiveness to a complete flotation stage. Sweet [2000] has done interesting work on the online identification of depressant and frother dosage rates on a rougher flotation stage with ten flotation cells. From the plant test work done on Merensky ore he proposes a control strategy that would manipulated the frother and depressant dosage rates according to the bubble size

distribution down the bank. Depending on whether the bubble size distribution down the bank is increasing or decreasing, identification is made to whether it is an over/under dosage of frother or depressant so that corrective action can be taken. This might still be considered as stabilisation control of the bubble area distribution down the bank. Optimisation of this would be to determine the optimal bubble size distribution down the bank, from metallurgical test work and passing these optimal setpoints to the lower level stabilisation control actions.

### *Online Circuit Configuration*

Somewhat out of the scope of this project, so only briefly mentioned for completeness, is the online manipulation of circuit configuration to achieve optimal performance. Lynch et al [1981] states that circuit configuration have a major effect on plant performance and that although online circuit configuration has not been widely applied, the equipment do so exists. Bazin et al [1999] discusses the application of online mass balancing to determine abnormal process deviations and to do online circuit optimisation. Online circuit configuration and mass balancing requires well instrumented plants with regard to OSA, flow rate and density measurements as well the equipment to do online circuit alterations.

From the literature as well as applications in the platinum industry, it can be said that online circuit configuration is still a very under utilised manipulated variable that could be used to improve flotation performance. The reason for this might be due to the fact that the decision-making on when to divert a stream would be based on a comparison of the current configuration performance with the estimated performance after the configuration has been altered. This would require an accurate process model to make such an estimate. Since the flotation process is mathematically not well defined, such a prediction might not be possible.

# Appendix G

# Metallurgical Terminology

This section gives an explanation of some common terminology used in extractive metallurgy.

| | | |
|---|---|---|
| Concentrate | → | The product of flotation (contained in the froth that over flows from the flotation cell. |
| Grade | → | The concentration of a valuable mineral in a process stream or sample. |
| Grinding | → | The process of reducing the particle size of a rock. Milling is an example of a grinding process. |
| Mass pull | → | The percentage of mass in flotation concentrate to the mass in the feed. |
| OSA | → | Online Stream Analysis. Measures metal content online. |
| Particle size distribution | → | A distribution that defines a composite of different particle sizes. |
| PGM | → | Platinum Group Metals. |
| ROM | → | Run-of-mine. |
| Pulp | → | Mixture of fine solids material and water. |
| Reagents | → | Chemicals that is added to the flotation process to enhance its performance, i.e. depressants, collectors, frothers and activators. |
| Recovery | → | The percentage of a valuable mineral or metal that is recovered in the concentrate. |
| Tails | → | The discard of flotation. |